The Role of Hydrogen Sulfide in Normal and Aberrant Late Lung Development

Inaugural Dissertation
submitted to the
Faculty of Medicine
in partial fulfillment of the requirements
for the PhD-Degree
of the Faculties of Veterinary Medicine and Medicine
of the Justus Liebig University Giessen

by

Madurga Hernández, Alicia
of
Valencia, Spain

Gießen 2015

From the Max Planck Institute for Heart and Lung Research, Bad Nauheim

Director / Chairman: Prof. Dr. Norbert Weissman of the Faculty of Medicine of the Justus Liebig University Giessen

First Supervisor and Committee Member: Prof. Dr. Werner Seeger
Second Supervisor and Committee Member: Prof. Dr. Martin Diener
Committee Members: Prof. Dr. Christine Wrenzycki, Prof. Dr. Maik Gollasch

Date of Doctoral Defense: 9th May 2016

1 Declaration

I declare that I have completed this dissertation single-handedly without the unauthorized help of a second party and only with the assistance acknowledged therein. I have appropriately acknowledged and referenced all text passages that are derived literally from or are based on the content of published or unpublished work of others, and all information that relates to verbal communications. I have abided by the principles of good scientific conduct laid down in the charter of the Justus Liebig University of Giessen in carrying out the investigations described in the dissertation.

“The basic mechanisms that regulate lung development and the link with human lung disease are among the most challenging and exciting areas of scientific inquiry”.

Edward E. Morrisey

2 Abstract

Bronchopulmonary dysplasia (BPD) is a chronic lung disease characterized by arrested alveolarization, a complication of premature birth. The gasotransmitter hydrogen sulfide (H_2S) is emerging as a mediator of lung physiology and disease. In this study, the impact of systemic application of H_2S on post-natal alveolarization was evaluated in a mouse BPD model. Exposure of newborn mice to 85% O_2 for 10 days decreased the total number of alveoli in the lung by 56% and increased mean alveolar septal wall thickness by 29%, assessed by stereological analysis. Systemically administration of GYY4137, the slow-release H_2S donor, for 10 days improved lung alveolarization in mouse pups breathing 85% O_2, compared with vehicle-treated littermates. Though without effect on lung oxidative status, systemic H_2S administration reduced leukocyte infiltration into alveolar airspaces caused by hyperoxia, and normalized lung interleukin (IL)-10 levels that were else diminished by 85% O_2. The rapid-release H_2S donor NaHS was used to treat primary mouse alveolar type II (ATII) cells; NaHS had no impact on cell viability but stimulated ATII cell migration. Glibenclamide attenuated the impact of NaHS on ATII cell migration, implicating ion channels; and was accompanied by activation of Akt, hinting at two possible mechanisms of H_2S action. Although exposure of ATII cells to 85% O_2 produced substantial changes in gene expression, exposure to either GYY4137 or NaHS had no impact on ATII cell gene expression, as determined by microarray suggesting that the effects observed were independent of changes in gene expression. H_2S can be generated endogenously by cystathionine β-synthase (Cbs) and cystathionine γ-lyase (Cth). In this study it is demonstrated that the expression of Cbs and Cth in mouse lungs is dynamically regulated during lung alveolarization, and that alveolarization is impaired in *Cbs*$^{-/-}$ and *Cth*$^{-/-}$ mouse pups, where a 50% reduction in the total number of alveoli was observed, with no influence on mean alveolar septal wall thickness. Immunofluorescence staining and laser-capture micro dissection revealed that CBS and CTH expression was present in the lung vessels and in the airway epithelium. Vessel remodeling occurred in the absence of Cbs and Cth, since it led to a 100-500% increase in vessel muscularization of small- and medium- size lung vessels. Inhibition of CBS or CTH expression in endothelial cells, using either small interfering RNA or via pharmacological inhibition (propargylglycine) respectively, diminished angiogenic capacity resulting in a 50% decrease in number of tubes formed, and a 30-40% decrease in tube length. On the other hand, administration of GYY4137, promoted endothelial tube formation. These data support the further investigation of H_2S as a candidate interventional strategy to limit the impaired alveolarization associated with BPD, also suggests a key role for the

H_2S-generating enzymes Cbs and Cth in lung alveolarization and pulmonary vascular development and homeostasis.

3 Kurzfassung

Die bronchopulmonale Dysplasie (BPD) ist eine chronische Lungenerkrankung, charakterisiert durch eine gehemmte Alveolarisierung und tritt als Komplikation bei Frühgeburten auf. Der Gasotransmitter Wasserstoffsulfid (H_2S) ist als ein Mediator in der Lungenphysiologie und in Erkrankungen bekannt. In dieser Studie wurde die Wirkung einer systemischen Applikation von H_2S auf die postnatale Alveolarisierung im BPD Modell evaluiert. Die Exposition neugeborener Mäuse zu 85% O_2 für 10 Tage verringerte die totale Anzahl der Alveoli in der Lunge um 56% und erhöhte die durchschnittliche Wanddicke der alveolaren Septen um 29%, festgestellt durch stereologische Analysen. Die systemische Verabreichung von GYY4137, einem H_2S Donor mit langsamer Freisetzung, für 10 Tage verbesserte die Alveolarisierung in den Jungtieren, die 85% O_2 ausgesetzt waren, im Vergleich zu den Jungtieren, die nur die Trägersubstanz verabreicht bekamen. Ohne Effekte auf den oxidativen Status der Lunge reduzierte die systemische H_2S Gabe die durch die Hyperoxie begründete Leukozyten-Infiltration in den alveolären Luftraum und normalisierte die Interleukin (IL)-10 Level, die durch 85% O_2 verringert werden. NaHS, ein H_2S Donor mit schneller Freisetzung, wurde zur Behandlung primärer alveolärer Typ II (ATII) Zellen verwendet. NaHS hatte keine Auswirkung auf die Lebensfähigkeit der Zellen, stimulierte jedoch die Zellmigration. Glibenclamide verringerte die Wirkung von NaHS auf die ATII Zellmigration, was eine Rolle von Ionenkanälen in diesem Prozess impliziert und wurde durch die Aktivierung von Akt begleitet, was Hinweise auf zwei mögliche Mechanismen der H_2S Aktivität gibt. Obwohl die Exposition von ATII Zellen zu 85% O_2 erhebliche Veränderungen der Genexpression bewirkt, hatte weder die Exposition zu GYY4137 noch zu NaHS eine Wirkung auf die Genexpression der ATII Zellen, wie durch Microarray Analysen festgestellt wurde. Dies lässt vermuten, dass die beobachteten Effekte unabhängig von Veränderungen in der Genexpression sind. H_2S kann endogen durch die Cystathionin β-Synthase (Cbs) und die Cystathionin γ-Lyase (Cth) generiert werden. In dieser Studie wurde gezeigt, dass die Expression von Cbs und Cth in der Lunge der Maus während der Alveolarisierung dynamisch reguliert wird und dass die Alveolarisierung in *Cbs*$^{-/-}$ und *Cth*$^{-/-}$ Jungtieren der Maus beeinträchtigt ist. Hier wurde eine Reduzierung der totalen Anzahl von Alveolen um 50% beobachtet, ein Einfluss auf die durchschnittliche Wanddicke

der alveolaren Septen wurde nicht festgestellt. Immunofluoreszenzfärbungen und Lasermikrodissektionen zeigten, dass eine Expression von CBS und CTH in den Lungengefäßen und dem Epithelium der Atemwege stattfand. Bei Abwesenheit von Cbs und Cth wurde ein Blutgefäß-*Remodeling* festgestellt, was zu einer 100 – 500%-igen Zunahme der Muskularisierung der kleinen und mittleren Blutgefäße führte. Die Inhibierung der CBS oder CTH Expression in Endothelzellen, entweder unter Verwendung von *small interfering* RNA oder einer pharmakologisch wirksamen Substanz (Propargylglycin) verminderte die angiogene Kapazität mit dem Resultat einer um 50% verminderten Anzahl der formierten *tubes* und einer Reduzierung der Länge der formierten *tubes* um 30 – 40%. Die Verabreichung von GYY4137 förderte die endotheliale *tube* Formierung. Diese Daten unterstützen eine weitere Untersuchung des H_2S als einen Kandidaten für Interventionsstrategien, um der beeinträchtigten Alveolarisierung, die mit BPD assoziiert ist, zu begegnen. Weiterhin kann vermutet werden, dass die H_2S-generierenden Enzyme Cbs und Cth in der Alveolarisierung und der pulmonalen vaskulären Entwicklung und Homöostase eine Schlüsselrolle einnehmen.

4 Index

5 List of figures

6 List of tables

7 List of abbreviations

%	*Per cent*
°C	Degree Celsius
αSMA	α smooth muscle actin
µ	Micro (10^{-6})
µg	Microgram
µl	Microliter
µM	Micromolar
A	Alveoli and ducts
Akt	Protein kinase B
Alv air	Alveolar air spaces
Alv epi	Alveolar epithelium
ATII	Primary alveolar type II
AV	Annexin V
B	Alveolar bridge
BAL	Bronchoalveolar lavage
bp	Base pair
Brg1	Brahma-related gene 1
BSA	Bovine serum albumin
C	Capillaries
CA	Carbonic anhydrase
cAMP	Cyclic adenosine monophosphate
CAT	Cysteine aminotransferase
CBS	Cystathionine-β synthase
cDNA	Complementary DNA
CDO	Cysteine dioxygenase
CE	Coefficient of error
cGMP	Cyclic guanosine monophosphate
CLY	Cysteine lyase
CO	Carbon monoxide
COPD	Chronic obstructive pulmonary disease
CPAP	Continuous positive airway pressure
CSD	Cysteine sulfinate decarboxylase

Ct	Cycle threshold
CTH	Cystathionine-γ lyase
CV	Coefficient of variation
DAB	3,3′-diaminobenzidine
dH_2O	Distilled water
DNA	Deoxyribonucleic acid
E	Embryonic
EDTA	Ethylendinitrilo-N, N, N′, N′-tetra-acetic-acid
eNOS	Endothelial NOS
et al.	Et alia
FBS	Fetal bovine serum
FC	Fold change
GD	Gestational day
GSH	Glutathione, reduced form
GSSG	Glutathione, oxidized form
GYY4137	4-methoxyphenyl(morpholino)phosphinodithioate morpholinium salt
HMOX	Heme oxygenase
H_2O	Water
HPAEC	Human pulmonary artery endothelial cell
HRPO	Horse radish peroxydase
H_2S	Hydrogen sulfide
IF	Immunofluorescence
IHC	Immunohistochemistry
IL-1β	Interleukin 1β
IL-6	Interleukin 6
IL-10	Interleukin 10
iNOS	Inducible NOS
i.p.	Intraperitoneal
K_{ATP}	ATP potassium
kDa	kilo Dalton
MAPK	Mitogen-activated protein kinases
mg	Milligram
min	Minute
ml	Milliliter

MLE-12	Murine lung epithelial cell line
mM	Millimolar
3-MPST	3-mercaptopyruvate sulfur transferase
mRNA	Messenger RNA
MTT	3-(4,5-dimethylthiazol-2-yl)-2,5-diphenyltetrazolium bromide
MWT	Index of medial wall thickness
N	Number
NaCl	Sodium chloride
NaHS	Sodium hydrosulfide
Na_3VO_4	Sodium vanadate
NFκβ	Nuclear factor κ-light-chain-enhancer of activated B cells
nM	Nanomolar
NO	Nitric oxide
Non-par	Non parenchyma
NOS	NO synthase
nNOS	Neuronal NOS
Nrf2	Nuclear factor (erythroid-derived 2)-like 2
O_2	Dimolecular oxygen
P	Postnatal
PAG	Propargylglycine
Par	Parenchyma
PBS	Phosphate-buffered saline
PCR	Polymerase chain reaction
PI	Propidium iodide
PLP	Pyridoxal 5′-phosphate
PPV	Positive pressure ventilation
R-SH	Thiol
S	Surface area
S_v	Surface density
SAM	S-adenosyl methionine
Sep	Septum
sGC	Guanylyl cyclase
siRNA	Small-interfering RNA
sO_2	Oxygen saturation

SUR	Systematic uniform random
TNFα	Tumor necrosis factor α
V	Volume
V_v	Volume density
vol/vol	Volume per volume
vWF	Von Willebrand factor
wt/vol	Weight per volume

8 Introduction

8.1 Lung development

The pulmonary system develops from a series of complex events that occur during prenatal and early postnatal life. During lung development, the embryonic lung arises as a protrusion from the foregut endoderm and undergoes a process called "branching morphogenesis", which begins a reproducible, bilaterally asymmetrical pattern of stereotypic branching into the surrounding splanchnic mesenchyme.

In the human lung, the branching is completed after 16 generations by week 16 post conception, and three lobes form on the right side and two on the left side of the lungs. These events require correct growth and differentiation of the epithelial and mesenchymal components of the immature lung to form the bronchial tree and alveoli; the pulmonary, bronchial, and lymphatic vasculatures; the nerves and the pleura.

In contrast to humans, the mouse has four lobes in the right side and one lobe on the left side. Moreover, the mouse only has 12 airway generations and alveolarization occurs postnatally.

Classically, lung development has been classified into five stages: embryonic, pseudoglandular, canalicular, terminal saccular, and alveolar. Lung development is an early process that starts around the third week of the embryonic period and that can last until early adulthood. During the earliest lung development stage, the pseudoglandular stage (5-17 weeks of human pregnancy, embryonic (E) E9.5-E16.6 days in the mouse embryo), branching morphogenesis occurs in epithelial tubes lined with cuboidal epithelial cells. At this point, the structure is still too immature for adequate gas exchange. During the canalicular stage (16-25 weeks of human pregnancy, E16.6-E17.4 days in the mouse embryo), the respiratory tree continues growing in length and diameter, along with vascularization and angiogenesis. An increase in capillary number occurs, and the terminal bronchioles are divided into respiratory bronchioles and alveolar ducts. The terminal saccular stage (24 weeks to late fetal period in human, E17.4 to postnatal (P) day P5 in the mouse) is characterized by thinning of the interstitium. The alveolar epithelial cells are more clearly differentiated into type I and type II pneumocytes. The capillaries grow and form an intricate network during this stage and the lymphatic network becomes well developed. Maturation of surfactant synthesis and secretion is a crucial event to prevent lungs from collapsing and allow gas exchange, and near the end of this stage, the fetal lung can support gas exchange in premature newborns. During the alveolar stage (late fetal period to childhood in human, P5 to P30 in mouse) terminal sacs develop into mature alveolar

ducts and alveoli. Contrary to early lung development, this stage remains poorly understood. During this latter phase of development, important events take place for the maturation of the lung: the peak of secondary septation occurs, with an increase in the number and a decrease in the size of the alveoli, together with a thinning of the pulmonary septa and maturation of the lung microvasculature, increasing exponentially the surface area for gas exchange and minimizing the distance between air and blood. A neonatal lung is estimated to have about 50 million alveoli, still, this number increases six-fold to about 300 million by the age 7-8 years when alveolarization is largely complete. In the meantime, the adult alveolar capillary bed is able of accommodating the entire cardiac output of 5 L/min, rising five-fold to 25 L/min during maximal exercise (Madurga et al., 2013; Massaro & Massaro, 2007; Morrisey et al., 2013; Warburton, 2012; Warburton et al., 2010; Warburton et al., 2000).

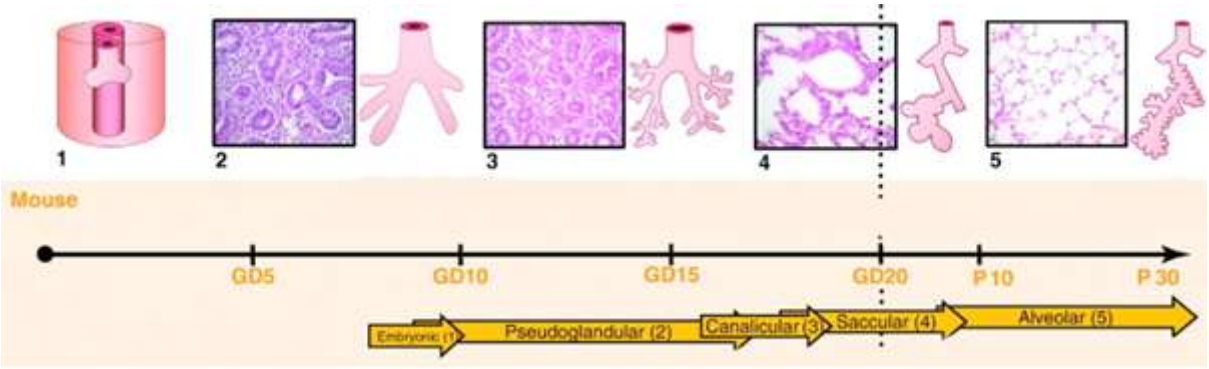

Figure 1 Scheme of the stages of lung development.

Scheme of the five stages of lung development: embryonic, pseudoglandular, canalicular, terminal saccular, and alveolar. In mice, birth takes place after 20 days of embryonic development and pups are born in the saccular stage. In contrast, humans give birth around the 38th week of gestation, during the alveolar stage of lung maturation. GD, gestational day, P, postnatal day. With the permission of Dr. Gianni Carraro.

8.2 Bronchopulmonary dysplasia

8.2.1 Introduction

The development of the airways, through epithelial tube branching and later septation of terminal air sacs, occurs in close conjunction with the development of the pulmonary vasculature. Alterations to these developmental processes give rise to abnormal lung structure, deficiency of gas exchange, and newborn respiratory failure. Clinical examples of such perturbation of normal lung growth include bronchopulmonary dysplasia (BPD), cystic adenomatoid malformation of the lung, and hypoplasia of the lung (Smith et al., 2010; Warburton et al., 2010).

8.2.2 Definition

The term bronchopulmonary dysplasia was first described in 1967 by Northway and colleagues (Northway et al., 1967). The definition of BPD is complicated and has evolved over the years. Nowadays, BPD refers to a newborn at 35-37 weeks postmenstrual age treated with mechanical ventilation, continuous positive airway pressure (CPAP), or in need of oxygen concentrations of 30% at rest on oxygen saturation (sO_2) of 90-96% or supplemental oxygen concentrations of 30% on sO_2 of more than 96% (Ambalavanan & Carlo, 2004; Ehrenkranz et al., 2005; Jobe & Bancalari, 2001; Jobe, 1999; Northway, 1992; Walsh et al., 2004).

The National Institute for Health in the USA has further divided the definition of BPD into:

-Mild: Requiring supplemental O_2 at 28 weeks of age, but in air by 36 weeks corrected age.

-Moderate: Requiring <30% supplemented O_2 at 36 weeks corrected age.

-Severe: Requiring >30% supplemental O_2 and/or requiring CPAP or ventilation, at 36 weeks of corrected age.

8.2.3 Incidence and prevalence

The BPD disease is a complex multifactorial chronic lung disease of the premature newborn that affects thousands of infants each year with an incidence of 23% of infants with birth weights are below 1500 g. It is the single most important factor determining the length of hospital stay in newborns born at less than 29 weeks. The more premature the newborns are, the more severely affected they are. The prevalence is higher among very low birth weight and extremely preterm infants. Improved medical management of BPD has increased substantially the survival of these patients and also the pathophysiological picture of BPD, but the prevalence of BPD has also increased, especially in small infants who may have been exposed to *in utero* infection (Bose et al., 2011; Laughon et al., 2011; Shennan et al., 1988; Van Marter, 2009).

8.2.4 Morbidity and mortality

Improvement in clinical management has decreased substantially the mortality rates of BPD infants. The survival and morbidity among infants older than 24 weeks of gestational age have improved since the introduction of antenatal corticosteroids treatment and surfactant therapy, and nowadays infants with BPD usually have a milder disease. However, the survival rate remain 25-50% in the most preterm neonates of 23-24 weeks gestation, reflecting the lack of maturation in alveolarization and vascular development. Neonates with severe BPD remain at high risk for mortality and pulmonary morbidity during the first two years of life. Finally, factors such as gender affect the severity of this disease, since male infants usually have a more severe phenotype with worse neurodevelopmental outcome (Ambalavanan et al., 2009; Ambalavanan et al., 2008; Ambalavanan et al., 2011; Shennan et al., 1988).

8.2.5 Risk factors

The BPD disease may be caused by factors such as perinatal infection (chorioamnionitis), peripartum inflammation, volotrauma, borotrauma, postnatal steroid treatment, premature delivery, and prolonged mechanical ventilation, among others (Ambalavanan et al., 2009; Bose et al., 2011; Hartling et al., 2012; Jobe, 2005; Jobe & Ikegami, 2001; Kakkera et al., 2005; Kallapur & Jobe, 2006; Kunzmann, et al., 2013; Laughon et al., 2011; Rocha et al., 2010; Schelonka et al., 2005).

8.2.6 Signs and symptoms

Infants with BPD exhibit abnormalities during clinical examination, chest radiography, pulmonary function testing, and histopathologic studies. Initial abnormalities are consistent with respiratory distress syndrome which if they persist have a higher risk of evolving into BPD. The symptoms include the following: Tachypnea, tachycardia, increased respiratory effort (with nasal flaring, retractions and grunting), frequent desaturations and significant weight loss during the first ten days of life.

Infants with BPD are usually extremely immature and have a very low weight birth. Often the requirements of oxygen and ventilator support are higher during the first two weeks of life. At weeks 2-4, either oxygen supplementation, ventilator support, or both, are frequently increased to maintain adequate ventilation and oxygenation. A classic scenario is a 23-26 weeks gestation infant who over a period of 4-10 weeks progresses from mechanical ventilation, CPAP through to requiring additional oxygen (Bancalari et al., 1979; Stoelhorst et al., 2005).

8.2.7 Pathophysiology

The pathogenesis of BPD remains poorly understood. Premature birth and subsequent events likely interfere with alveolarization and vascularization, leading to a decrease in alveolar number, and overall to a reduced surface area for gas exchange. Today, BPD is characterized by arrested alveolarization in the saccular stage, lung inflammation with variable interstitial fibrosis and discontinuance of microvessel maturation (Abman, 2007; Blackwell et al., 2011; Madurga et al., 2013; Morrisey et al., 2013; O'Reilly et al., 2013).

8.2.8 Diagnosis

Today, the diagnosis of BPD is defined by oxygen need and postmenstrual age, but the pathological characteristics and mechanisms that underlie the disease remain to be better understood. Different tests and procedures are useful tools for the diagnosis and monitoring, BPD such as laboratory tests (blood gasometry tests), oxygenation monitoring, chest radiography, high-resolution chest computed tomography scanning, chest magnetic resonance imaging, lung biopsy, pulmonary function tests (airway resistance, lung compliance, and airway reactivity) and echocardiographic assessment (Ambalavanan & Carlo, 2004; Bancalari et al.,

1979; Jobe & Bancalari, 2001; Smith et al., 2005; Stoelhorst et al., 2005; Van Marter et al., 2000; Walsh et al., 2006; Walsh et al., 2004).

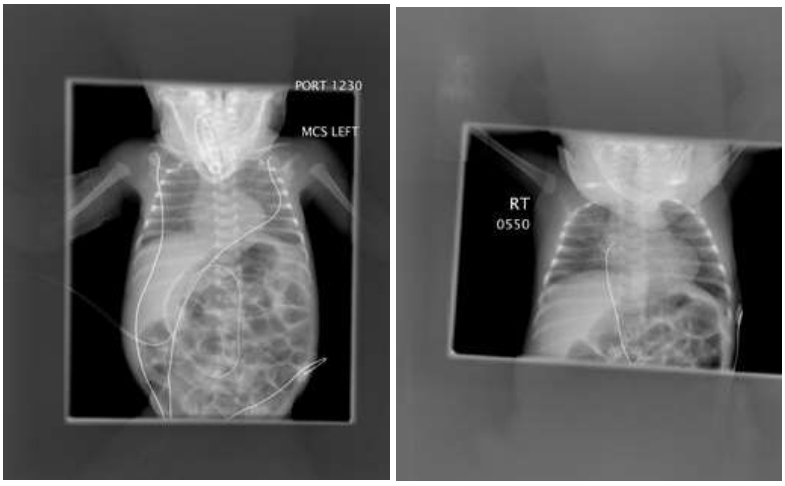

Figure 2 Chest X-ray of a one month old female patient with BPD.
Initial chest X-ray revealing minimal coarsening of the interstitial markings radiating from the hilia. One month later after prolonged incubation, the chest X-ray reveals bilateral, interstitial thickening and diffuse haziness in the lungs. Courtesy of Northeastern Ohio Universities College of Medicine-Canton Affiliated Hospitals.

8.2.9 Treatment

In most therapies, BPD infants are treated by surfactant replacement (Kresch & Clive, 1998; Mbuyamba et al., 1998), with oxygen supplementation, CPAP and mechanical ventilation (Northway et al., 1967). Different models and strategies of ventilation have been studied to potentially reduce lung injury and systematic reviews judge that optimal use of conventional ventilation may be as effective as high-frequency oscillatory ventilation in improving pulmonary outcomes. Many centers use "gentler ventilation" with more CPAP and less intubation to lower the rates of BPD. Infants with BPD that require mechanical ventilation, small tidal volumes are preferable to lower the risk of lung injury, although in the very preterm infants, higher tidal volumes are necessary to maintain effective ventilation (Morley et al., 2008; Nanan et al., 2008). For infants requiring oxygen and positive pressure ventilation (PPV), efforts are made to minimize oxygen toxicity, lung, and retina injury. Optimal ventilation levels include a pH level of 7.2-7.3, a partial pressure of carbon dioxide of 45-55 mm Hg, and a partial pressure of oxygen level of 50-70 mm Hg (with sO_2 at 91-95 %) (Network et al., 2010).

Nonetheless, the normal oxygen requirement for a preterm infant is unknown, and repeated episodes of desaturation and hypoxia may appear in infants with BPD receiving mechanical ventilation, as a result of altered pulmonary mechanics, bronchospasm, excessive stimulation, decreased of respiratory drive and enforced exhalation efforts.

The use of other medications is also common, diuretics, bronchodilators and corticosteroids, which have many pharmacologically benefits but clinically significant adverse effects (Brion & Soll, 2001; Brundage et al., 1990; Halliday & Ehrenkranz, 2001a, 2001b, 2001c; Kersbergen et al., 2013; Papile et al., 1998). Patients with BPD have higher nutrition requirements, therefore nutritional strategies are important to manage these infants: Early administration of parenteral nutrition, supplementation with antioxidant vitamins (vitamin A), and caffeine treatment, avoid of fluid overload and early enteral feeding in small amounts (Darlow & Graham, 2007; Rocha et al., 2010; Schmidt et al., 2006). Postnatal growth failure is frequent in BPD patients, and may have extensive effects on long-term development outcomes. Therefore, strategies to optimize postnatal weight gain are necessary to improve pulmonary, retinal and neurologic development. Prenatal management of the pregnant mother to lower the risk of BPD includes treatment of maternal inflammatory conditions (chorioamnionitis) and treatment of maternal infection (*Ureaplasma urealyticum*) (Hartling et al., 2012; Schelonka et al., 2005).

Overall, present therapies palliate the symptoms, but there is a lack of better treatments that promote lung maturation, and prognostic factors to detect which neonates are more prone to develop BPD (Jobe, 2011; Madurga et al., 2013).

8.2.10 Complications

Patients with BPD have a higher risk of developing pulmonary hypertension and *cor pulmonale*, which affects at least one in six extremely low birth weight infants with moderate-severe BPD, which increases the morbidity and mortality rates. Infants with BPD are at high risk of respiratory infections in the first two years of life (respiratory syncytial virus) that can endanger the life of these babies. Infants with BPD are at higher risk of poor growth and abnormal neuro- and lung- development. Chronic pulmonary morbidities are common in BPD infants. Abnormal growth occurs in 50-60% of infants with BPD. Patients with BPD have more than double risk to suffer neurodevelopmental impairment, cerebral palsy and low intelligent quotient. Other risks include severe retinopathy of prematurity, hearing impairment, severe intraventricular hemorrhage and ventriculomegaly (Ambalavanan et al., 2008; Ambalavanan et al., 2011; Bader et al., 1987; Kirpalani et al., 2006; Massie et al., 2011; O'Reilly et al., 2013).

8.2.11 Prognosis

Most neonates with BPD survive but are at high risk for long-term pulmonary and neurologic sequelae. Persistent pulmonary hypertension or right ventricular hypertrophy are associated with a poor prognosis (Ambalavanan et al., 2008; Bader et al., 1987; Blayney et al. 1991; Kirpalani et al., 2006; Laughon et al., 2011; Massie et al., 2011; O'Reilly et al., 2013; Shennan et al., 1988; Smith et al., 2005).

8.3 Hydrogen sulfide

8.3.1 Introduction to gasotransmitters

The gasotransmitter family consists of three endogenous molecules of gases or gaseous signaling molecules: nitric oxide (NO), carbon monoxide (CO) and hydrogen sulfide (H_2S). The criteria defining gasotransmitters were proposed by Rui Wang in 2003 (Wang, 2003): (i) Gasotransmitters are small molecules of gas (ii) that are freely permeable to membranes, and can have endocrine, paracrine and autocrine effects. (iii) Gasotransmitters are endogenously and enzymatically generated, and their production is regulated. Moreover, (iv) gasotransmitters have specific functions at specific physiologically relevant concentrations, and (v) their functions can be mimicked by exogenously applied counterparts. Finally, (vi) the cellular effect of gasotransmitters may or may not be mediated by second messengers but should have specific and molecular targets. The gasotransmitters NO, CO, and H_2S are different from classic neurotransmitter and humoral factors while sharing some common characteristics, as it is documented in Table 1, first described in 1981 from clinical work with NO as a molecule that transmits information between cells in various parts of the body (Gillman & Lichtigfeld, 1981, 1983).

Table 1 Comparison of the modes of action of gasotransmitters and neurotransmitters.

	Release	Re-uptake	Removal mechanism	Revert direction	Membrane receptors
Gasotransmitter	Cytoplasm release	No	Nonenzymatic: oxidation, scavenging, methilation, etc.	Bidirectional	Not necessary
Neurotransmitter	Exocytotic vesicle	Yes	Enzyme dependent	Pre-postsinaptic membrane (one direction)	Necessary

Under physiological conditions gasotransmitters are maintained at low levels, ensuring homeostasis of specific cells and organs, since the effects may not always be beneficial (gasotransmitters may cause inhibition of physiological cellular function). Nevertheless, these three gasotransmitters function in a regulatory capacity, controlling important physiologic functions including host defense against pathogens, vascular tone, apoptosis, neuromodulation, and energy metabolism (Kajimura et al., 2010).

8.3.2 Nitric oxide and carbon monoxide

The molecule NO was established as gasotransmitter in the brain and peripheral nervous system as a physiologic vasodilator, and NO is responsible of tumoricidal and bactericidal actions of macrophages. The physiologic role of NO as an endothelial derived relaxing factor is very well-known. The generation of NO is through the enzyme NO synthase (NOS), which has three different isoforms derived from different genes that convert arginine to citrulline and NO (Gadalla & Snyder, 2010). The neuronal NOS (nNOS) is localized in the brain and peripheral nervous system and in few non-neural tissues, whereas endothelial NOS (eNOS) generates NO that regulates blood vessels and inducible NOS (iNOS) is present ubiquitously throughout the body, but with highest abundance in inflammatory cells (macrophages). The nNOS and eNOS are calcium-calmodulin dependent constitutive enzymes, meanwhile iNOS is an inducible enzyme, produced in response to inflammatory stimuli, and is not dependent on calcium. The NO binds with high affinity to the heme group in the active site of soluble guanylyl cyclase (sGC), promoting the catalytic activity of the enzyme. Generation of cGMP leads to smooth muscle cell relaxation. The concentration of NO in tissues is likely to be in the 0.1 to 100 nM

range, but it has been noted of having a higher concentration up to 500 to 600 nM in arterioles (Kajimura et al., 2010).

The CO gasotransmitter is physiologically generated and can mediate neural activity in the brain and non-adrenergic non-cholinergic neurotransmission in the intestine. The CO molecule is enzymatically generated through two different isoforms of the enzyme heme oxygenase, heme oxygenase 1 (HMOX 1) and 2 (HMOX 2), with HMOX 1 being inducible, particularly activated through stressful and oxidative situations, and highly expressed in different tissues such as liver, kidney and spleen in the micromolar range. The HMOX 1 enzyme is responsible of degrading heme into biliverdin and CO (Kajimura et al., 2010; Nicholson & Calvert, 2010). In contrast, HMOX 2 is constitutively expressed and activated by calcium-calmodulin, much like nNOS and eNOS, and is mainly localized in the brain and the endothelial layer of blood vessels. The CO molecule also activates sGC but it is less potent than NO. Like eNOS and HMOX 2, CO is localized in the endothelial layer of blood vessels and behaves as an endothelial relaxing factor (Gadalla & Snyder, 2010).

8.3.3 Introduction to hydrogen sulfide

Hydrogen sulfide is an endogenous gas, considered to be the third gasotransmitter together with NO and CO, first described in 1989 as an endogenous "sulphide" in rat brain tissues and in normal human post-mortem brainstem that suggested endogenous production of H_2S in the brain (Nicholson & Calvert, 2010; Wang, 2010). In 1996 Abe and Kimura reported the role of H_2S in human neuromodulation that was the beginning of research into H_2S as a biological signaling molecule (Gu & Zhu, 2011). Nowadays, it is acknowledged that H_2S is produced endogenously in mammals in the brain, blood vessels, liver, kidneys, lung, upper and lower gastrointestinal tract, reproductive organs, synovial joints, connective tissue, cochlea and adipose tissues. The H_2S molecule is implicated in a series of physiological and pathological processes in humans (Kabil et al., 2011; Predmore et al., 2012).

8.3.4 Biochemistry of hydrogen sulfide under physiological conditions

The H_2S is small, lipid and water-soluble molecule and acts as a weak acid. The H_2S molecule can interact with receptors and can pass through biological membranes to employ its effects. At 37 ºC and pH 7.4 in aqueous solution, two thirds of H_2S dissociates into protons and HS^- and one third of H_2S does not dissociate. The H_2S molecule is presumed to exist in an ionized

form in extracellular fluids and plasma as HS^- whereas within the cell (pH about 7.2) the amounts of H_2S and HS^- are nearly equal (Nicholson & Calvert, 2010; Predmore et al., 2012).

8.3.5 Hydrogen sulfide donors

There are reagents that are able to release H_2S, which have been very useful tools to study the biological effects and drug development of H_2S. The most frequently used H_2S donor in biological experiments is NaHS. Considered a fast release donor, NaHS can release H_2S within seconds in aqueous solutions (Li et al., 2008). On the other hand, GYY4137 is a slow-release H_2S donor that mimics in a more physiological way the actions of H_2S; the GYY4137 compound was synthesized by the Moore group on the basis of the structure of Lawesson's compound, which releases H_2S in organic solvents. The rate of H_2S release from GYY4137 (1 mmol/L) is 4.17±0.5 nmol/25min in aqueous solution, and when incubated in aqueous buffer (pH 7.4, 37 ºC), the rate of H_2S release climbs for 15 min and then plateaus at 75 min. Release of H_2S from GYY4137 is pH and temperature dependent, with less release at 4 ºC and more release at pH 3.0 (Li et al., 2008). When administered intravenously or intraperitonealy, GYY4137 increases plasma H_2S at 30 min and H_2S plasma levels remain elevated over 180 min time course. In contrast, NaHS does not elevate plasma H_2S at these time points (Li et al., 2008). It has been proved that GYY4137 has vasorelaxant effects, antihypertensive and anti-inflammatory activity, showing that GYY4137 is a useful tool for studying the biological effects of H_2S (Gu & Zhu, 2011; Lee et al., 2011; Li et al., 2008).

8.3.6 Toxicology of hydrogen sulfide

The presence of H_2S in the environment is easily recognized by the peculiar smell of rotten eggs. The H_2S gas has been regarded as a toxic pollutant for decades, since small concentrations of this gas can make the perceived quality of the air as unpleasant (1-3 ppm). With increasing concentrations, in an extremely dose-effect response and duration of exposure, H_2S can cause symptoms such as irritation of the eyes and the respiratory tract (20-50 ppm), headache, loss of appetite and decline in cognitive functions (200-500 ppm). When the concentration reaches around 1000 ppm H_2S can be lethal due to saturation of the mitochondria and inhibition of cytochrome c oxidase (Gu & Zhu, 2011; Kabil et al., 2011; Mathew et al., 2011; Olson, 2011).

8.3.7 Endogenous hydrogen sulfide synthesis, regulation and catabolism

Cysteine is a semi-essential amino acid and one of the two sulfur-containing amino acids together with methionine. The source of cysteine is the diet, and partly also methionine processing. Cysteine is the major source of H_2S in mammals and H_2S is generated mainly through three different enzymes (Figure 3): cystathionine β-synthase (Cbs), cystathionine γ-lyase (Cth, also called Cse and Cgl) and 3-mercaptopyruvate sulfur transferase (Mpst) (Nicholson & Calvert, 2010; Olson, 2011; Wang, 2010). In most peripheral tissues Cth levels are much higher than the levels of Cbs, while in the brain Cbs is the most predominant form (Nagahara, 2011; Robert et al., 2003). In lower amounts, Mpst has been found in the brain, mostly in neurons, and in the vascular endothelium (Gu & Zhu, 2011; Olson, 2011; Wang, 2010). Both Cbs and Cth are localized in the cytosol whereas Mpst exist both in the mitochondria and in the cytosol (Kajimura et al., 2010; Predmore et al., 2012). The Cbs enzyme condenses homocysteine with serine to generate the thiol ether cystathionine, during the condensation the hydroxyl group of serine is replaced with the thiolate of homocysteine. The human Cbs gene is located in chromosome 21 at 21q22.3. In humans and rats Cbs exists primarily as a homotetramer with a subunit molecular mass of 63 kDa. Each subunit also binds to the cofactors pyridoxal 5-phosphate (PLP), S-adenosyl methionine (SAM) and heme. The cofactor SAM is an allosteric activator of the Cbs enzyme while heme appears to be a redox sensor. The C-terminus of Cbs contains two domains of tandem repeats that seem to inhibit the enzymatic function, as the deletion of these domains activates Cbs. The Cbs enzyme can be sumoylated, inhibiting the catalytic activity of Cbs. The Cth enzyme can also form H_2S from cysteine, it hydrolyzes cystathionine into cysteine with ammonia and α-ketobutyrate as byproducts. The Cth enzyme converts cysteine to thiocysteine, pyruvate and ammonia, in a β-disulfide elimination reaction, with the thiocysteine then reacting with cysteine or other thiols to produce H_2S and cysteine or the corresponding disulfide. The Cth enzyme is also dependent on PLP, and it is selectively activated by calcium-calmodulin similar to the activation of eNOS, nNOS and HMOX 2 (Gadalla & Snyder, 2010). The Mpst enzyme catalyzes only sulfur transferases reactions from 3-mercaptopyruvate to various donors, and needs cysteine aminotransferase and further redox reactions with biological thiols such as glutathione to yield H_2S (Gu & Zhu, 2011; Predmore et al., 2012; Wang, 2010).

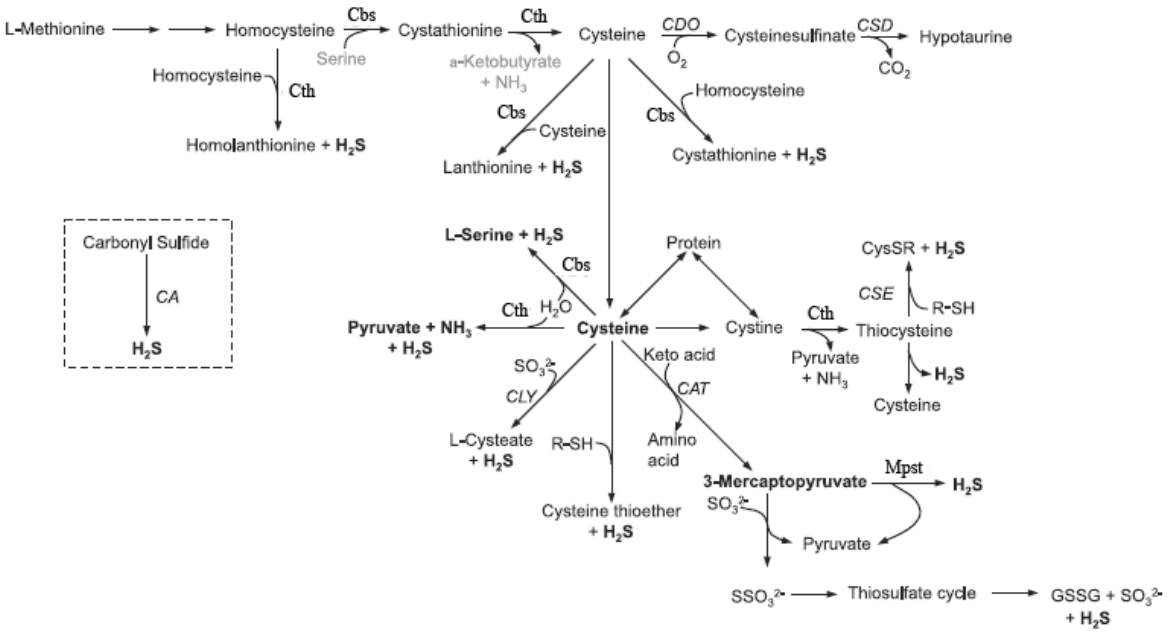

Figure 3 Potential pathways of H_2S production and metabolism.
Transsulfuration reactions that involve cystathionine β-synthase (Cbs), cystathionine γ-lyase (Cth) and 3-mercaptopyruvate sulfur transferase (Mpst) in the production and metabolism of H_2S. CDO, cysteine dioxygenase; CAT, cysteine aminotransferase; CLY, cysteine lyase; CSD, cysteine sulfinate decarboxylase CA, carbonic anhydrase; R-SH, thiol; GSSG, glutathione oxidized form. (Olson, 2011).

The catabolic pathways of H_2S are not fully understood, one catabolic pathway of H_2S is oxidation in the mitochondria and excretion in the urine, sulfate being the major end product of H_2S catabolism. Another catabolism pathway is the thiol S-methyltransferase mediated methylation of H_2S to yield monomethylsulfide and dimethylsulfide. A third pathway involves binding of H_2S to methemoglobin to yield sulfhemoglobin. It has also been reported that H_2S can diffuse across the alveolar membrane (Kajimura et al., 2010).

8.3.8 *Cbs*$^{-/-}$ and *Cth*$^{-/-}$ mice

The *Cbs*$^{-/-}$ mice were generated through insertion of a neomycin selection cassette that replaced a genomic fragment containing exons 3 and 4 of the Cbs gene (Watanabe et al., 1995). The *Cbs*$^{-/-}$ mice have a manifest phenotype and are broadly used as a mental retardation model, as a model for hyperhomocysteinemia and as a thromboembolism model. The *Cbs*$^{-/-}$ mice display several pathophysiologic features similar to hyperhomocysteinemic patients, including endothelial dysfunction and hepatic steatosis. The mice usually die during the weaning period between the 2-4 weeks of age, probably due to severe hepatic dysfunction and require sufficient

supplementation of cysteine for survival. The *Cbs*$^{-/-}$ mice have a severe retardation in body mass that might be caused by taurine deficiency and an abnormal lipid metabolism. The *Cbs*$^{-/-}$ mice also have cerebellar malformation and impaired learning ability. The adult *Cbs*$^{-/-}$ mice display lung fibrosis and airspace enlargement in the absence of increased inflammatory cell infiltrates (Akahoshi et al., 2008; Hamelet et al., 2007; Namekata et al., 2004). The *Cth*$^{-/-}$ mutant mice were generated thorough exons 1 to 6 being replaced with a LacZ and neomycin selection cassette (Ishii et al., 2004). The *Cth*$^{-/-}$ mice have a milder phenotype compared to the *Cbs*$^{-/-}$ mice, the *Cth*$^{-/-}$ mice have a slight retard in growth, but homozygotes can reach adulthood and breed. The *Cth*$^{-/-}$ mice are normally used as a cystathionemia/cystathionuria model. The *Cth*$^{-/-}$ mice develop hypertension and have an impaired endothelium derived vasorelaxation capacity, are very sensitive to oxidative stress, and have lower taurine levels. When fed with low cysteine in diet, the *Cth*$^{-/-}$ mice exhibit acute skeletal muscle atrophy (Ishii et al., 2010; Ishii et al., 2004; Wang et al., 2013).

8.3.9 Endogenous levels of hydrogen sulfide in health and disease

A role for H_2S in health and disease is supported by the correlations found between the plasma/tissue levels of H_2S/sulfane sulfur or H_2S generating enzymes and the progression of diseases such as insulin resistance, hypertension, hyperhomocysteinemia, diabetes, exacerbated cardiac injury following ischemia-reperfusion injury, cirrhosis, Alzheimer-disease, progression of adiposity, chronic kidney disease, gastrointestinal tract irritation, asthma and cancer among others (Gu & Zhu, 2011; Predmore et al., 2012). Like in the case of NO and CO, measuring the concentrations of a gas with a short half-life that can form complex with other molecules in biological samples, is still very challenging. Conventional methods for the determination of H_2S fall into two categories: measuring “free” H_2S or “labile” H_2S. An example of the first would be a polarographic sensor, and examples of the second would be colorimetric assays, gas-chromatography-mass spectrometry and high-performance liquid chromatography. Reported values of labile H_2S in plasma and blood range between 20 and 30 µM, in contrast to polarographic sensors with detection limit near 10 nM. In tissues from rat brain the values of free H_2S varied from 14 nM to 70 µM (Kajimura et al., 2010).

8.3.10 Mechanism of action of hydrogen sulfide

The molecular targets of H_2S include enzymes, proteins, transcription factors and membrane ion channels (Predmore et al., 2012).

8.3.10.1 Sulfhydration of proteins

The H_2S molecule can sulfhydrate different proteins, and sulfhydration can alter protein function suggesting sulfhydration as an important physiologic signaling pathway. An example would be that H_2S can sulfhydrate nuclear factor κ-light-chain-enhancer of activated B cells (NFκB) and cause anti-apoptosis actions (Predmore et al., 2012).

8.3.10.2 Interaction with potassium channels

The H_2S molecule can stimulate ATP potassium (K_{ATP}) channels. The K_{ATP} channels contain nine cysteines with C43 that lies close to the surface, which is selectively influenced by oxidative insults. The mechanism of action of how H_2S interacts with K_{ATP} channels is not completely understood, but it has been reported that H_2S can interact with the sulfonylurea receptor subunit of the K_{ATP} channel with selective cysteine residues located at the extracellular loop of the receptor subunit. The activation of K_{ATP} channels has been described as the molecular basis of H_2S-elicited cardiac protection, blood pressure lowering, or insulin release inhibition (Wang, 2010).

8.3.10.3 Vasorelaxation

The H_2S molecule can relax blood vessels, H_2S resembles the principal properties of endothelial derived relaxing factor, and it is localized in the endothelial layer of blood vessels. The H_2S vasorelaxation, reflects hyperpolarization mediated by the opening of K_{ATP} channels via the sulfhydration at C43. Unlike NO and CO, H_2S does not activate guanylate cyclase (Gu & Zhu, 2011).

8.3.10.4 Oxygen sensitive responses

The vessel wall produces H_2S, and it has been proposed that H_2S is an O_2 sensor in both vascular and non-vascular smooth muscle as well as a putative chemoreceptor (Olson et al., 2010). Catabolism of H_2S is mainly through oxidation in the mitochondria; since oxidation depends mainly on O_2 availability, depending on the concentration of O_2 it will affect the total amount of biologically active H_2S. In agreement with this theory, high O_2 concentration correlates with low H_2S activity and a dilated pulmonary artery. Inversely, low O_2 concentrations correlate with higher H_2S activity and artery contraction. Indeed, H_2S has been found to have both vasodilatory and vasoconstrictive effects depending on its concentration. It has also been reported that O_2 can modulate the activity of both Cbs and Cth, which may have an additive impact on the H_2S mediated vascular response (Kajimura et al., 2010; Olson, 2011; Wang, 2010).

8.3.10.5 Anti-inflammatory effects

The H_2S molecule is thought to have anti-inflammatory effects through action on K_{ATP} channels, inhibition of activation of NFκB and p38 MAPK, scavenging of oxidants, up regulation of intracellular cAMP, and inhibition of caspase-3 cleavage. Considered a powerful inhibitor of leukocyte adherence to the vascular endothelium, H_2S may obstruct inflammatory processes by diminishing the tissue injury induced by neutrophils via induction of apoptosis and/or scavenging of neutrophils derived hypochlorous acid. Reactive oxygen species are mediators of NFκB activation and this process can be blocked by antioxidants such as GSH and cysteine. It has been described that H_2S can down-regulate several pro inflammatory cytokines including: NFκβ, TNFα, IL-1β, IL-6 and IL-8 (Chen et al., 2009; Predmore et al., 2012; Wallace et al., 2012; Zhang et al., 2013) and that it can activate anti-inflammatory chemokines such as IL-10 (Wang, 2010). Promotion of tissue repair by H_2S is likely due to its vasodilatory properties and activation of cyclooxygenase 2 expression and through promotion of angiogenesis. Another property of H_2S is that can also act as an energy source substituting for oxygen mitochondrial respiration, which may contribute significantly to protection and repair of tissue injury (Wallace et al., 2012). Other data support that H_2S can also be pro-inflammatory, mostly at high concentrations, promoting formation of pro-inflammatory cytokines and chemokines by up-regulation of NFκB of activated B cells or by activating the metabolism of substance P (Gadalla & Snyder, 2010; Wallace et al., 2012; Wang, 2010).

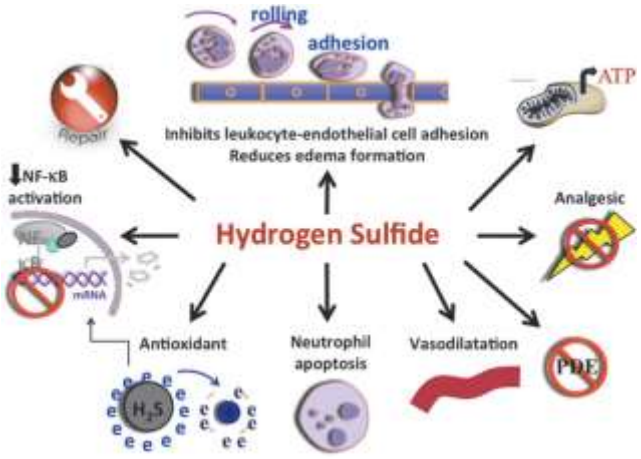

Figure 4 Anti-inflammatory effects of hydrogen sulfide.

Illustration of several mechanism of action involved in the anti-inflammatory effects of hydrogen sulfide that include inhibition of leukocyte-endothelial cell adhesion, vasodilation, neutrophil apoptosis, antioxidant, reduction of NFκB, inhibition of PDE, nociception, repair, and modulation of K_{ATP} channels (Wallace et al., 2012).

8.3.10.6 Cytoprotective effects

H_2S can strongly influence the redox status through different mechanisms, such as increasing GSH levels in the cytosol, the mitochondria, and nucleus of the cell, by increasing the GSH/GSSG ratio, activating the protective heat-shock proteins, activating the nuclear factor (erythroid-derived2)-like 2 (Nrf2) that results in activation of the antioxidant response elements of several antioxidant genes. By activating K_{ATP} channels, H_2S can also have an anti-apoptotic, anti-inflammatory and blood-pressure lowering effects. The cytoprotective effects of H_2S also involves activation of signaling pathways such as Akt pathways (Kimura et al., 2012; Predmore et al., 2012).

8.3.10.7 Antioxidant effects

The H_2S molecule is capable of quenching free radicals, since HS^- anions have reducing chemical properties. The oxidation of HS^- by biochemical relevant two-electron oxidants, yields hydrogen disulfide which also has oxidizing activity and is capable of regenerating H_2S. However, since the concentration of H_2S and HS^- is very low in blood and tissues, the anti-oxidative capacity against free radicals is quite limited (Predmore et al., 2012).

A major antioxidant protein in the human body is GSH, and the action of H_2S influencing the generation of GSH is often described in the literature: (i) H_2S enhances the cellular glutamate uptake, (ii) H_2S- induced increase in the level of gamma-glutamylcysteine synthethase and cysteine transporter activity in the cell, (iii) reduction of cystine into cysteine by H_2S in the extracellular space, and transport of cysteine into cells by the cysteine transporter, (iv) H_2S stimulation of the nuclear transcription factor Nrf2, which then up regulates GSH synthesis and transport, and (v) a decrease in the activity of the enzymes that catabolize GSH (Predmore et al., 2012; Wang, 2010).

8.3.11 Interaction with other gasotransmitters

There are many similarities between the three gases NO CO and H_2S, at physiological concentrations the three of them act as vasodilators, as cytoprotective and anti-inflammatory molecules. When it concerns cross talk between NO and H_2S, it has been demonstrated that H_2S can relax SMCs through release of endothelium-derived hyperpolarizing factor and NO from the endothelium. H_2S can react with NO to form a nitrosothiol and reducing the availability of NO to cause SMCs contraction, and through inhibition of eNOS as well as reduction in SMCs cAMP concentration (Kajimura et al., 2010; Li et al., 2009). Moreover, the group heme binds to the N-terminal portion of Cbs, comprising about 70 amino acids. In its ferrous state, this heme binds both CO and NO. The group heme has more affinity to CO than to Cbs, therefore CO can inhibit Cbs activity. The powerful influence of CO upon Cbs raises the possibility of cross talk between CO and H_2S as messenger molecules (Gadalla & Snyder, 2010).

8.3.12 Effects of hydrogen sulfide in the nervous system

In the brain H_2S is produced mainly in the astrocytes. H_2S may have a neuro-protectant role, since the first recognized sign of Cbs deficiency in humans is mental retardation and Alzheimer's disease (Enokido et al., 2005; Olson, 2011; Robert et al., 2003). It is suggested that Cbs plays a crucial role in the development and maintenance of the central nervous system (Kimura et al., 2012; Robert et al., 2003). Cbs-deficient patients also suffer other symptoms such as seizures, abnormal electroencephalogram, extrapyramidal disturbances and psychiatric disorders (Gadalla & Snyder, 2010). In the nervous system H_2S has been shown to have

protective effects, preventing the activation of neurotoxins, neuron degeneration, neuron apoptosis and gliosis in mice (Predmore et al., 2012).

8.3.13 Role of hydrogen sulfide in different lung diseases

The three H_2S-generating enzymes are variably expressed in the lung depending on the species: Cth and Mpst are widely expressed in bovine pulmonary arterial smooth muscle cells, while Cbs has only been found in bovine pulmonary arterial endothelial cells. In humans, both airway SMCs and primary fibroblast express Cth and Cbs. In contrast, in mice, both Cth and Cbs were found in pulmonary blood vessel SMCs and endothelial cells as well as in airway SMCs (Olson et al., 2010; Wang et al., 2011). The role of H_2S in different chronic lung disease has been recently reviewed by Chen et al. (Chen & Wang, 2012) and it is summarized in Figure 5. In chronic obstructive pulmonary disease (COPD), H_2S has proven to be an anti-inflammatory and bronchi dilatant agent, decreasing the expression of TNFα and IL-8 lung tissue of chronic cigarette smoke exposed rats treated with NaHS in comparison to control rats. Similar results were found by another group, using a tobacco smoke induced emphysema mouse model, where NaHS treatment ameliorated inflammation measured in bronchoalveolar lavage (BAL), reduced the increase in right ventricle systolic pressure, the thickness of pulmonary vascular walls and right ventricular hypertrophy. The serum levels of H_2S COPD patients varied depending on stage and tobacco exposure and further studies are needed to use it as a marker (Chen et al., 2005). In the case of asthma, lower levels of H_2S were found in asthmatic patients, related negatively to sputum counts and positively to forced expiratory volume capacities. In an experiment with ovalbumin treated rats, exogenous administration of NaHS increased peak expiratory flow, decreased goblet cell hyperplasia and collagen deposition score, decreased total cells in BAL and influx of eosinophils and neutrophils (Benetti et al., 2013; Chen & Wang, 2012; Chen et al., 2009). Moreover, the *Cth*$^{-/-}$ mice when challenged with ovalbumin, had worsen airway inflammation and elevated cytokines such as IL-5 and IL-13 in BAL when compared to wild type littermates, and interestingly, recovery treatment with NaHS supplement rescued the *Cth*$^{-/-}$ mice from the aggravated pathological picture (Zhang et al., 2013). In pulmonary fibrosis, NaHS has been reported to decrease pulmonary fibrosis caused by bleomycin, decreasing lung hydroxyproline content and malondialdehyde. The authors speculated about an anti-oxidative effect of NaHS against lipid peroxidation produced by ROS. Treatment with NaHS has been proven to arrest cultured human fibroblasts in the G1 phase of the cell cycle, and trigger them into apoptosis. Furthermore, treatment with H_2S decreased

pSmad2/3 phosphorylation in A549 cultured cells stimulated with TGF-β1, and prevented epithelial to mesenchymal transition (Chen & Wang, 2012; Fang et al., 2009). Finally, H_2S has demonstrated a regenerative effect in two different models of acute lung injury, in a mouse model of lipopolysaccharide-induced lung injury, it improved lung structure in histological examination and prevented cytokine release in BAL fluid, clarified in Figure 6 (Faller et al., 2012). In a mechanical ventilation rat model, NaHS treatment improved inflammation and oxygenation in comparison to the control group (Aslami et al., 2010).

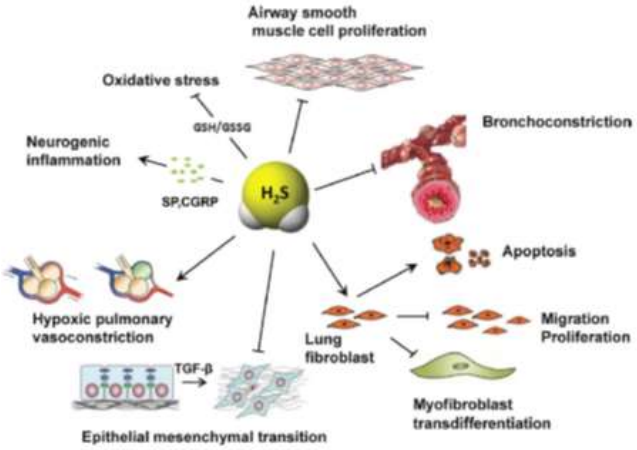

Figure 5 Mechanism of action of H_2S in chronic lung diseases.

Several mechanism of action of H_2S: Inhibition of airway smooth muscle cell proliferation, inhibition of bronchoconstriction, modulation of lung fibroblast differentiation, inhibition of epithelial to mesenchymal transition, modulation of hypoxic pulmonary vasoconstriction, neurogenic inflammation and inhibition of oxidative stress. Glutathione reduced form (GSH), glutathione oxidized form (GSSG), substance P (SP), calcitonin gene-related peptide (CGRP), transforming growth factor beta (TGF-β) (Chen & Wang, 2012).

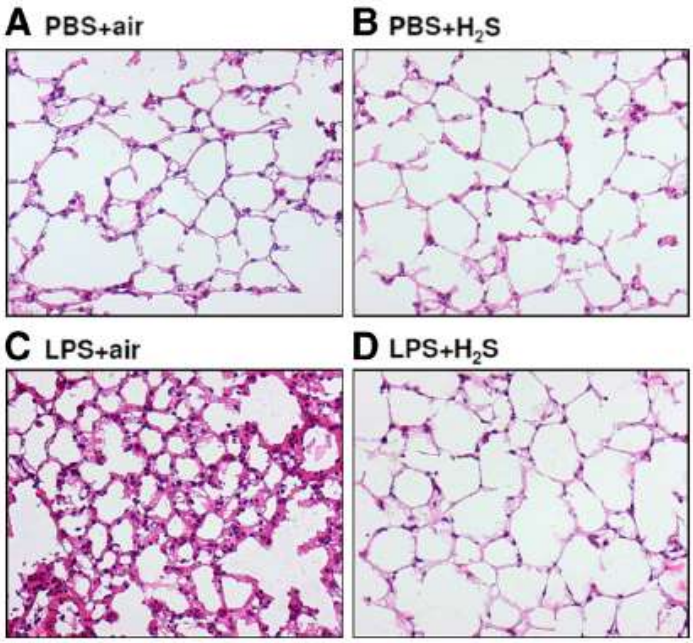

Figure 6 Effect of lipopolysaccharide induced acute lung injury and effect of H_2S inhalation on lung structure.

Control mice treated with phosphate buffer saline intranasal and room air (A), 80 ppm hydrogen sulfide (H_2S) for 6 h (B), lipopolysaccharide (LPS) treated mice and room air (C) and LPS and 80 ppm H_2S treated mice for 6 h (D). Sections stained with hematoxylin and eosin (Faller et al., 2012).

9 Hypothesis and aims

Bronchopulmonary dysplasia is a dangerous complication of the premature newborn. There is a lot of effort in the scientific community to unravel the disease mechanisms and identify therapies that could improve lung growth from these infants. It is thought that anti-inflammatory, cytoprotective, antioxidant and vascular protective approaches, which are meant to be properties of H_2S, could be beneficial treating BPD.

In this context, it was also observed that the expression levels of the H_2S generating enzymes Cbs and Cth, changed over the course of normal mouse late lung development.

Thus it was hypothesized that:
In the BPD model H_2S can be used as a potential treatment, due to cytoprotective, anti-inflammatory, antioxidant and pulmonary vasodilatory properties and that Cbs and Cth play a role in normal late lung development.

Hence, the aims of the study were:
(a) Using a hyperoxia BPD mouse model to expose the animals either to vehicle or to a H_2S donor, and study the effect of the treatment on lung structure during normal and aberrant late lung development.
(b) In the case of improved in alveolarization in (a), to study the possible mechanisms of action that would impact lung development.
(c) To study the role of Cbs and Cth during mouse late lung development.

10 Materials and methods

10.1 Equipment and software

Equipment and software	Manufacturer
Adobe Photoshop Software	Adobe Systems, USA
Autoclave	Systec, Germany
BD FACS Canto™ flow cytometer	BD Biosciences, USA
Cell culture incubator HERAcell 150i	Thermo Scientific, USA
Cell culture plates (6-, 24-, 96- well plates)	Greiner Bio-One, Germany
Cell culture flasks (75 ml)	Greiner Bio-One, Germany
Cell counter, Countess®	Invitrogen, UK
Corning® Costar® cell culture plates	Sigma-Aldrich, Germany
Culture-insert µ-dish©	Ibidi® cells in focus, USA
Electrophoresis chambers	Bio-Rad, USA
FACSDiva™ software	BD Biosciences, USA
Filter Tip FT: 10, 20, 100, 200, 1000	Greiner Bio-One, Germany
Freezer -20 °C	Bosch, Germany
Freezer -40 °C	Kryotec, Germany
Freezer -80 °C	Heraeus, Germany
Fridge +4 °C	Bosch, Germany
Gel blotting paper 70 x 100 mm	Bioscience, Germany
Hood with laminar flow	Thermo Scientific, USA
Image J Software	NIH, USA
Image Quant™ LAS4000	GE Healthcare, UK
Microscope (light, phase contrast, fluorescent, Laser-capture micro dissection, confocal)	Leica, Germany
Microtome (paraffin-, plastic-, cryo- sections)	Leica, Germany
Mini spin centrifuge	Eppendorf, Germany
Multifuge centrifuge, 3 s-R	Heraeus, Germany
NanoDrop® ND 1000	Peqlab, Germany
NanoZoomer-XR C12000 Digital slide scanner	Hamamatsu, Japan
PCR-thermo cycler: peqSTAR	Peqlab, Germany
PCR-tubes (0.2 ml)	Applied Biosystems, USA

Petri dishes	Eppendorf, Germany
Pipetboy	Eppendorf, Germany
Pipetmans: P10, P20, P100, P200, P1000	Gilson, France
Precellys® 24 Homogenizer	Peqlab, Germany
QWin software	Leica, Germany
Single-use syringe	Braun, Germany
Reaction tubes: 0.5, 1.5, 2 ml	Eppendorf, Germany
Stepanizer© stereology software	Tschanz, Switzerland
StepOnePlus™ Real-Time PCR	Applied Biosystem, Germany
Test tubes: 15, 50 ml	BD Biosciences, USA
Trans blot transfer membrane (0.2 µm)	Bio-Rad, USA
Visiopharm NewCast™ computer-assisted stereology system (VIS 4.5.3)	Visiopharm, Denmark
VersaMax Micro plate reader	Molecular Devices, Germany
Vortex machine	Eppendorf, Germany
Vacuum centrifuge	Eppendorf, Germany
Western blot chambers, Mini Trans-Blot	Bio-Rad, USA
Western blot chambers, Mini-Protean 3 Cell	Bio-Rad, USA
WIMASIS Software WimTube	Wimasis GmbH, Deutschland

10.2 Reagents

Reagents	Manufacturer
Acetone	Roth, Germany
Acrylamide solution, Rotiphorese Gel 30	Roth, Germany
Agar-agar	Merck, Germany
Agarose	Invitrogen, UK
Accutase	Invitrogen, UK
AlexaFluor® 488 Annexin V/Dead Cell Apoptosis Kit	Invitrogen, UK
BD BioCoat™ BD Matrigel™ plate	Becton Dickinson, USA
Bioxytech© GSH/GSSG kit	OxisResearch, USA
Bovine serum albumin	Sigma-Aldrich, Germany
Bromophenol blue	Sigma-Aldrich, Germany

Ceramic beads	PeqLab, Germany
Complete™ Protease inhibitor	Roche, Germany
Diaminobenzidine	Vector Laboratories, USA
DNA Ladder (1 kb, 100 bp)	Promega, USA
DNase I	Serva, Germany
DTT	Promega, USA
Dulbecco's modified Eagle's medium (DMEM)	Gibco BRL, Germany
Dulbecco´s phosphate buffered saline 10×	PAA Laboratories, Austria
Dulbecco´s phosphate buffered saline 1×	PAA Laboratories, Austria
Ethylendinitrilo-N, N, N′,N′tetra-acetic-acid (EDTA)	Promega, USA
Ethanol absolute	Riedel-de Haen, Germany
ECL Plus Western Blotting Detection System Amersham	Bioscience, UK
ELISA kit (TNFα, IL-10)	BD Biosciences, USA
ELISA kit (IL-6, I-1β)	Qiagen, Germany
Fetal bovine serum	Gibco BRL, Germany
Ethidium bromide	Roth, Germany
Fe-Hematoxylin Weigert	Waldeck, Germany
Fuchsin-Resorcin	Waldeck, Germany
Giemsa solution	Merck, Germany
Glibenclamide	Tocris Bioscience, UK
Glutaraldehyde	Sigma-Aldrich, Germany
Glycine	Roth, Germany
GoTaq® DNA polymerase	Promega, USA
GYY4137	Enzo, USA
Hanks' balanced salt solution (HBSS)	Euro lone, Italy
HEPES buffer	Sigma-Aldrich, Germany
Hydrogen peroxide	Sigma, Germany
iScript™ cDNA Synthesis Kit	BioRad, USA
ImmPRESS kit	Vector Laboratories, USA
Lipofectamine™ 2000	Invitrogen, UK
May-Grünwald solution	Merck, Germany
β-mercaptoethanol	Sigma-Aldrich, Germany
Meta-phosphoric acid	Sigma-Aldrich, Germany
Methanol	Fluka, Germany

Methyl green	Sigma, Germany
MES buffer	OxisResearch, USA
MM HRP polymer	Zytomed Systems, Germany
MuLV reverse transcriptase	Applied Biosystems, Germany
NaHS	Sigma-Aldrich, Germany
Nuclease free water	Ambion, USA
Oligo(dT) primer	Promega, USA
Opti-MEM® Medium	Gibco BRL, Germany
Osmium tetroxide	Carl Roth, Germany
Penicillin/streptomycin	GE Healthcare, UK
PCR Nucleotide Mix	Promega, USA
PfuUltra™ High-Fidelity DNA polymerase	Thermo Scientific, Germany
Platinum® SYBR® Green qPCR SuperMix UDG Kit	Invitrogen, UK
Propidium iodide	Invitrogen, UK
Proteinase K	Promega, USA
2-Propanol	Merck, Germany
Quick Start™ Bradford Dye Reagent	Bio-Rad, USA
Paraformaldehyde	Sigma-Aldrich, Germany
PeqGold total RNA kit	Peqlab, Germany
Pertex mounting media	Leica, Germany
RNAase Inhibitor	Applied Biosystems, USA
RNeasy Midi Kit	Qiagen, Germany
Rodent block M	Zytomed Systems, Germany
Roti®-Histol	Roth, Germany
Scott's tap water substitute	Leica, Germany
SDS 10% solution	Promega, USA
Sodium cacodylate	Serva, Germany
Sodium vanadate	Sigma-Aldrich, Germany
Staurosporine	Sigma-Aldrich, Germany
SuperSignal® West Pico Chemi luminescent Substrate	Thermo Scientific, USA
Technovit 7100	Heareus Kulzer, Germany
Tissue Tek®	Sakura, Japan
Triethanolamine	Sigma-Aldrich, Germany
Tris	Roth, Germany

Trypsin	Invitrogen, UK
Tween® 20	Sigma-Aldrich, Germany
Uranyl acetate	Serva, Germany
Van Gieson stain	Applichem, Germany
Vector Vip substrate kit	Vector laboratories, USA
Xylol	Roth, Germany

10.3 Cell lines

MLE-12; CRL-2110	ATCC, USA
HPAEC; CC-2530	Invitrogen, USA

10.4 Primer list

Table 2 Primers for RT-PCR analysis

Gene	Sequence (5´→3´)
Cth m.m. Forward primer	GGGATGGCGGTGGCTCGTTT
Cth m.m. Reverse primer	AGCCCGAGCACTGGCGTTTG
Cbs m.m. Forward primer	TGAACCAGACGGAGCAAACA
Cbs m.m. Reverse primer	CCAGGACTGTCGGGATGAAG
Polymerase r 2a m.m. Forward primer	CTAAGGGGCAGCCAAAGAAAC
Polymerase r 2a m.m. Reverse primer	CCATTCAGCATACAACTCTAGGC

m.m. = *Mus musculus*.

Table 3 Primers for genotyping

Gene	Sequence (5´→3´)
Cbs m.m. Forward primer common	GATTGCTTGCCTCCCTACTG
Cbs m.m. Reverse primer wild type	AGCCAACTTAGCCCTTACCC
Cbs m.m. Reverse primer mutant	CGTGCAATCCATCTTGTTCA
Cth m.m. Forward primer common	TGCCGACCAATAAGCAGGGC
Cth m.m. Reverse primer wild type	CCGAGGACTGGCCCGGGAAGT
Cth m.m. Reverse primer mutant	CCAGACCGGCAACGAAAATCA

m.m. = *Mus musculus.*

10.5 Antibodies

Table 4 Antibodies

Name	Catalogue number	Dilution	Manufacturer
α–smooth muscle actin	A-2547	1:900	Sigma-Aldrich, Germany
α–smooth muscle actin-Cy3	C6198	1:400	Sigma-Aldrich, Germany
Akt pan 11E7	4685	1:1000	Cell Signaling, USA
βactin	4970	1:3000	Cell Signaling, USA
CBS	LS-C154538	1:1000; 1:10 (IF)	LS Bioscience, USA
CD 31	Ab28364	1:500	Abcam, UK
CTH	HPA023300	1:600; 1:100 (IF)	Sigma-Aldrich, Germany
DAB	SK4100	1:100	Vector Laboratories, USA
DAPI	D21400	1:100	Invitrogen, USA
FITC-conjugated mouse IgG1, isotype control	551954	1:1000	BD Biosciences, USA
Goat anti-mouse IgM	31440	1:3000	Thermo Scientific, USA
Goat anti-mouse IgG (H+L) Alexa Fluor® 568	A-11031	1:1000	Life Technologies, Germany
Goat anti-rabbit IgG	31460	1:3000	Thermo Scientific, USA
Goat anti-rabbit IgG (H+L) Alexa Fluor® 488	A-11034	1:1000	Life Technologies, Germany
IgG anti mouse Alexa Fluor A568	A-11031	1:1000	Molecular probes, USA
IgG anti rabbit Alexa Fluor A448	A-11034	1:1000	Molecular probes, USA
IgG_1 PETexas Red® conjugate	MG117	1:1000	Invitrogen, USA
Mouse IgG isotype control	10400C	1:400	Invitrogen, USA
Anti-rabbit IgG-HRPO	MP-7401	1:100	Immpress Vector Laboratories, USA
Anti-mouse IgG-HRPO	MM620	1:900	Biocare Medical USA
Propidium iodide	V13241	1:1000	Sigma-Aldrich, Germany
phospho-Akt Ser473	4060	1:500	Cell Signaling, USA
Rabbit IgG isotype control	2729	1:100, 1:10	Cell signaling, USA
von Willebrand factor	A0082	1:900 (IHC); 1:100 (IF)	Dako, Germany

IHC=Immunohistochemistry; IF=Immunofluorescence.

10.6 siRNA

For the assessment of the role of Cbs and Cth in angiogenesis *in vitro*, HPAEC cells were transfected with a mixture of opti-mem (Opti-MEM® Medium, Gibco BRL, Germany), lipofectamine (LipofectamineTM 2000, Invitrogen, UK) and either with scrambled (200 nM; Santa Cruz Technology, USA, sc-37007) or siRNA CBS (200 nM; Santa Cruz Technology, USA, sc-60335) and cultured during 6 h in a humidified 5% (vol/vol) CO_2 atmosphere. After that, the transfection media was changed to DMEM media supplemented with LVES 2% (vol/vol), and cells were cultured during 48 h prior to detachment with Accutase and counted and re-seeded for the endothelial tube-formation assay.

Several attempts with different CTH siRNA (Santa Cruz Technology, USA) were tested but not successful. Instead, the CTH inhibitor propargylglycine (PAG) was used (1 mM or 3 mM during 24 h).

10.7 Mouse model of bronchopulmonary dysplasia

Exposure to normobaric hyperoxia (85% O_2) induced an arrest in alveolarization to mouse pups, as described previously (Alejandre-Alcazar et al., 2008). This model has formerly been characterized in our research group (Alejandre-Alcazar et al., 2008) and other groups (Buczynski et al., 2013; Fernandez-Gonzalez et al., 2012), where a pronounced arrest of lung development is seen in response to hyperoxia exposure. Both groups, the normoxia (21% O_2) and the hyperoxia (85% O_2) group, were further divided into two groups, treated with daily intraperitoneal (i.p.) injections of either water (used as vehicle control) or with GYY4137 a slow-release H_2S donor (Li et al., 2008), at a dose of 50 mg/kg dissolved in water, for nine days. To minimize oxygen toxicity and to prevent potential cofounders of milk production caused by changes in inspired oxygen levels, nursing dams were rotated every 24 h between normoxia and hyperoxia conditions. Dams and mouse pups received food *ad libitum* and were kept on 12 h light-dark cycle. Mouse pups were sacrificed on the tenth day of life, by euthanasia with an overdose of isofluorane, followed by thoracotomy and lung extraction. All animal experiments and procedures were approved by the local authorities, the Regierungspräsidium Darmstadt (approval B2/327).

10.8 Lung processing

Isolation of lungs was processed differently depending on the posterior analysis. The lungs from transgenic and wild-type mice were harvested on different postnatal days depending on the experiment. Lungs were embedded in glycol methacrylate for stereological analysis; lungs were embedded in paraffin for immunohistochemistry and immunofluorescence analysis, lungs were cryopreserved for laser-capture micro dissection analysis, and lungs were frozen in liquid nitrogen and stored in -80 ºC for RNA and protein isolation analysis.

10.9 Design-based stereology

The methods used in this study were based on newly published American Thoracic Society/European Respiratory Society recommendations for quantitative evaluation of lung structure (Hsia et al., 2010). Mouse pup lungs were instillation-fixed via a tracheal cannula at a hydrostatic pressure of 20 cm H_2O with 1.5% (wt/vol) glutaraldehyde, 1.5% (wt/vol) paraformaldehyde, in 150 mM HEPES pH7.4, at 4°C for 24 h as defined previously (Knudsen et al., 2007). Lung tissue blocks were collected via systematic uniform random (SUR) sampling for stereological analysis (Ochs, 2006; Weibel et al., 2007). Whole lungs were embedded in agar and cut into pieces of 2 mm thickness. Using the Stepanizer© stereology software (Tschanz et al., 2011), the total volume of the lungs was measured by Cavalieri's principle. Because the neonatal lungs are very small in size, whole lungs were treated with 0.1 M sodium cacodylate, 1% (wt/vol) osmium tetroxide and 4.5% (wt/vol) uranyl acetate, and embedded in glycol methacrylate. Each tissue block was cut into sections of 2 μm, and every first and third section of a consecutive series of sections was stained with Richardson's stain. The NanoZoomerXR C12000 Digital slide scanner was used to scan all slides. The SUR sampling was continued throughout all steps of microscopic analysis, as described previously for adult lungs (Fehrenbach et al., 2008; Knudsen et al., 2013; Muhlfeld & Ochs, 2013; Ochs & Muhlfeld, 2013; Schneider & Ochs, 2013; Voswinckel et al., 2004). The Visiopharm NewCast™ computer-assisted stereology system was employed to do all investigations. Structural analyses included the determination of alveolar number, surface area, total alveolar septal volume, mean linear intercept (MLI), and mean alveolar septal wall thickness. The number of alveoli was counted using a physical disector (disector height 4 μm). Surface densities and alveolar septal volumes were determined by intersection and point counting, respectively, and were multiplied

by the reference volume (total lung volume) to get absolute values. The microtome was calibrated prior to use. An example of the tools used for the stereological analysis is illustrated in Fig. 7. The stereological analysis was applied to the first experiment, where two control groups of mice, which received daily injections (i.p.) of vehicle alone (water) from the first day of life (P1), until the tenth day of life (P10), that were exposed either to 21% O_2, or to 85% O_2. Moreover, two experimental groups were also evaluated, which received daily injections (i.p.) of the slow-release H_2S donor molecule GYY4137 (50 mg/kg body mass, in H_2O), from the first day of life (P1), until the tenth day of life (P10), that were exposed either to 21% O_2, or to 85% O_2. The same type of analysis was also applied to the second experiment to study the course of normal late lung development on two different time points: On P7.5 and P14.5, either wild type mice, *Cbs*$^{-/-}$ or *Cth*$^{-/-}$ mice. The coefficient of error (CE), the coefficient of variation (CV) and the squared ratio between both (CE^2/CV^2) were measured for each stereological parameter to be <0.5 to validate the precision of the measurements.

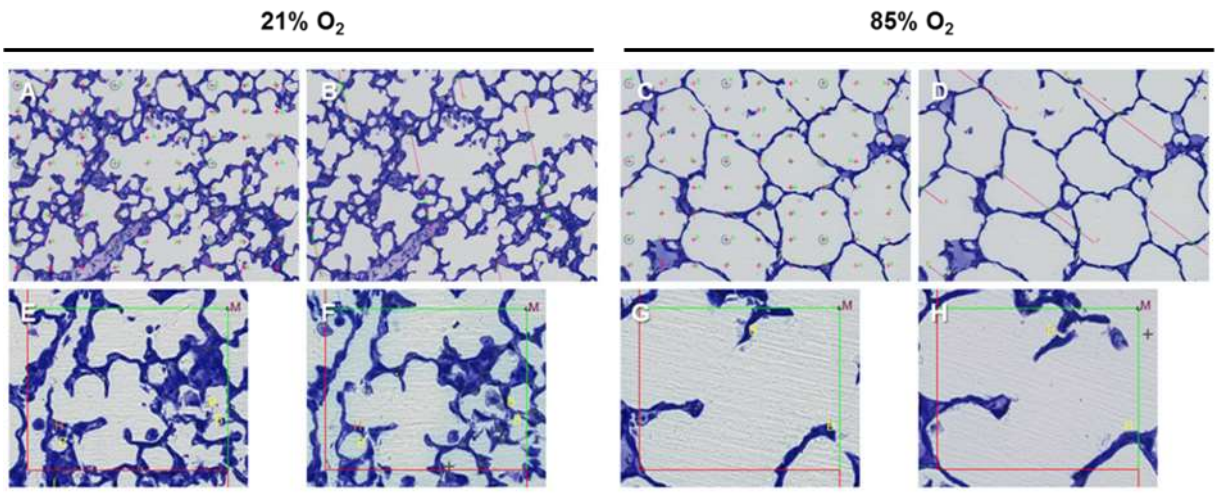

Figure 7 Example of stereological analysis of neonatal mouse lungs exposed to either 21% O_2 or 85% O_2 pressure, fixed via the airways, and stained with Richardson's stain.

A, point grid superimposed randomly into a field of view of a virtual Nanozoomer-scanned lung tissue section from a mouse pup at P10 exposed to 21% O_2 for the first 10 days of life (20× magnification). The counted points need to fall on the reference space (i.e. parenchyma) to be counted, and were subdivided into different categories, namely alveolar air spaces (A; alveoli and ducts), capillaries (C) and septal wall (S). B, representation of same situation as (A) but with a line grid. Each line was associated with two points that when fell on the reference space (i.e. parenchyma) were counted. The length of the test-line is approximately 110 µm. Intersection of the test lines with the alveolar surface were also counted (green crosses). C, the same situation as (A) is represented, but in a lung from a mouse pup exposed to 85% O_2. D, The same situation as in (B) is represented, but in a lung from a mouse pup exposed to 85% O_2. E and F, fields of view with a counting frame superimposed over the image of virtual Nanozoomer-scanned slides at 40× magnification from the first and third histological sections in a consecutive series of serial sections for the alveolar count, each of 2 µm thickness (disector height, 4 µm). An alveolar bridge (B) is counted if an alveolar opening is open in one section (E) and closed in the other section (F) or vice versa. In this illustration (E) is considered the reference section, and (F) the look-up section. G and H, representation of the same situation as in (E) and (F), respectively, but in a lung from a hyperoxia-exposed mouse pup (Madurga et al., 2014).

10.10 Bronchoalveolar lavage

Bronchoalveolar lavage was performed for each mouse pup (four groups; n=6 per group), and cytoslides with lung leukocytes were stained for May-Grünwald Giemsa following the protocols described in (Regal, 2004).

10.11 Immunofluorescence staining of mouse lung sections

Paraffin-embedded lung tissue sections (3 μm) were stained as described previously (Alejandre-Alcazar et al., 2007) to localize Cbs and Cth in the lung. Serial sections were stained to ease antigen localization since co-staining of the same section was not successful. Shortly, paraffin sections were warmed for 20 min at 65 ºC, de-paraffinized with a series of Roti®-Histol (Roth), 100% (vol/vol), 90% (vol/vol) and 70% (vol/vol) ethanol, and processed for antigen-retrieval, for which different protocols were applied depending on the antigen. For von Willebrand factor (vWF), antigen-retrieval was by boiling in 10 mM Tris-Cl, pH 10.0 for 10 min, followed by a trypsin digestion 37 ºC for 10 min, while for α-smooth muscle actin (αSMA), antigen-retrieval was by boiling in citrate buffer (10 mM, pH 6.0) 10 min. Slides were cooled and washed with dH_2O and with 1×PBS. Sections were incubated with blocking buffer, and with the appropriate primary antibodies overnight at 4 ºC. The antibodies employed were rabbit anti-human Cbs, rabbit anti-human Cth, rabbit anti-human vWF and mouse anti-human αSMA-Cy3 conjugate. For unconjugated primary antibodies, the next secondary antibodies were employed: goat anti-mouse IgG (H+L)-Alexa Fluor® 568 conjugate and goat anti-rabbit IgG (H+L) -Alexa Fluor® 488 conjugate. As IgG control the next non-immune antibodies were used at the concentration as the corresponding primary antibody: mouse IgG and rabbit IgG. Nuclear staining was performed with 4′,6-diamidino-2-phenylindole (DAPI). Images were analyzed with a Leica DFC 360FX microscope.

10.12 Determination of medial wall thickness index and degree of vessel muscularization

The index of medial wall thickness (MWT) and the degree of muscularization of small (internal diameter 20-70 μm), medium (internal diameter 70-150 μm), and large (internal diameter >150 μm) pulmonary vessels were evaluated in paraffin-embedded lung sections (3 μm), exactly as described previously (Dahal et al., 2010; Malczyk et al., 2013). The methodology used for this study gives a general idea of whether changes in the MWT and vessel muscularization occur. On the other hand, this methodology does not follow design-based stereological principles, and there was no SUR sampling of tissue samples. MWT was indexed as a percentage of the vessel diameter, using the formula MWT (%) = 100 × [(2×medial wall thickness)/(outer vessel diameter)] (Ambalavanan, et al. 2005; Rabinovitch et al., 1979). Staining of sections was

performed with van Gieson's stain for MWT determination, or by immunohistochemistry for αSMA and vWF for muscularization assessment. The antibodies rabbit anti-human vWF and mouse anti-human αSMA were used. As secondary antibodies, anti-rabbit IgG-HRPO conjugate and anti-mouse IgG-HRPO conjugate were employed.

10.13 Assessment of vascular supply in lung sections

Paraffin-embedded lung tissue sections (3 μm) were stained for vWF using rabbit anti-human vWF. Then, sections were rinsed with 1×PBS and incubated with an anti-rabbit IgG HRPO conjugate. Immune complexes were visualized with 3,3′-diaminobenzidine (DAB) and counterstained with methyl green. After that, sections were dehydrated in 96% (vol/vol) ethanol, isopropanol and xylol, and then mounted. Sections were analyzed by light microscopy using a Leica microscope (CTR6000) with the QWin software. All images were taken at 20× magnification. The cross-sections of vWf-positive vessels were counted in four representative high-power fields per animal, a parameter that depends on the length of the vascular system. As with the MWT index and vessel muscularization methodology described above, this methodology does not follow design-based stereological principles, and there was no SUR sampling of tissue samples.

10.14 Endothelial tube-formation assay

Human pulmonary artery endothelial cells (HPAEC; Lonza, Walkersville, MA, U.S.A.; #CC-2530) were transfected to determine endothelial tube formation capacity. Cells were transfected either with siRNA directed against human CBS (200 nM; Santa Cruz, Heidelberg, Germany; #sc-60335) or with scrambled siRNA (200 nM; Santa Cruz, Heidelberg, Germany; #sc-37007), or the CTH inhibitor PAG 1 mM or 3 mM during 24 h, or after treatment with the slow release H_2S donor GYY4137 (100 μM during 24 h) or vehicle alone (DMEM Media 200 with LVES supplement 2% (vol/vol); Gibco, Karlsruhe, Germany; #ATCC 30-2002 and #A14608-01, respectively). The HPAEC were seeded (100.000 cells/well) into Matrigel-coated wells of a 24-well plate (BD BioCoat™ BD Matrigel™ plate; Becton Dickinson, Heidelberg, Germany; #3554480). Prior to loading on the Matrigel plate, HPAEC had been transfected with siRNA for 48 h, detached with Accutase and cells were counted prior to re-seeding. Total tube length and numbers of tubes were measured using a Leica CTR6000 microscope, with the aid

of WimTube software (Wimasis, Munich, Germany). Cell viability in response to siRNA, GYY4137 and PAG treatment was calculated using 3-(4,5-dimethylthiazol-2-yl)-2,5-diphenyltetrazolium bromide (MTT).

10.15 Primary ATII cells and cell-lines

Primary mouse lung alveolar type II (ATII) cells were isolated from the lungs of adult C57Bl/6J mice as described previously (Alejandre-Alcazar et al., 2007; Morty et al., 2007). The ATII cells were cultured on an air/liquid interface for three days after isolation and used on day three after isolation. The ATII cells were cultured in DMEM supplemented with 10% (vol/vol) FBS and 1% (wt/vol) penicillin/streptomycin in a humidified 5% (vol/vol) CO_2 atmosphere. Transformed mouse lung epithelial cells (MLE-12; ATCC, USA;# CRL-2110) were cultured in DMEM supplemented with 10% (vol/vol) FBS in six-well tissue culture plates, as described above. Equally primary mouse lung ATII cells and MLE-12 cells were maintained in starvation media (DMEM without FBS) for 6 h and treated with NaHS (100 μM) dissolved in DMEM for 10, 15, 20, 30 and 60 min.

10.16 ATII cell isolation and staining for flow cytometry

Primary mouse lung ATII cells were treated either with vehicle (DMEM, supplemented with 10% (vol/vol) FBS), NaHS (100 μM) for 24 h, or with staurosporine 0.5 μM for 1.5 h. Cells were detached with Accutase and proceeded according to established protocols for the detection of apoptosis by flow cytometry (Rieger et al., 2011). Shortly, cell staining with performed using an AlexaFluor® 488 Annexin V/Dead Cell Apoptosis Kit, or with FITC conjugated mouse IgG1, isotype control, mouse IgG_1 PETexas Red® conjugate. Using a BD FACS Canto™ flow cytometer, 10.000 ATII cells/sample were analyzed (n=5 per group). The samples were analyzed with FACSDiva version 6.1.3.

10.17 ATII cell isolation and staining for immunofluorescence

Primary mouse lung ATII cells were treated either with vehicle (DMEM, supplemented with 10% (vol/vol) FBS), the fast release H_2S donor NaHS (100 μM) for 24 h, or with staurosporine 0.5 μM for 1.5 h. Cells were stained with propidium iodide and DAPI and analyzed with a Leica

microscope (DFC 360FX). Representative images of every sample were taken at 10× magnification, and >300 cells were counted per sample, (n=4 per group).

10.18 RNA isolation and cDNA synthesis for RT-PCR analysis

Either mouse lung homogenates or cells (both primary cells and cell lines) were homogenized in RNA lysis buffer in Precellys® 24-Dual Homogenisator using 1.4 mm ceramic beads to disrupt tissue (n=4-6). The RNA isolation was performed using a peqGOLD Total RNA Kit from Peqlab following the manufacturer´s instructions. The RNA concentration was measured using a Nanodrop Spectophotometer. Taking 1000 ng of total RNA, cDNA was obtained using a MuLV reverse transcriptase from Applied Biosystems, and RNAse free water.

10.19 Laser-capture micro dissection

Frozen cryosections from wild type mouse at P7.5 and P14.5 (n=4 per group) were cut in 10 µm thickness using a Leica microtome (RM2255). The sections were afterwards treated with a series of ethanol (70%, 90%, and 99% (vol/vol) ethanol), washed with RNAse free water, and with Scott's tap water, and finally stained with Hematoxylin. Compartmentalization of tissue was taken from different samples, falling into the categories: Parenchyma, airway, and lung vascular compartment, using a Leica laser micro dissection system (LMD 6500). As pulmonary arteries and pulmonary veins are difficult to discriminate in unstained cryosections, all vessels were harvested together, and no discrimination between arteries and veins has been attempted. Samples were collected in RLT-buffer that contained β-mercaptoethanol. Isolation of RNA was performed using a PeqGold total RNA kit isolation kit following the manufacturer's indications. Synthesis of cDNA was fulfilled using iScript™ cDNA Synthesis Kit, from BioRAD, following the manual's instructions.

10.20 RT-PCR analysis

Quantitative changes in mRNA expression of genes was determined using a quantitative real time PCR method. The RT-PCR analysis were performed using a Platinum® SYBR® Green qPCR SuperMix UDG Kit (Invitrogen) and a StepOnePlus PCR Machine (Applied Biosystems). The primers were synthesized in Eurofins MWG Operon. As a house-keeping

gene for mouse samples, the gene POL2RA was used as a reference gene. The table of primer sequences can be found in Table 2.

10.21 Protein isolation for immunoblots

Cells were homogenized by scraping in lysis buffer: 20 mM Tris-Cl, 150 mM NaCl, 1 mM EDTA, 1 mM EGTA, 1% (vol/vol) NP-40, 1 mM sodium ortho-vanadate and 1× Complete™ protease inhibitor cocktail. Proteins from mouse lung tissue were homogenized in lysis buffer by disruption in Precellys® 24-Dual Homogenisator using 1.4 mm ceramic beads to disrupt tissue (n=3-8 per group). Protein concentration was determined by Bradford assay.

10.22 Protein expression analysis

Immunoblotting was performed as described previously, (Alejandre-Alcazar et al., 2007; Morty et al., 2007), using the following primary antibodies: anti-phospho-Akt, anti-Akt, anti-Cbs, anti-Cth, anti-CD31 and anti β-actin. Immune complexes were detected with a secondary antibody anti-rabbit IgG horseradish peroxidase conjugate, employing enhanced chemiluminescence. Densitometric analysis of immunoblot bands was determined using the Multi Gauge MFC Application version 3.0.0.0.

10.23 Wound healing assay

The ATII cells were cultured in in DMEM supplemented with 10% (vol/vol) FBS on an ibidi culture-insert μ-dish© that contained a grid, until a confluent monolayer was formed. The cells were maintained for 24 h in starvation media (DMEM without FBS supplementation) prior to remove the insert of the grid. Once the insert was removed, it left a wound in the ATII cell monloayer. Next, the cells were treated either with DMEM, NaHS (100 μM) dissolved in DMEM, glibenclamide (10 μM) dissolved in DMEM, or with glibenclamide (10 μM) dissolved in DMEM, for 30 min, followed by the addition of NaHS (100 μM; final concentration). Three representative images of every sample were taken at 0, 4, 8, 12 and 24 h at 5× magnification (n=6 per group), with a Leica (DMI3000B) microscope. Using Image J Software and Adobe Photoshop CS5 Software, the wound distance and the number of cells that migrated over time were measured.

10.24 ELISA

Proteins from mouse lung tissue were homogenized in MES buffer by disruption in a Precellys® 24-Dual Homogenisator using 1.4 mm ceramic beads to disrupt tissue (n=5-6 per group). Protein concentration was determined using Bradford assay. Using 5 mg of lung extract proteins, mouse ELISA kits R&D and Qiagen were used following the manufacturer´s instructions to measure changes in the protein abundance of IL-10, IL-6, IL-1β and tumor necrosis factor (TNFα). ELISA measurements were performed in a VersaMAX microplate spectrophotometer.

10.25 Glutathione assay

Proteins from mouse lung tissue were homogenized in gluthatione assay buffer by disruption in Precellys® 24-Dual Homogenisator using 1.4 mm ceramic beads to disrupt tissue (n=8 per group). Protein concentration was measured using the Bradford assay. Proteins were treated with 4 M triethanolamine and 5% (wt/vol) meta-phosphoric acid. Using a Bioxytech®GSH/GSSG kit following the manufacturer's instructions, the ratio of reduced glutathione (GSH) was compared to oxidized glutathione (GSSG).

10.26 Microarray analyses

Primary mouse ATII cells were either treated with vehicle (DMEM, supplemented with 10% (vol/vol) FBS) or GYY4137 (100 μM; dissolved in DMEM, supplemented with 10% (vol/vol) FBS) for 24 h. In another set of experiments primary mouse ATII cells were either treated with vehicle (DMEM, supplemented with 10% (vol/vol) FBS) or NaHS (100 μM; dissolved in DMEM, supplemented with 10% (vol/vol) FBS) for 6 h or 24 h. Total RNA was harvested using the PeqGold total RNA kit. The company IMGM Laboratories (Martinsreid, Germany) performed the microarray analyses by using an Agilent SurePrint G3 Mouse Gene Expression Microarray (8×60K) in combination with a one-color based hybridization protocol. Signals were detected using an Agilent DNA Microarray Scanner. Based on the PANTHER analysis, the induced and repressed genes were additionally categorized for involvement in molecular functions, functional biological processes, cellular components, and protein classes and pathways.

10.27 Transgenic mice

All animal procedures were approved by the local authority, the *Regierungspräsidium Darmstadt* (approval B2/327). The generation of *Cbs*$^{-/-}$ mice, where a neomycin selection cassette replaced a genomic fragment containing exons 3 and 4 of the Cbs gene, has previously been reported (Watanabe et al., 1995). These mice referred to here as *Cbs*$^{-/-}$, (strain designation B6.129P2-*Cbs*^{tm1Unc}/J), were obtained from The Jackson Laboratory (stock number 002853). The generation of *Cth*$^{-/-}$ mutant mice has already been defined, where exons 1 to 6 were replaced with a LacZ and neomycin selection cassette (Ishii et al., 2004) herein referred to as *Cth*$^{-/-}$.

10.28 Genotyping of mouse genomic DNA

To genotype transgenic mice semi-quantitative PCR analysis was performed using genomic DNA isolated from tail-cuts as template. The DNA extraction from mouse tail cuts was achieved according to the Nature protocol ISSN: 1754-2189, EISSN: 1750-2799. The PCR for genotyping *Cbs*$^{-/-}$ mice, was assessed following the protocol described in the Jackson Laboratory (category: stock number: 002461, strain name: B6.129P2-*Cbs*^{tm1Unc}/J). The polymerase used for the PCR reaction was PfuUltra™ High-Fidelity DNA polymerase (Thermo Scientific). The PCR for genotyping *Cth*$^{-/-}$, was performed as described previously (Ishii et al., 2004) using a Hot GoTaq® DNA polymerase (Promega). The primer sequences for genotyping are described in Table 3.

10.29 Statistical analyses

Differences between groups were compared by one-way analysis of variance (ANOVA) with Tukey's *post hoc* test (when more than two groups were compared), or Student's *t* test (in the case of a comparison of two groups, or pair-wise comparisons of wild-type lungs with either Cbs$^{-/-}$ mouse lungs or Cth$^{-/-}$ mouse lungs). Plus, a two-way ANOVA was used for the wound healing assay assessed at multiple time-points. Statistical analyses were performed with GraphPad Prism 6.0, and statistical outliers were identified by Grubb's test. A p value <0.05 was considered significant.

11 Results

11.1 Systemic H_2S administration partly restores normal alveolarization in an experimental animal model of BPD

11.1.1 Stereological analysis of lung structure in normally and aberrantly developing lungs

Neonatal mouse pups exposed to 85% O_2 for the first 10 days of life presented an evident increase in MLI. In normally-developing lungs (21% O_2 group) the MLI ranged from 47.2 ± 1.2 µm whereas in the aberrantly-developing lungs (85% O_2 group) the MLI increased to 83.3 ± 4.8 µm without any changes in total lung volume (Fig. 8E; Table 5). An increase of 29% in mean septal thickness was also observed in the aberrantly-developing lungs, the mean septal thickness ranged from 11.69 ± 0.10 µm compared to 9.05 ± 0.61 µm in normally-developing lungs (Fig. 8F). Accordant with the changes in MLI (Fig. 8E), the total number of alveoli decreased 56%, from 2.10 ± 0.23 × 10^6 alveoli/both lungs in normally-developing lungs to 0.92 ± 0.08 × 10^6 alveoli/both lungs in aberrantly-developing lungs (Fig. 8G).

11.1.2 Stereological analysis of the impact of H_2S donor administration on normal and aberrant late lung development

Mouse pups maintained at 21% O_2 environment and treated with the slow-release H_2S donor GYY4137 did not have alterations of total number of alveoli per lung, septal thickness or MLI (Fig. 8). Still, mouse pups maintained at 85% O_2 environment and treated with GYY4137 resulted in a partial normalization of lung structure. The total number of alveoli per lung was almost doubled, increasing from 0.92 ± 0.08 × 10^6 alveoli/both lungs in vehicle-treated mice to 1.70 ± 0.15 × 10^6 alveoli/both lungs in GYY4137-treated mice (Fig. 8F). Accordant with this tendency, the MLI was decreased by 21%, from 83.3 ± 4.8 µm in vehicle-treated mice to 65.7 ± 4.3 µm in GYY4137-treated mice (Fig. 8E). Moreover, the mean septal wall thickness also was normalized, decreasing by 23%, from 11.69 ± 0.10 µm in vehicle-treated mice to 8.99 ± 0.34 µm in GYY4137 treated mice (Fig. 8D). Altogether, these data (additional parameters in

Table 5) indicate that treatment of an H_2S donor to hyperoxia-exposed mice partially normalizes lung structure.

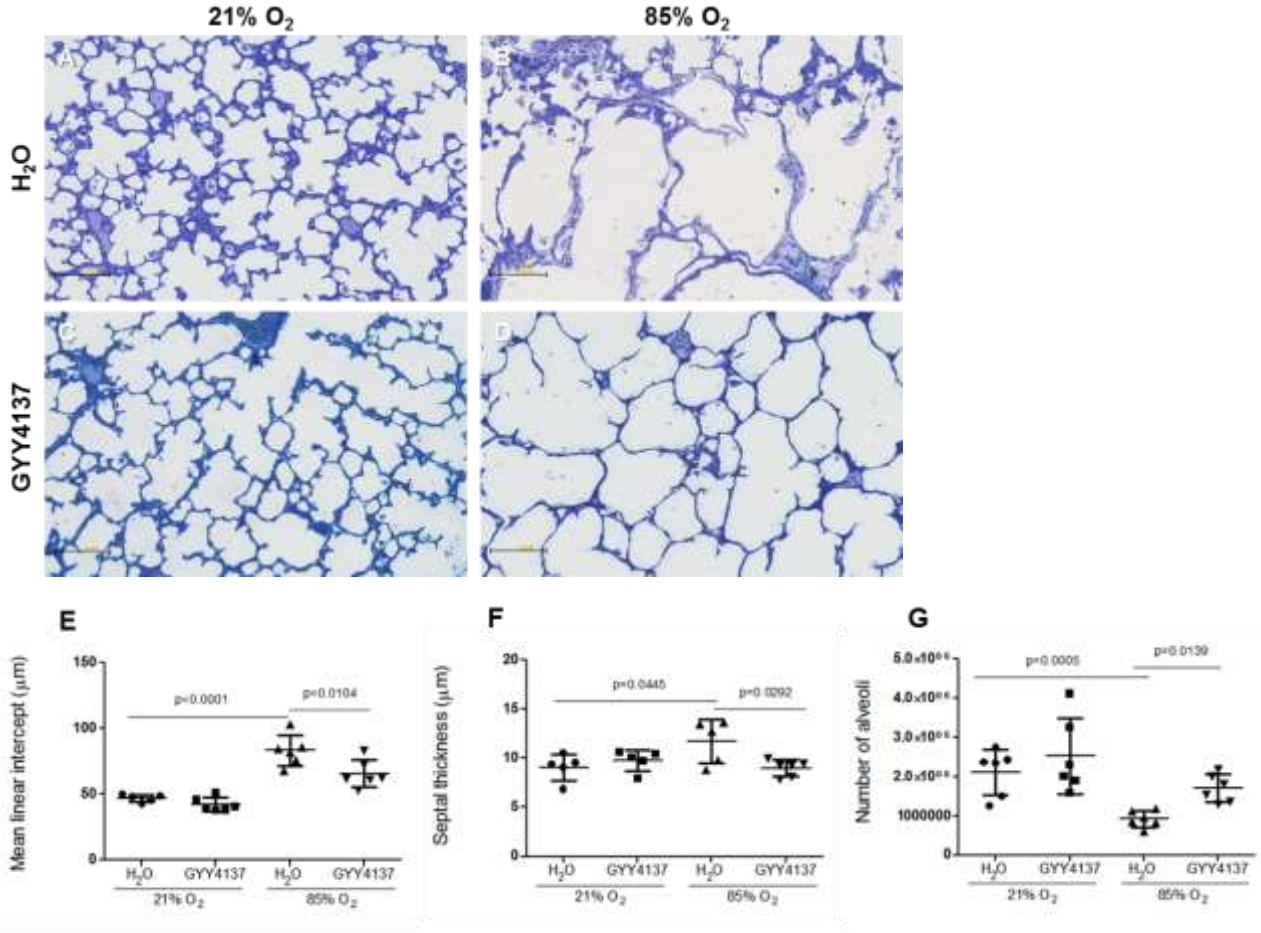

Figure 8 GYY4137 administration decreased impaired alveolar development in an experimental mouse model of bronchopulmonary dysplasia.

Illustrative lung tissues sections from mouse pups at postnatal day 10. Mouse pups were exposed either to normoxia conditions, 21% O_2 (A, C), or to normobaric hyperoxia 85% O_2 (B, D) for the first 10 days of life. Mouse pups were treated either with a vehicle control (A, B) or with GYY4137 (C, D). Structural lung changes were assessed via stereology analysis, including the parameters number of alveoli (E), septal thickness (F) and mean linear intercept (G), additional parameters are presented in Table 5. Data represent the mean ± S.E. (n=6, per group). The p values were determined by one-way ANOVA with a Tukey's *post hoc* test (Madurga et al., 2014).

Table 5 Structural parameters of developing mouse lungs during exposure to 21% O_2 or 85% O_2 assessed by stereological analysis (Madurga et al., 2014).

Parameter	21% O_2		85% O_2			
	H_2O	GYY4137	H_2O		GYY4137	
	mean ± S.E.	mean ± S.E.	mean ± S.E.	*p* value *versus* H_2O/21% O_2	mean ± S.E.	*p* value *versus* H_2O/85% O_2
V (lung) [cm^3]	0.19 ± 0.02	0.22 ± 0.01	0.19 ± 0.01	0.9984	0.20 ±0.01	0.9874
CV [*V* (lung)]	0.25	0.11	0.17		0.13	
V_V (par/lung) [%]	90.9 ± 2.0	95.0 ± 1.3	92.1 ± 2.2	0.9580	91.5 ± 1.0	0.9922
V_V (non-par/lung) [%]	9.06 ± 1.95	5.05 ± 1.32	7.87 ± 2.21	0.6926	8.53 ± 1.03	0.7804
S_V (alv epi/par) [cm^{-1}]	576.4 ± 34.3	598.3 ± 26.1	383.3 ± 18.9	0.0002	480.1 ± 23.5	0.0739
S (alv epi, lung) [cm^2]	96.0 ± 10.9	127.4 ± 8.3	66.1 ± 6.4	0.0530	83.8 ± 6.7	0.4498
CV [S (alv epi, lung)]	0.28	0.16	0.24		0.20	
V (alv air, lung) [cm^3]	0.16 ± 0.01	0.12 ± 0.02	0.14 ± 0.01	0.5332	0.14 ± 0.01	>0.9999
CV [*V* (alv air, lung)]	0.22	0.24	0.19		0.12	
V (sep, lung) [cm^3]	0.05 ± 0.01	0.08 ± 0.01	0.04 ± 0.01	0.5349	0.04 ± 0.003	0.9933
CV [*V* (sep, lung)]	0.13	0.37	0.35		0.21	

V, volume; V_V, volume density; *S*, surface area; S_V, surface density; *CV*, coefficient of variation; *par*, parenchyma; *non-par*, non-parenchyma; *alv air*, alveolar airspaces; *alv epi*, alveolar epithelium; *sep*, septum. Values are presented as mean ± S.E, n=6 lungs per group. *p* values were calculated by one-way ANOVA with Tukey's *post-hoc* analysis.

11.1.3 Analysis of H_2S donor administration on inflammatory cell infiltration in neonatal mouse pup lungs

The anti-inflammatory properties of H_2S have been previously described by other groups (Li et al., 2011; Wallace et al., 2012). It has also been noted the importance of inflammatory cells to normal and aberrant late lung development (Ambalavanan et al., 2009; Deng et al., 2000; Hartling et al., 2012; Kunzmann et al., 2013). For that reason, the inflammatory cell infiltration into the alveolar airspaces was determined in both 21% O_2- and 85% O_2-exposed lungs, with either vehicle or GYY4137 administration, in cytospins from BAL fluid (Fig. 9). Mouse pups exposed to 85 % O_2 presented an increase in the abundance of leukocytes in BAL fluid (Fig. 9B versus Fig. 9A; quantified in Fig. 9E). In detail, the 85% O_2-exposed mouse pups had an increase in the abundance of macrophages and neutrophils in BAL fluid (Fig. 9G). Plus, the hyperoxia exposed mice also had an elevated abundance of monocytes (Fig. 9H), eosinophils (Fig. 9I) and lymphocytes (Fig. 9J) in the BAL fluid. Administration of GYY4137 to mouse pups exposed to 85% O_2 environment changed the BAL fluid inflammatory cell profile (Fig. 9D versus Fig. 9C; quantified in Fig. 9E). In detail, the infiltration that was provoked by exposure to 85% O_2 of macrophages (Fig. 9F), neutrophils (Fig. 9G), monocytes (Fig. 9H), and eosinophils (Fig. 9I) decreased after GYY4137 treatment, but not lymphocytes (Fig. 9J). Therefore, the reduction of inflammatory response by exposure to hyperoxia conditions after GYY4137 administration, may represent a mechanism by which GYY4137 was able to partially restore normal lung structure to 85 % O_2-exposed mouse pups.

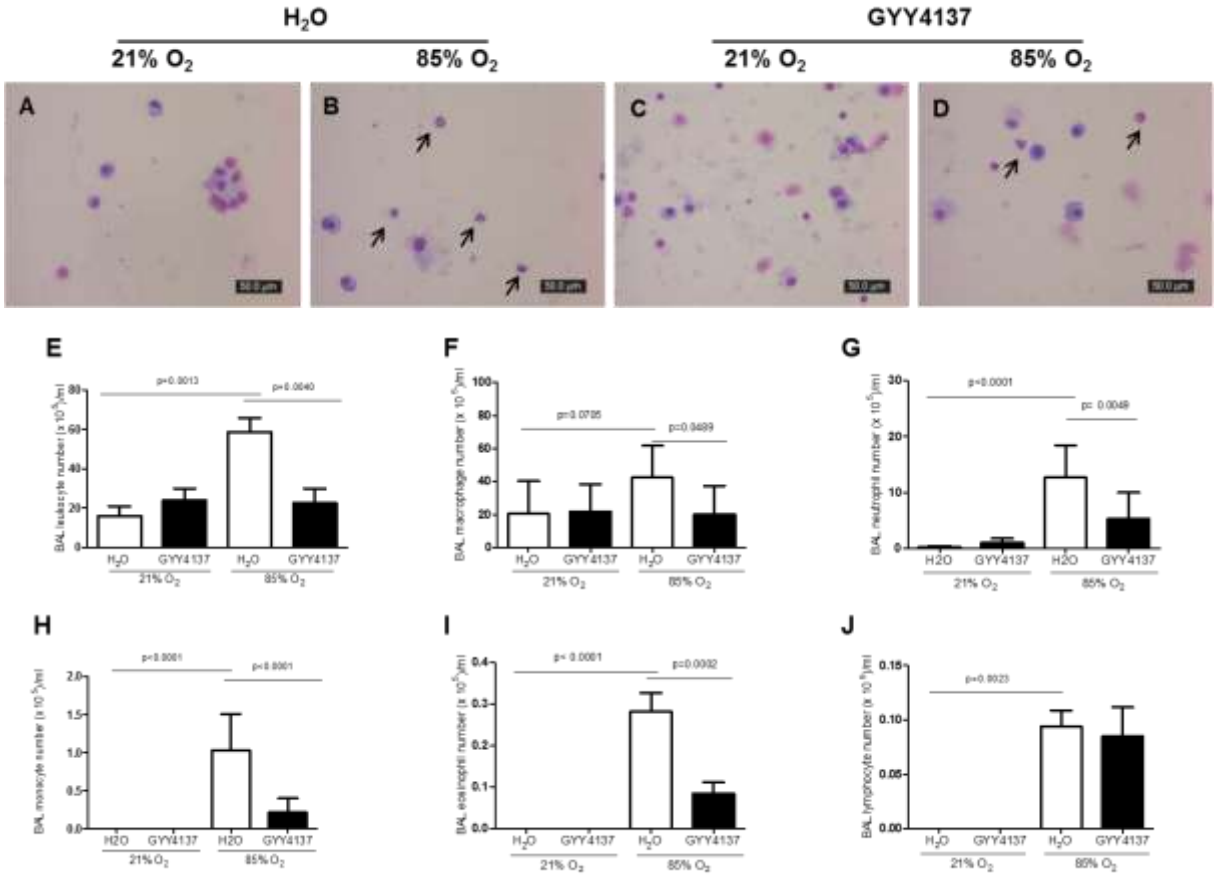

Figure 9 GYY4137 administration diminished leukocyte recruitment into the alveolar airspaces that was provoked by exposure to hyperoxia.

Representative cytospins images from bronchoalveolar lavage (BAL) fluid from mouse pups at post-natal day 10. Mouse pups were exposed either to 21% O_2 (A, C) or 85% O_2 (B, D) for the first 10 days of life, and treated either with a vehicle control (water) (A, B) or with GYY4137 (50 mg/kg/day, intraperitoneal) (C, D). Arrows indicate neutrophils. E, assessment of the total leukocyte number in BAL fluid cytospins; F, number of macrophages present in BAL fluid cytospins; G, number of neutrophils present in BAL fluid cytospins; H, number of monocytes present in BAL fluid cytospins; I, number of eosinophils present in BAL fluid cytospins; J, number of lymphocytes present in BAL fluid cytospins. Data represent the mean ± S.E. (n=6, per group). The p values were determined by one-way ANOVA with a Tukey's *post hoc* test (Madurga et al., 2014).

11.1.4 Cytokine response to GYY4137 administration

Lung homogenates of mouse pups exposed to 21% O_2 or 85% O_2, with and without concomitant GYY4137 administration were evaluated to study the expression levels of the cytokines IL-6 (Fig. 10A), IL-10 (Fig. 10B), TNFα (Fig. 10C) and IL-1α (Fig. 10D) by ELISA in an effort to comprehend the anti-inflammatory properties of GYY4137 administration. In mouse pup lungs exposed to 85% O_2 the expression levels of the pro-inflammatory IL-6 were increased, and the expression levels of the anti-inflammatory IL-10 were decreased (Fig. 10) generating a pro-inflammatory environment. Meanwhile the IL-6 expression levels were not impacted in the developing lungs of mouse pups treated with GYY4137 and exposed to 85% O_2 (Fig: 10A), the IL-10 expression levels were otherwise restored (Fig. 10B). Remarkably, it was also noted that mouse pups exposed to 21% O_2 environment and treated with GYY4137 had a reduction of IL-10 expression levels. In sum, GYY4137 may partially restore the pro-inflammatory environment provoked by hyperoxia conditions that caused an increase of IL-6 and a decrease of IL-10, restoring pulmonary IL-10 levels that were otherwise depressed in the 85 % O_2 environment (Fig. 10).

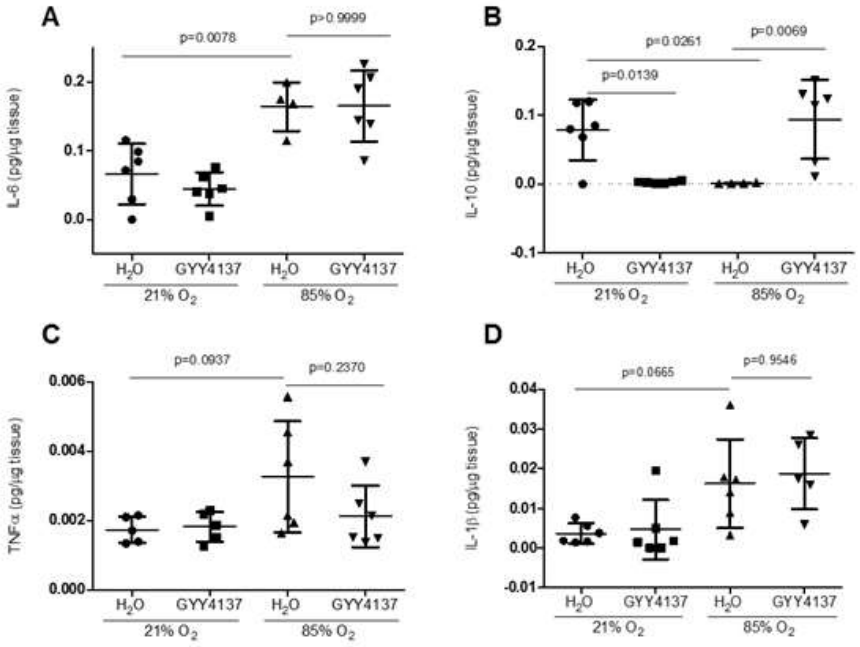

Figure 10 GYY4137 administration alters the pulmonary expression of inflammatory mediators in neonatal mouse lungs.

Changes in protein expression levels of IL-6 (A), IL-10 (B), tumor necrosis factor alpha (TNFα) (C), and IL-1β (D) by ELISA determination in lung tissue homogenates of mouse pups exposed to either 21% O_2 or 85% O_2 for the first 10 days of life, that received either vehicle (water) or GYY4137 (50 mg/kg/day, intraperitoneal). Data represent the mean ± S.E. (n=5-6, per group). The p values were determined by one-way ANOVA with a Tukey's *post hoc* test (Madurga et al., 2014).

11.1.5 Impact of GYY4137 on the oxidative status of the developing lung

The gasotransmitter H_2S has also been reported to have anti-oxidant properties in addition to anti-inflammatory properties (Li et al., 2011; Wallace et al., 2012). Hence, the oxidative status of the developing lungs was studied, assessed via the ratio of GSH to GSSG in protein extracts from mouse pup lung homogenates. Meanwhile mouse pups lungs exposed to hyperoxia conditions decreased the GSH/GSSG ratio (Fig. 11), GYY4137 administration did not impact the GSH/GSSG ratio (Fig. 11). From this data it is suggestive that the ability of GYY4137 to partially restore normal lung structure to 85% O_2 exposed mouse pups was not dependent upon the anti-oxidative properties of H_2S.

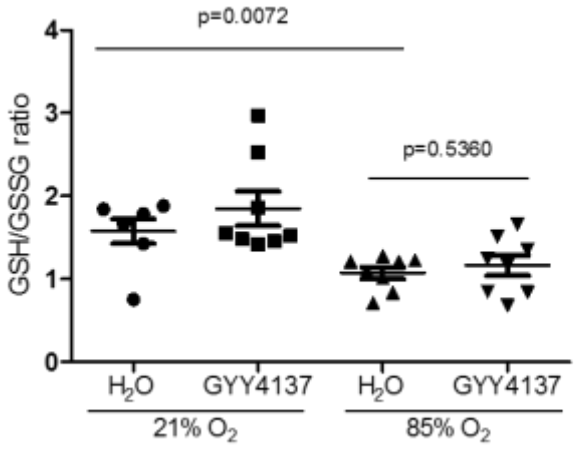

Figure 11 GYY4137 administration does not impact the oxidative status of neonatal mouse lung as assessed by glutathione oxidation.

Assessment of oxidative status from mouse pup lung homogenates via ratio of reduced glutathione (GSH) to oxidized glutathione (GSSG). Mouse pups were exposed either to 21% O_2 or 85% O_2 for the first 10 days of life, and received either vehicle (water) or GYY4137 (50 mg/kg/day, intraperitoneal). Data represent the mean ± S.E. (n=6-8, per group). The p values were determined by one-way ANOVA with a Tukey's *post hoc* test (Madurga et al., 2014).

11.1.6 Impact of NaHS on viability of primary mouse alveolar type II cells

Further studies were focused in the alveolar epithelium, since the epithelium that lines the alveolar air spaces would be in direct contact with the increased oxygen levels and therefore prone to oxygen-induced injury. Moreover, the epithelium may promote or inhibit inflammation in the developing lung since is an important site of generation of inflammatory mediators. In addition, if H_2S gas would be administered to ventilated patients, the epithelium would be likely the first tissue barrier to encounter H_2S.

For the evaluation of how H_2S would impact the alveolar epithelium, the H_2S donors were employed in microarray studies, in cell wounding and cell signaling studies.

First, the impact of cell viability on ATII cells was assessed using the NaHS donor (100 µM) to confirm that the dose used was not toxic to ATII cells over the time-frame of treatment (24 h) employed. No noticeable apoptosis was detected on ATII cells by flow cytometry based on annexin V translocation and propidium iodide permeability (Fig. 12A, quantified in Fig. 12C). Likewise, NaHS treatment did not cause appreciable apoptosis to ATII cells, as assessed by fluorescence microscopy based on propidium iodide permeability and DAPI nuclear staining (Fig. 12B, quantified in Fig. 12D).

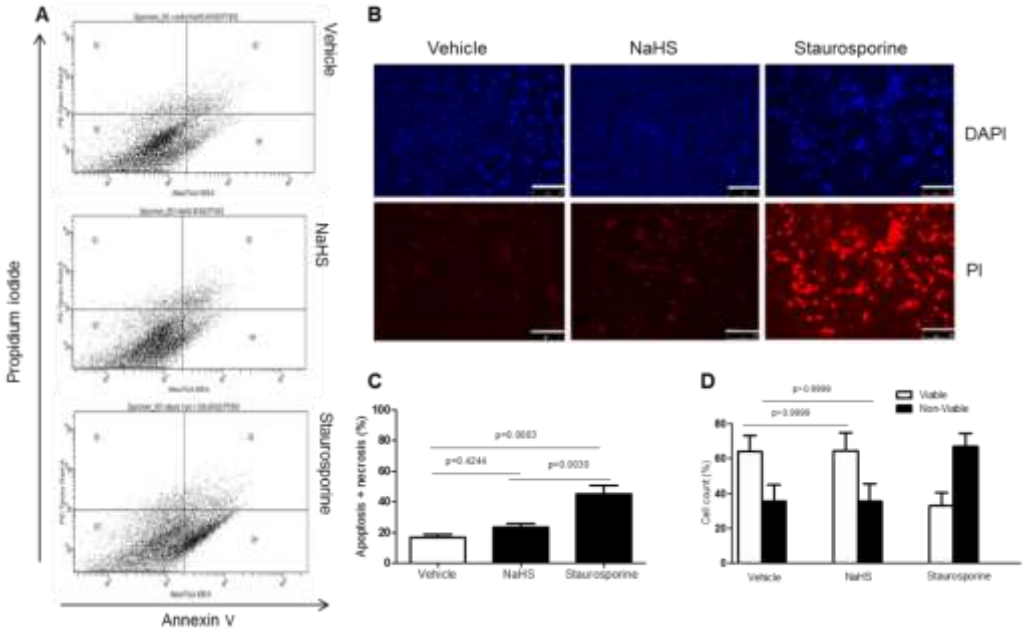

Figure 12 H_2S delivered exogenously by a chemical donor does not cause apoptosis or cell death of primary mouse alveolar type II cells.

The fast release H_2S donor NaHS (100 μM, 24 h) was employed for all *in vitro* studies. As positive apoptosis control, cells were treated with staurosporine (1.5 μM, 1.5 h). A, by flow cytometry apoptosis was assessed in primary mouse ATII cells to detect annexin V in the outer surface of the cell membrane and propidium iodide entry into cells. B, representative images of ATII cells treated either with vehicle (DMEM media), NaHS or staurosporine staining with DAPI and propidium iodide (PI) to detect apoptosis of cells. C, data were quantified from multiple experiments depicted in (A). D, data were quantified from multiple experiments depicted in (B). Data represent the mean ± S.E. (n=4-5, per group). The p values were determined by one-way ANOVA with a Tukey's *post hoc* test. The scale bar indicates 75 μm (Madurga et al., 2014).

11.1.7 Impact of NaHS and GYY4137 treatment on gene expression in primary mouse alveolar type II cells

Primary ATII cells were treated either with vehicle (DMEM media) or with H_2S donors (delivered by NaHS or GYY4137 100 μM for 24 h) both at 21% O_2 and 85% O_2 conditions, to study the changes of gene expression in the alveolar epithelium via microarray analysis (Fig. 13). Dramatic changes in mRNA expression profiles occurred when primary mouse ATII cells were exposed to an 85% O_2 environment for 24 h, measured by microarray analysis. The 20 most up-regulated genes and 20 most down-regulated genes are indicated in Table 6 and Table

7, respectively. Yet, GYY4137 and NaHS administration did not have any effect on gene expression in primary mouse ATII cells. From this data, it is suggestive that the partially restore of lung structure to oxygen-injured developing mouse lungs treated with H_2S donors was not dependent on changes in gene expression in alveolar epithelial cells

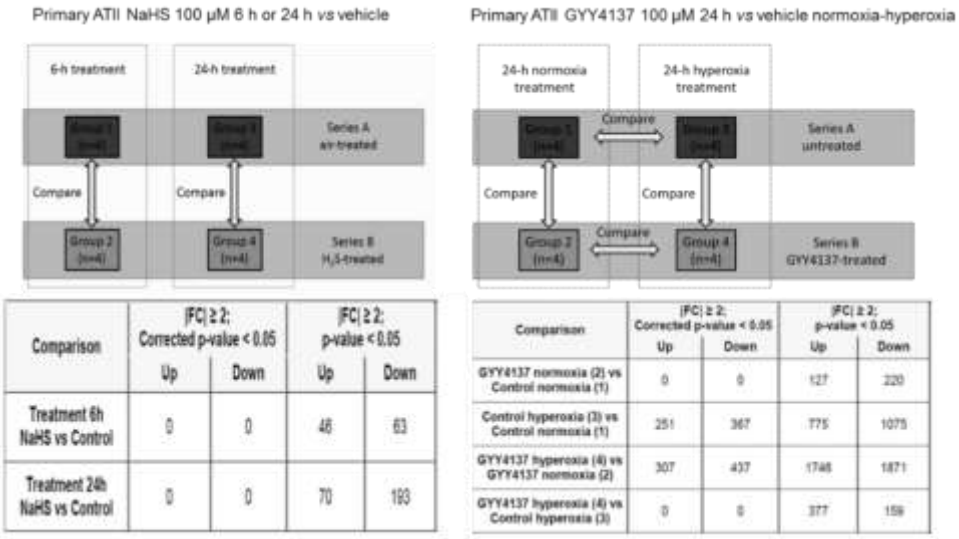

Comparison	|FC| ≥ 2; Corrected p-value < 0.05		|FC| ≥ 2; p-value < 0.05	
	Up	Down	Up	Down
Treatment 6h NaHS vs Control	0	0	46	63
Treatment 24h NaHS vs Control	0	0	70	193

Comparison	|FC| ≥ 2; Corrected p-value < 0.05		|FC| ≥ 2; p-value < 0.05	
	Up	Down	Up	Down
GYY4137 normoxia (2) vs Control normoxia (1)	0	0	127	220
Control hyperoxia (3) vs Control normoxia (1)	251	367	775	1075
GYY4137 hyperoxia (4) vs GYY4137 normoxia (2)	307	437	1748	1871
GYY4137 hyperoxia (4) vs Control hyperoxia (3)	0	0	377	159

Figure 13 Scheme representing the experimental settings of primary alveolar type II cells exposed to hydrogen sulfide donors.

Scheme of experimental settings of primary alveolar type II (ATII) cells treated either with vehicle or NaHS 100 µM for 6 or 24 h (left side panel) or ATII cells treated either in normoxia or hyperoxia conditions, treated either with vehicle (DMEM media) or with GYY4137 100 µM for 24 h (right side panel). Both schemes are accompanied by a table showing the gene regulation caused by the treatment administration and analyzed by microarray analysis. FC=Fold change (Madurga et al., 2014).

Table 6 Gene expression in primary mouse alveolar type II cells up-regulated by exposure to 85% O_2 *in vitro.*

Gene symbol (NCBI)	**Fold change**	**Gene name**
Svop	8.67	SV2 related protein
H2-M9	8.54	histocompatibility 2, M region locus 9
Prl2c5	7.53	prolactin family 2, subfamily c, member 5
Robo3	6.65	roundabout homolog 3 (Drosophila)
Zfp750	5.84	zinc finger protein 750
Tmem45b	5.62	transmembrane protein 45b
Krtap3-2	5.46	keratin associated protein 3-2
Apol7d	5.29	apolipoprotein L 7d
Rprm	5.18	reprimo, TP53 dependent G2 arrest mediator candidate
Dusp15	5.12	dual specificity phosphatase-like 15
Nkx2-9	4.98	NK2 transcription factor related, locus 9 (Drosophila)
Kcnj4	4.86	potassium inwardly-rectifying channel, subfamily J, member 4
Nr1d1	4.78	nuclear receptor subfamily 1, group D, member 1
Lrdd	4.70	leucine-rich and death domain containing
Dcxr	4.55	dicarbonyl L-xylulose reductase
Cdkn1a	4.28	cyclin-dependent kinase inhibitor 1A (P21)
Lrdd	4.24	leucine-rich and death domain containing
Olfr1020	4.15	olfactory receptor 1020
Dcxr	4.14	dicarbonyl L-xylulose reductase
Crct1	4.01	cysteine-rich C-terminal 1

NCBI, national center for Biotechnology Information.

Table 7 Gene expression in primary mouse alveolar type II cells down-regulated by exposure to 85% O_2 *in vitro.*

Gene symbol (NCBI)	**Fold change**	**Gene name**
Hist1h1b	-15.89	histone cluster 1, H1b
Hist2h2bb	-11.84	histone cluster 2, H2bb
Cep55	-9.94	centrosomal protein 55
Cdc6	-8.78	cell division cycle 6 homolog (S. cerevisiae)
Mki67	-8.35	antigen identified by monoclonal antibody Ki 67
Casc5	-8.18	cancer susceptibility candidate 5
Kif11	-8.14	kinesin family member 11
Mxd3	-8.13	Max dimerization protein 3
Aspm	-8.10	asp (abnormal spindle)-like, microcephaly associated (Drosophila)
Ndc80	-7.88	NDC80 homolog, kinetochore complex component (S. cerevisiae)
Mki67	-7.84	antigen identified by monoclonal antibody Ki 67
Sgol2	-7.80	shugoshin-like 2 (S. pombe)
Hist1h1a	-7.74	histone cluster 1, H1a
Plk1	-7.15	polo-like kinase 1 (Drosophila)
Fbxo5	-7.08	F-box protein 5
Kif2c	-6.98	kinesin family member 2C
Kif2c	-6.51	kinesin family member 2C
Nuf2	-6.51	NUF2, NDC80 kinetochore complex component, homolog (S. cerevisiae)
Depdc1b	-6.17	DEP domain containing 1B
E2f8	-6.14	E2F transcription factor 8

NCBI, national center for Biotechnology Information.

11.1.8 Impact of NaHS on primary mouse alveolar type II cell wound closure

Taken into account that H_2S administration (delivered by NaHS and GYY4137) did not impact gene expression in primary ATII cells, it was likely that H_2S could influence other processes during lung development and repair that implied ATII cells. Thus, using the fast release H_2S donor NaHS, a classical wound repair assay was performed on primary ATII cell monolayers. The NaHS promoted wound repair assessed by the rate of wound closure (Fig. 14B versus Fig. 14D, quantified in Fig. 14I and Fig. 14J). Though glibenclamide, a sulfonylurea that inhibits ATP-sensitive potassium channels and the cystic fibrosis transmembrane conductance regulator, was with no effect on ATII cell wound closure, glibenclamide (Fig. 14F versus Fig. 14B; quantified in Fig. 14I and Fig. 14J) did blunt the ability of NaHS to promote would closure (Fig. 14H versus Fig. 14D; quantified in Fig. 14I and Fig. 14J). Taken together this data suggest that H_2S (released from NaHS) can promote wound healing in ATII cells, and that this process depends on the interaction of H_2S with glibenclamide, implying involvement of ion channels in ATII cells. Moreover, this data suggest a hint in the mechanism of action of H_2S to restore proper lung development in oxygen-injured lungs.

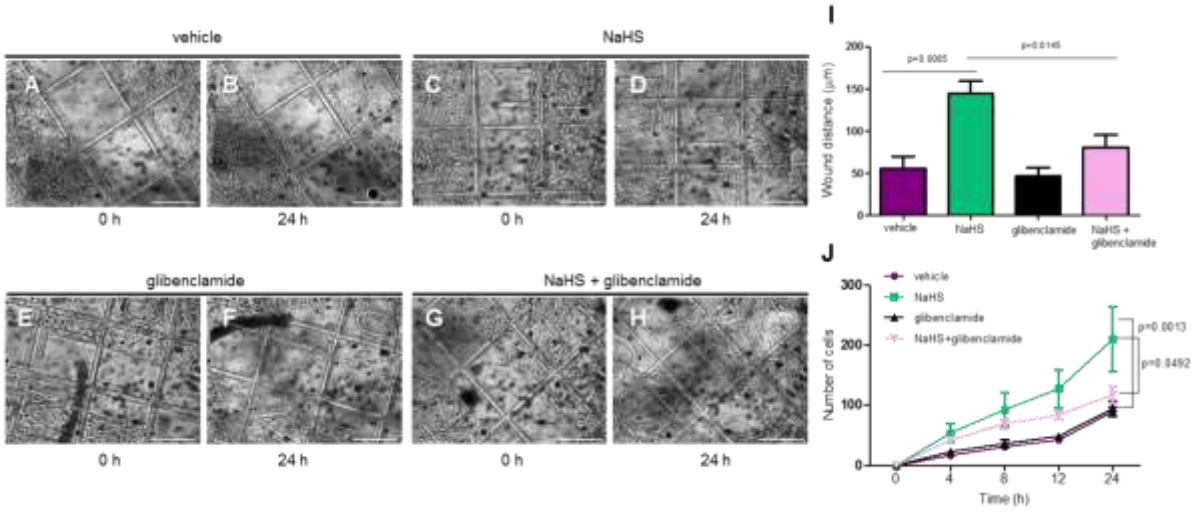

Figure 14 NaHS promotes wound closure in monolayers of primary mouse alveolar type II cells. Illustrative images taken at 0 h and 24 h representing wound closure in primary mouse alveolar type II (ATII) cell monolayers, in vehicle-treated (A, B), NaHS-treated (C, D), glibenclamide-treated (E, F), NaHS and glibenclamide-treated (G, H) ATII cells. I, data quantification for multiple experiments assessing wound closure at 24 h. Data represent the mean ± S.E. (n=6, per group). The p values were determined at one-way ANOVA with a Tukey's *post hoc* test. J, wound closure dynamics in primary mouse ATII cell monolayers over 24 h. Data represent the mean ± S.E. (n=6, per group). The p values were determined by two-way ANOVA (Madurga et al., 2014).

11.1.9 Impact of NaHS on Akt signaling in primary mouse alveolar type II cells

Further studies focused in the effect of NaHS treatment on protein kinase B (Akt) (Fig. 15), since Akt is known to play a role in repair processes in epithelial cells and to protect against hyperoxia-induced damage to the lung (Alphonse et al., 2011).

Measuring Akt phosphorylation as activation of the Akt pathway, NaHS (100 µM) treatment into ATII cells (Fig. 15A) and the MLE-12 mouse lung epithelial cell line (Fig. 15B) resulted in a fast (with 30 min) activation of the Akt pathway. Thus, H_2S delivery through NaHS may have a cell wound healing effect on ATII cells through activation of the Akt pathway. Moreover, the effect of H_2S administration (through GYY4137 treatment) on the activation of the Akt pathway was also assessed *in vivo*, in mouse pup lungs exposed either to 21% O_2 or 85% O_2 environment conditions (Fig. 15C). Hyperoxia conditions reduced the total levels of Akt protein, nonetheless GYY4137 administration although also had reduced levels of total Akt, promoted activation of Akt pathway (as assessed by phosphorylation) in the developing lung. Therefore, these data encourages the idea that Akt activation by GYY4137 might underlie some of the lung-protective effects in oxygen-injured lungs from mouse pups.

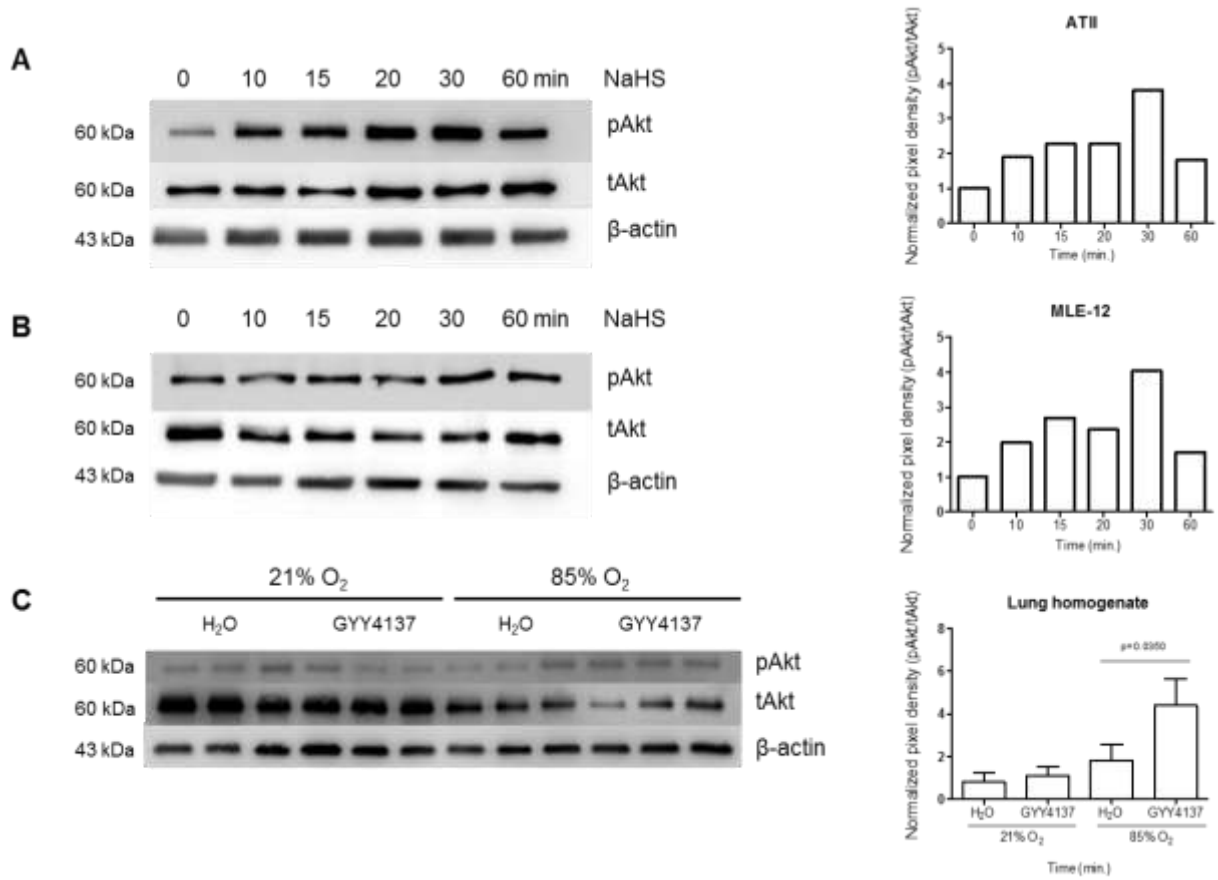

Figure 15 H_2S donors promote activation of Akt.

A, immunoblot representing protein expression levels of total Akt (tAkt) and levels of phosphorylated Akt (pAkt) from primary mouse alveolar type II (ATII) treated with NaHS, for 10, 15, 20, 30 or 60 min in cell protein extracts (25 µg). Data quantification of activated Akt was measured the ratio of phosphorylated to total Akt. B, similar data were obtained using MLE-12 cells. C, immunoblot representing protein expression levels of total (tAkt) and levels of phosphorylated Akt (pAkt) of protein extracts (20 µg) from mouse pup lungs exposed to either 21% O_2 or 85% O_2 for the first 10 days of life, that received either H_2O or GYY4137 (50 mg/kg/day, intraperitoneal). Data represent the mean ± S.D. (n=3, per group). The p values were determined by one-way ANOVA with a Tukey's *post hoc* test (Madurga et al., 2014).

11.2 The role of Cbs and Cth during late lung development

11.2.1 The expression of Cbs and Cth is dynamically regulated during alveolarization

Cbs and Cth are both enzymes that generate and regulate the release of H_2S in human and mouse (Nagahara, 2011; Olson, 2011; Wang, 2003, 2010). The expression mRNA levels of Cbs and Cth was dynamically regulated over the course of late lung development (Figure 16). Regarding Cbs, the data illustrates that the expression of Cbs was 16-fold down regulated between P2.5 and P3.5 over a period of 24 h, an remained down-regulated on P5.5 concomitant with the peak of septation at P5.5 (Massaro & Massaro, 2007; Warburton et al., 2010; Warburton et al., 2000). At P9.5, after secondary septation was mostly completed, the expression of Cbs was up-regulated 32-fold. Regarding Cth, the data illustrates that the expression of Cth was regulated in an opposite manner in comparison to Cbs. The expression of mRNA encoding Cth was four-fold up-regulated between P2.5 and P3.5, over a period of 24 h, and the peak of up-regulation was highest on P5.5, after which decreased by eight-fold on P9.5. This changing regulation of Cbs and Cth in an inverse manner with one another, points a role for Cbs and Cth during post-natal lung development.

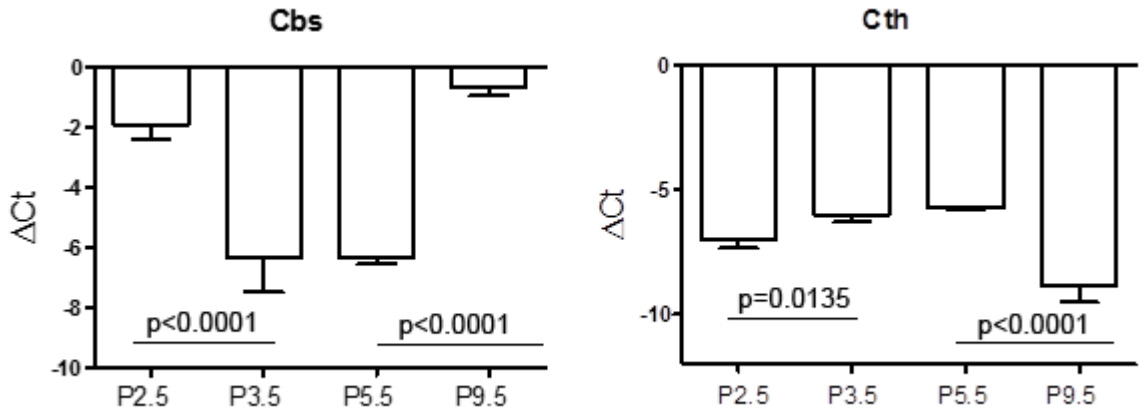

Figure 16 RT-PCR to assess changes of mRNA expression of Cbs and Cth, on different time points during normal late lung development.

Data represent the mean ΔCt ± S.E. (n=4, per group). The ΔCt values were compared by one-way ANOVA and Tukey's *post hoc* test. The primers used for the RT-PCR are listed in Table 2.

11.2.2 The expression of both Cbs and Cth can be abrogated during post-natal lung development in mice

To genotype transgenic mice semi-quantitative PCR analysis was performed using genomic DNA isolated from tail-cuts as template (primers listed in Table 3). Regarding Cbs, pups were generated from heterozygous parental animals, a single 450-bp band identified *Cbs*$^{-/-}$ homozygotes, a single 300-bp band identified wild type mice, or a 300-bp band together with a 450-bp band identified heterozygous mice (Fig. 17A). Immunoblot was used to confirm loss of Cbs protein expression (Fig. 18A). Regarding Cth, the homozygous *Cth*$^{-/-}$ pups were obtained by mating homozygous *Cth*$^{-/-}$ parental animals, a single 199-bp band identified *Cth*$^{-/-}$ pups, while a single 299-bp band identified wild-type animals (Fig. 17B). Immunoblot was used to confirm loss of CTH protein expression (Fig. 18B).

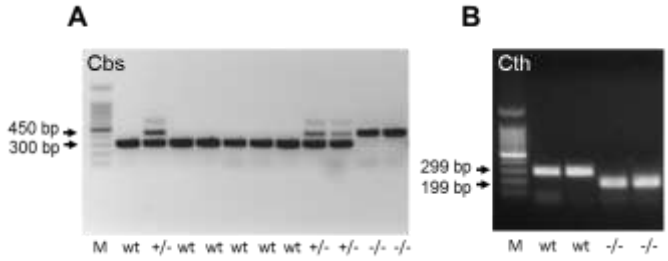

Figure 17 Genotyping of mouse pups for Cbs and Cth.
A, illustration of PCR genotyping wild type mice (wt; 300 bp), Cbs heterozygote mice (+/-; 300-bp and 450-bp) and *Cbs*$^{-/-}$ mice (-/-; 450-bp). B, illustration of PCR genotyping of wild type mice (wt; 299-bp) and *Cth*$^{-/-}$ mice (-/-; 199-bp). M, marker; wt, wild type.

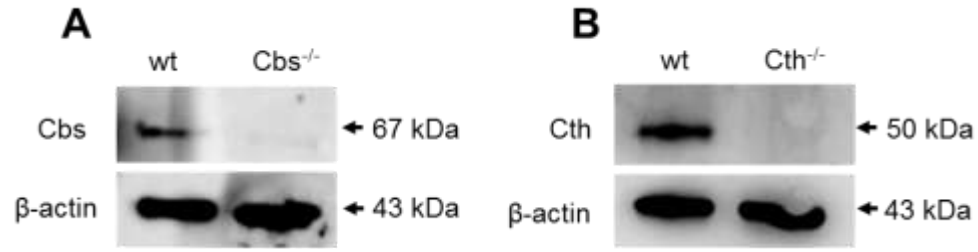

Figure 18 Loss of Cbs and Cth expression in lungs of *Cbs*$^{-/-}$ and *Cth*$^{-/-}$ mice by immunoblot.
A, immunoblot from whole-lung homogenates resolved with an anti-Cbs antibody (67 kDa) in wild-type mice and Cbs-null homozygotes (-/-). B, same situation as (A) but probed with an anti-Cth antibody (50 kDa) in wild type mice and Cth-null homozygotes (-/-). β-actin was used as loading control; wt, wild type.

11.2.3 Loss of Cbs or Cth impairs normal lung alveolarization in mice. Lung histology

When inspecting lung histology sections from wild-type mice at P7.5 (Fig. 19A) in comparison to age-matched *Cbs*$^{-/-}$ mice (Fig. 19B) and *Cth*$^{-/-}$ mice (Fig. 19C), the lung structure of *Cbs*$^{-/-}$ and *Cth*$^{-/-}$ mice suggested to be less complex - implying fewer but larger alveoli - indicating that both Cbs and Cth were necessary for proper late lung development. On P14.5, this effect was more evident, and both *Cbs*$^{-/-}$mice (Fig. 19E) and *Cth*$^{-/-}$ mice (Fig. 19F) presented a more immature lung structure, with less alveoli and enlarged air spaces compared to wild type mice (Fig. 19D).

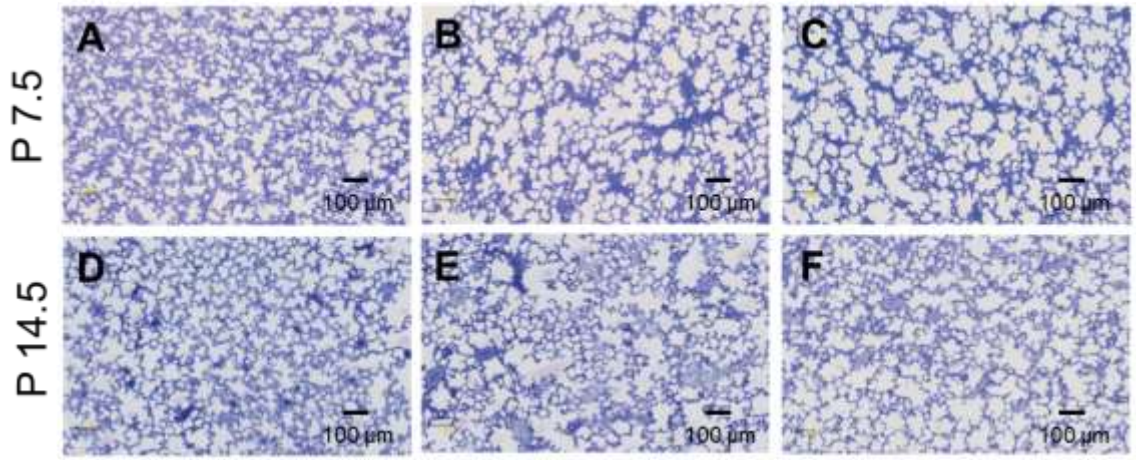

Figure 19 Representative lung histology of postnatal day P7.5 and P14.5 of wild type mice, *Cbs*$^{-/-}$ mice, and *Cth*$^{-/-}$ mice.

Lung histology representative images at postnatal day P7.5 of wild type mice (A), *Cbs*$^{-/-}$ mice (B) and *Cth*$^{-/-}$ mice (C). Lung histology representative images of postnatal day P14.5 of wild type mice (D), *Cbs*$^{-/-}$ mice (E) and *Cth*$^{-/-}$ mice (F). Sections stained with Richardson's staining at 10 × magnification, scale bar of 100 µm.

11.2.4 Loss of Cbs or Cth impairs normal alveolarization in mice. Stereology analysis

The histological observations were confirmed by stereological analysis which were fully evident on P14.5 (Table 8, 9 and Figures 20 and 21). Lung volumes of both *Cbs*$^{-/-}$ and *Cth*$^{-/-}$ mice decreased approx. 25 % compared to wild type mice. The lung volumes values decreased from 0.31 ± 0.01 cm^3 in the wild type mice, to 0.23 ± 0.009 cm^3 in the *Cbs*$^{-/-}$ mice and to 0.24 ± 0.02 cm^3 in the *Cth*$^{-/-}$ mice. The number of alveoli of both *Cbs*$^{-/-}$ and *Cth*$^{-/-}$ mice lowered down to approx. 50% compared to the wild type mice. The number of alveoli decreased from 4.74 ± 0.42 × 10^6 alveoli/both lungs in the wild type mice, to 2.30 ± 0.20× 10^6 alveoli/both lungs in the *Cbs*$^{-/-}$ mice, and to 2.81 ± 0.78 × 10^6 alveoli/both lungs in the *Cth*$^{-/-}$ mice. Regarding the mean linear intercept, it changed, increasing from 30.85 ± 1.0 µm in wild type mice to 38.15 ± 3.4 µm in the *Cbs*$^{-/-}$ mice, and it also increased to 43.2 ± 6.8 µm in the *Cth*$^{-/-}$ mice. In regards of septal thickness, the values were similar among all the groups, from 10.4 ± 0.4 µm in the wild type mice to 12.9 ± 1.8 µm in the *Cbs*$^{-/-}$ mice and of 9.4 ± 0.6 µm in the *Cth*$^{-/-}$ mice. Moreover, the surface area for gas exchange was smaller in both *Cbs*$^{-/-}$ and *Cth*$^{-/-}$ mice when compared to the wild type mice. The surface area values decreased almost 50 %, ranging from 220.8 ± 13.1 cm^2 in the wild type mice, to 134.2 ± 5.9 cm^2 in the Cbs$^{-/-}$ mice and to 154 ± 22.6 cm^2 in the *Cth*$^{-/-}$ mice. Taken together, this data suggest that both Cbs and Cth play a role during normal late lung development.

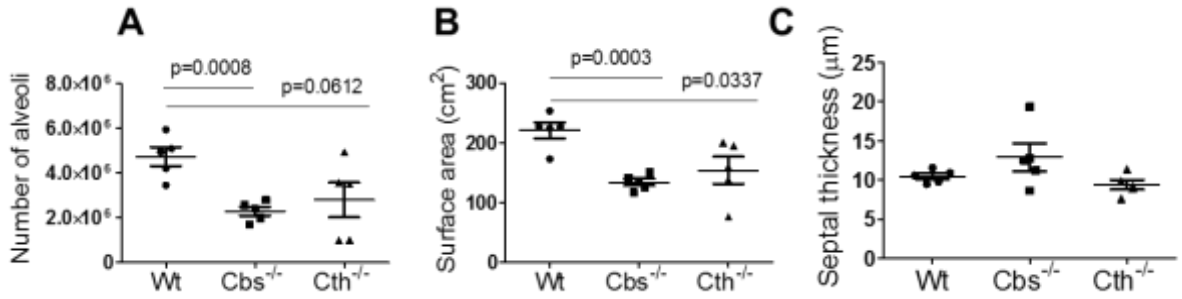

Figure 20 Aberrant late lung development in the *Cbs*$^{-/-}$ mice and *Cth*$^{-/-}$ mice assessed via stereology methods.

Stereology analysis on postnatal day P14.5 of wild type mice (wt), *Cbs*$^{-/-}$ mice and *Cth*$^{-/-}$ mice representing number of alveoli (A), surface area (B) and septal thickness (C). Data represent the mean ± S.E. (n=5 per group). The differences between groups were determined by unpaired Student *t* test.

Table 8 Stereological parameters of wild type mice, *Cbs*$^{-/-}$ mice and *Cth*$^{-/-}$ mice on postnatal day P7.5.

Parameter	P7.5				
	Wt	Cbs$^{-/-}$	*p* values Wt to Cbs$^{-/-}$	Cth$^{-/-}$	*p* values Wt to Cth$^{-/-}$
V (lung) [cm^3]	0.20 ± 0.02	0.17 ± 0.03	0.448	0.17 ± 0.02	0.2649
CV [V (lung)]	0.24	0.36		0.22	
V_V (par/lung) [%]	89.24 ± 2.09	91.01 ± 1.46	0.5076	89.00 ± 1.81	0.9336
V_V (non-par/lung) [%]	10.76 ± 2.01	8 ± 1.46	0.5076	11.00 ± 1.81	0.9336
S_V (alv epi/par) [cm^{-1}]	599.1 ± 34.18	589.7 ± 30.86	0.8423	628.5 ± 22.87	0.4955
S (alv epi, lung) [cm^2]	106.2 ± 14.62	89.42 ± 13.01	0.4149	92.64 ± 10.21	0.4672
CV [S (alv epi, lung)]	0.31	0.32		0.25	
V (alv air, lung) [cm^3]	0.09 ± 0.01	0.08 ± 0.01	0.3997	0.09 ± 0.01	0.9150
CV [V (alv air, lung)]	0.24	0.24		0.23	
V (sep, lung) [cm^3]	0.09 ± 0.01	0.08 ± 0.01	0.5030	0.06 ± 0.007	0.0440
CV [V (sep, lung)]	0.32	0.49		0.29	

Wt, wild type mice; *V*, volume; V_V, volume density; *S*, surface area; S_V, surface density; *CV*, coefficient of variation; *par*, parenchyma; *non-par*, non-parenchyma; *alv air*, alveolar airspaces; *alv epi*, alveolar epithelium; *sep*, septum. Values are presented as mean ± S.E, n=5 lungs per group. *p* values were calculated by Student *t* test.

Table 9 Stereological parameters of wild type mice, *Cbs*$^{-/-}$ mice and *Cth*$^{-/-}$ mice on postnatal day P14.5

Parameter	P14.5				
	Wt	Cbs$^{-/-}$	*p* values Wt to Cbs$^{-/-}$	Cth$^{-/-}$	*p* values Wt to Cth$^{-/-}$
V (lung) [cm^3]	0.31 ± 0.01	0.23 ± 0.009	0.0023	0.24 ± 0.02	0.0471
CV [*V* (lung)]	0.12	0.09		0.22	
V_V (par/lung) [%]	93.01 ± 2.2	91.72 ± 2.0	0.6727	92.33 ± 1.8	0.8151
V_V (non-par/lung) [%]	6.99 ± 2.2	8.28 ± 2.0	0.6728	7.68 ± 1.8	0.8151
S_V (alv epi/par) [cm^{-1}]	756.5 ± 15.9	641.2 ± 41.5	0.0320	676.9 ± 65.9	0.2741
S (alv epi, lung) [cm^2]	220.8 ± 13.1	134.2 ± 5.9	0.0003	154 ± 22.6	0.0337
CV [S (alv epi, lung)]	0.13	0.10		0.33	
V (alv air, lung) [cm^3]	0.17 ± 0.01	0.13 ± 0.01	0.0281	0.15 ± 0.02	0.4956
CV [*V* (alv air, lung)]	0.16	0.19		0.27	
V (sep, lung) [cm^3]	0.12 ± 0.01	0.09 ± 0.01	0.0259	0.07 ± 0.01	0.0045
CV [*V* (sep, lung)]	0.18	0.24		0.28	

Wt, wild type mice; *V*, volume; V_V, volume density; *S*, surface area; S_V, surface density; *CV*, coefficient of variation; *par*, parenchyma; *non-par*, non-parenchyma; *alv air*, alveolar airspaces; *alv epi*, alveolar epithelium; *sep*, septum. Values are presented as mean ± S.E, n=5 lungs per group. *p* values were calculated by Student *t* test.

11.2.5 Loss of Cbs or Cth affects lung development, transition from P7.5 to P14.5

During the transition between P7.5 and P14.5, the changes in lung structure for wild type mice (illustrated in blue color), *Cbs*$^{-/-}$ mice (illustrated in grey color) and *Cth*$^{-/-}$ mice (illustrated in black color) are resumed in figure 21. Interestingly, the rate of lung volume (Fig. 21A), alveoli number (Fig. 21C) and surface area (Fig. 21E) augmented more exponentially in the case of wild type mice in comparison to both *Cbs*$^{-/-}$ and *Cth*$^{-/-}$ mice. These changes were more obvious in the case of the *Cbs*$^{-/-}$ mice. For instance, the number of alveoli per cm^3 (Fig. 21B) between P7.5 and P14.5 was equivalent between wild type mice and *Cth*$^{-/-}$ mice whereas was reduced in *Cbs*$^{-/-}$ mice. This situation was also observed in other parameters, like the alveolar septal volume (Table 9), suggesting fewer alveoli per unit volume being produced in the *Cbs*$^{-/-}$ mice. Taken together, this data indicates an alveolar impairment during late lung development in *Cbs*$^{-/-}$ and *Cth*$^{-/-}$ mice, highlighting roles for Cbs and Cth in normal lung growth and maturation.

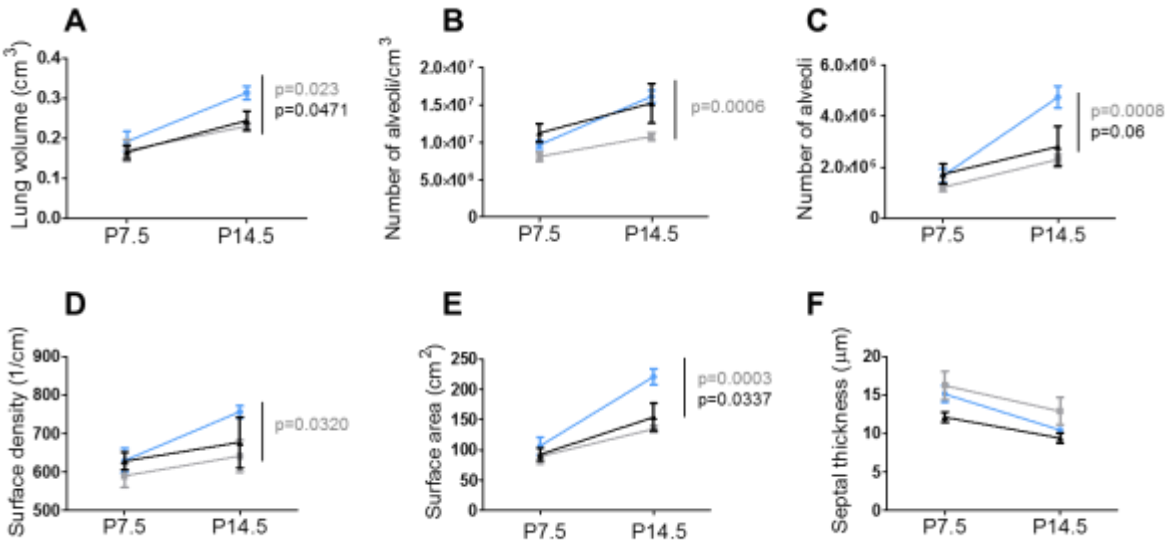

Figure 21 Aberrant late lung development in the *Cbs*$^{-/-}$ mice and *Cth*$^{-/-}$ mice assessed via stereology methods, evolution from P7.5 to P14.5.

Stereology representation of lung volume (A), number of alveoli per cm^3 (B), number of alveoli (C), surface density (D), surface area (E) and septal thickness (F). Wild type mice are represented in blue color, *Cbs*$^{-/-}$ mice represented in grey color, and *Cth*$^{-/-}$ mice represented in black color. Data represent the mean ± S.E. (n=5 per group). The p values show the statistics on P14.5 and, the differences between groups were determined by unpaired Student *t* test.

11.2.6 Both Cbs and Cth are preferentially expressed in specific lung compartments

To identify if Cbs and Cth expression was confined to specific lung compartments, cryopreserved sections from mouse pup lungs at P7.5 and P14.5 were micro dissected using a laser-capture micro dissection system (Leica LMD 6500). A RT-PCR analysis was used to screen the expression of mRNA encoding Cbs and Cth in micro dissected tissue. These two time points during late lung development were chosen, the first on P7.5 close to the peak of septation, and the other on P14.5 close to the micro vessel maturation (Massaro & Massaro, 2007; Warburton et al., 2010; Warburton et al., 2000). As is illustrated in figure 22, Cbs was more expressed in the airway at P7.5 (Fig. 22A), and in the vascular compartment at P14.5 compared with the parenchymal compartment (Fig. 22B). In the case of Cth expression, at P7.5 Cth expression was equivalent in all three compartments (Fig. 22C), but more elevated in the airway compartment at P14.5 (Fig. 22D). A representation of the laser-capture micro dissection process is presented for the vascular compartment (in this case, most likely a pulmonary artery), as an example, in Fig. 22E, 22F, and 22G.

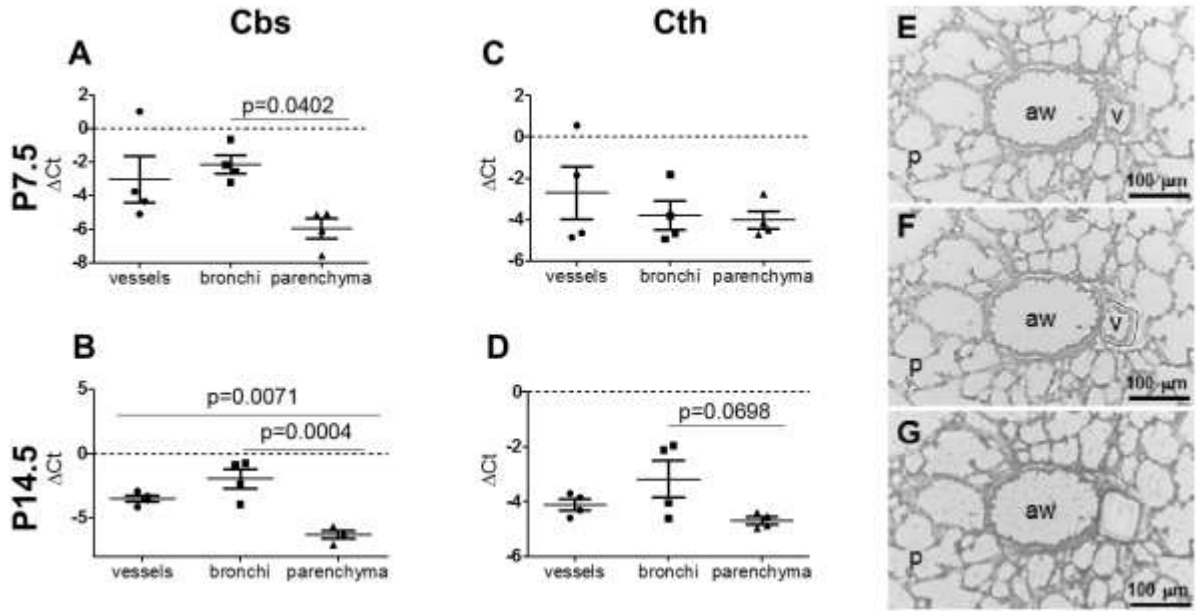

Figure 22 Cbs and Cth are mostly expressed in the airway and vascular compartment.

RT-PCR analysis of Cbs (A) and Cth (C) on P7.5, and of Cbs (B) and Cth (D) on P14.5 to assess the expression in the vascular, airway and parenchymal compartment. Data represent the ΔCt ± S.E. (n=4 per group). The differences between groups were determined by one-way ANOVA with Tukey's *post hoc* test. The laser-capture micro dissection process is offered for the vessel compartment (in this case most likely a pulmonary artery), as an example in E, F and G. Parenchyma compartment (p), airway compartment (aw) and vascular compartment (v). Scale bar of 100 µm.

11.2.7 Both Cbs and Cth localize to the airways and vessel walls in the lungs of mouse pups

Serial sections of wild-type mouse pup lungs were stained by immunofluorescence to detect the expression of CBS and CTH in the lung architecture. Serial sections were stained with vWF (Fig. 23B) and αSMA staining (Fig. 23B) to discriminate the vascular and airway compartments. The immunoreactivity for CBS was detected in the airway epithelium and the lung vessel walls (Fig. 23A and Fig. 23C). The better immunoreactivity of anti-Cbs antibodies in Fig. 23A compared with Fig. 23C is due to the superior performance of anti-Cbs antibodies in the vWF staining protocol (Fig. 23A, B) compared with the αSMA staining protocol (Fig. 23C, D). In the same manner as CBS, CTH immunoreactivity was positive in the lung vessel walls and the airway epithelium (Fig. 24A and Fig. 24C, respectively). Both CBS and CTH were weakly detected in the lung parenchyma (Fig. 23 and Fig. 24, respectively). As negative controls, a pre-immune isotype-matched primary antibody (Fig. 23E and Fig. 24E) or lung sections from *Cbs*$^{-/-}$ and *Cth*$^{-/-}$ mice (Fig. 23F and Fig. 24F, respectively) were immunofluorescence stained for both CBS and CTH. The data presented here, validates the previously presented data on laser-capture micro dissection gene expression for Cbs (Fig. 22A, B) and Cth (Fig. 22C, D), and highlight plausible roles for Cbs and Cth in the in the airways and pulmonary vasculature during late lung development.

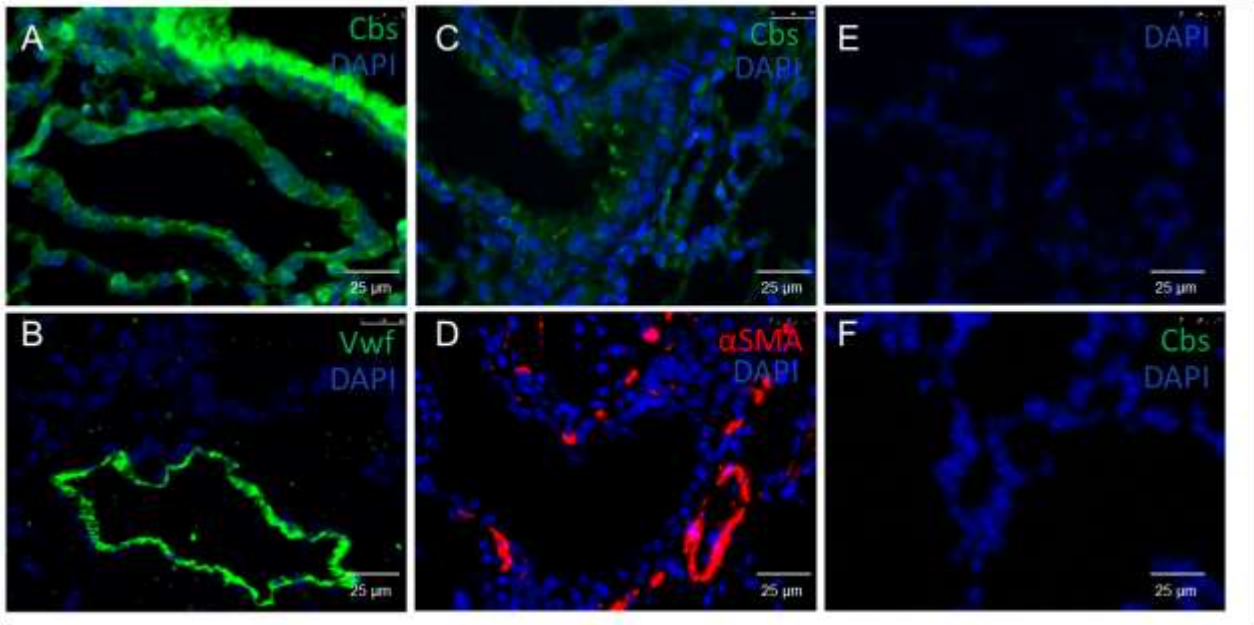

Figure 23 Localization of CBS in the airways, vessel walls and alveolar epithelium.

Serial sections (A combined with B; and C combined with D) were co-stained, to determine CBS localization in a mouse lung on P14.5. Serial sections stained for CBS and von Willebrand Factor (vWF), to assess Cbs expression in the lung vasculature (A, B); serial sections stained for CBS and alpha smooth muscle actin (αSMA) to assess expression in the pulmonary smooth muscle (C, D). As controls, lung sections were stained using a non-immune IgG as primary antibody instead of the anti-Cbs antibody (E), and staining for CBS on *Cbs*$^{-/-}$ mouse lung tissue (F). Cell nuclei were revealed with 4′,6-diamidino-2-phenylindole (DAPI). Scale bar of 25 µm.

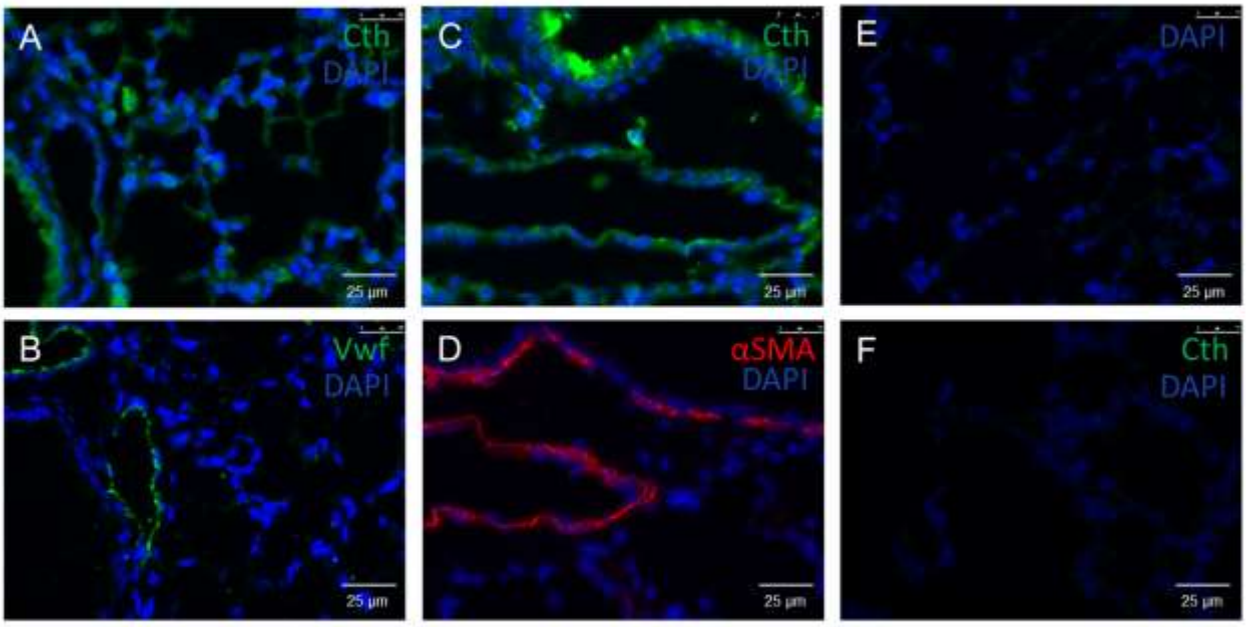

Figure 24 Localization of CTH in the airways, vessel walls and alveolar epithelium.

Serial sections (A combined with B; and C combined with D) were co-stained, to determine CTH localization in a mouse lung on P14.5. Serial sections stained for CTH and von Willebrand Factor (vWF), to assess CTH expression in the lung vasculature (A, B); serial sections stained for CTH and alpha smooth muscle actin (αSMA) to assess expression in the pulmonary smooth muscle (C, D). As controls, lung sections were also stained using a non-immune IgG as primary antibody instead of the anti-Cth antibody (E), and staining for CTH on *Cth*$^{-/-}$ mouse lung tissue (F). Cell nuclei were revealed with 4′,6-diamidino-2-phenylindole (DAPI). Scale bar of 25 µm.

11.2.8 Both Cbs and Cth contribute to the development or maintenance of normal pulmonary vasculature

Blood vessels in the lung play an important role promoting normal lung development and preserving correct alveolar structures throughout alveologenesis. An incorrect or poor blood flow distribution may outcome in lung abnormality (Iosef et al., 2012; Pereda et al., 2013; Thebaud, 2007).

Taking into account that both *Cbs*$^{-/-}$ mice and *Cth*$^{-/-}$ mice have an impaired lung development, and that both CBS and CTH are mainly expressed in the vessel and airway compartment, attention was driven to the density of vessels for both *Cbs*$^{-/-}$ and *Cth*$^{-/-}$ mice.

Using antibodies against αSMA, vWF, and performing a Van Gieson staining with Fuchsin-Resorcin in paraffin embedded neonatal lung mouse sections, the vessel density, the vessel muscularization and the MWT index of vessels was counted. As it is illustrated in Figure 25, an approximation of vascular supply by visual inspection of histological sections from developing mouse lungs was diminished (Fig. 25) in both *Cbs*$^{-/-}$ mice (Fig. 25C) and *Cth*$^{-/-}$ mice (Fig. 25D) compared to wild type mice (Fig. 25B). Furthermore, lung homogenates from postnatal wild type mice, *Cbs*$^{-/-}$ mice and *Cth*$^{-/-}$ mice were evaluated for measuring the expression of CD31 [platelet endothelial cell adhesion molecule (PECAM)-1], an endothelial marker. Remarkably, the expression of CD31 was lower in lung homogenates from both *Cbs*$^{-/-}$ and *Cth*$^{-/-}$ mice when compared to wild type mice as it is shown in Figure 25 (Fig 25 E and F) suggesting that the loss of Cbs or Cth may result in deficient vascular growth in developing mouse lungs.

The degree of muscularization of pulmonary vessels (Fig. 26) indicated that the genetic absence of Cbs (Fig. 26E) and Cth (Fig. 26F) led to a pronounce increase in the degree of muscularization of small vessels (diameter 20-70 µm). Additionally, increased muscularization of medium vessels (diameter 70-150 µm) was also noted in the *Cbs*$^{-/-}$ mice. The degree of muscularization had no affection on the large vessels (diameter >150 µm). Consistent with this experiment, the measurement of the MWT index showed the same trend as the degree of muscularization for both *Cbs*$^{-/-}$ and *Cth*$^{-/-}$ mice (Figure 27). Taken together, this data suggests that both Cbs and Cth play a role in the development or maintenance of the normal pulmonary vasculature in developing mouse lungs.

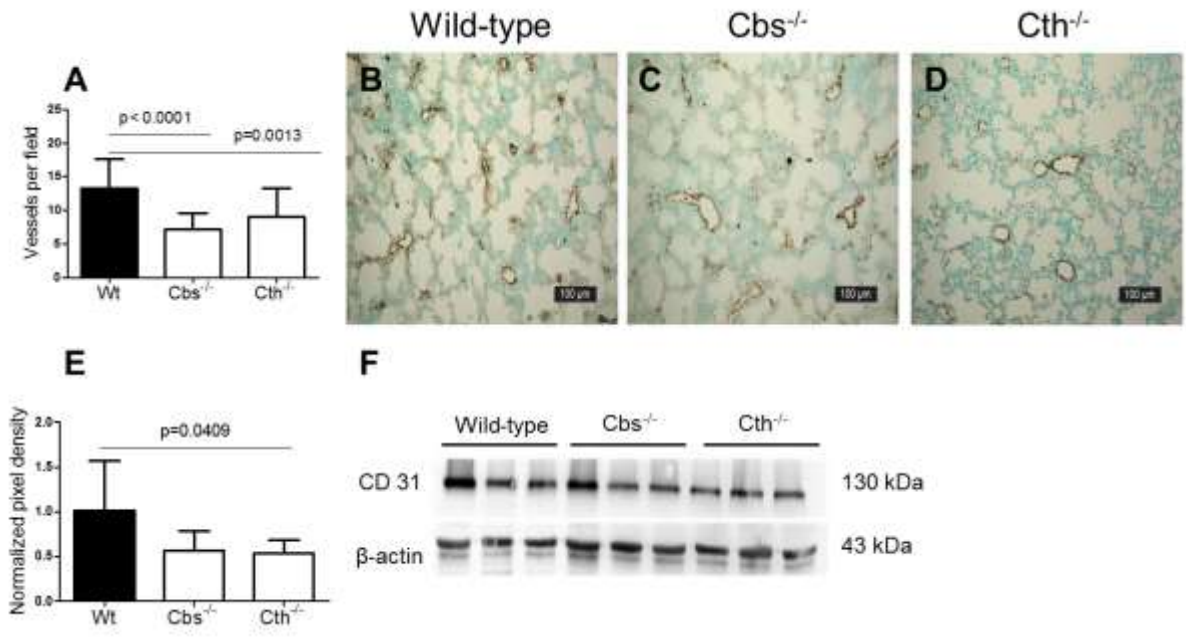

Figure 25 Decreased vascular supply in the *Cbs*$^{-/-}$ mice and the *Cth*$^{-/-}$ mice.

A, quantification of vascular supply per field and per group: Wild type mice (wt), *Cbs*$^{-/-}$ mice and *Cth*$^{-/-}$ mice. Representative stained sections are illustrated for wild type mice (B), *Cbs*$^{-/-}$ mice (C) and *Cth*$^{-/-}$ mice (D), stained with von Willebrand factor (brown) and alpha smooth muscle actin (purple). Magnification 20×, scale bar of 100 µm. Data represent the mean number of vessels cross-section per microscopic field ± S.E. (n=3-4, per group). The p values were determined by one-way ANOVA with Tukey's *post hoc* test. E and F, total mouse pup lung homogenates were tested for CD31 expression by immunoblot. The histogram represents the mean ± S.E. normalized pixel density were the CD31 band was normalized for the pixel density of the β-actin band from the same sample (n=3, per group). Differences between groups were determined by one-way ANOVA with Tukey's *post hoc* test.

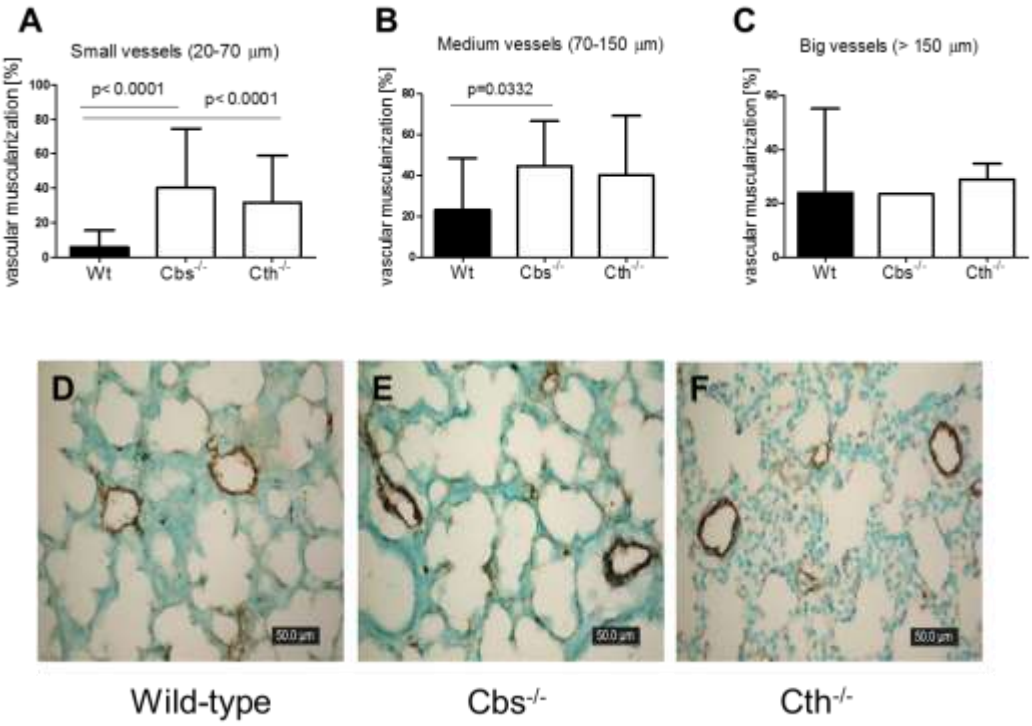

Figure 26 Loss of Cbs or Cth promotes increased muscularization of small pulmonary vessels. The degree of muscularization of lung vessels were calculated in three different groups: Small vessels (diameter 20-70 µm) (A), medium vessels (diameter 70-150 µm) (B) and large vessels (diameter >150 µm) (C). Illustrative stained sections are represented for wild type (D), *Cbs*$^{-/-}$ mice (E) and *Cth*$^{-/-}$ mice (F). Staining of alpha smooth muscle actin (purple) and von Willebrand factor (brown), 40× magnification, scale bar of 50 µm. Data represent the mean muscularization (%) ± S.E. (n=3-4, per group). Differences between groups were determined by one-way ANOVA with Tukey's *post hoc* test.

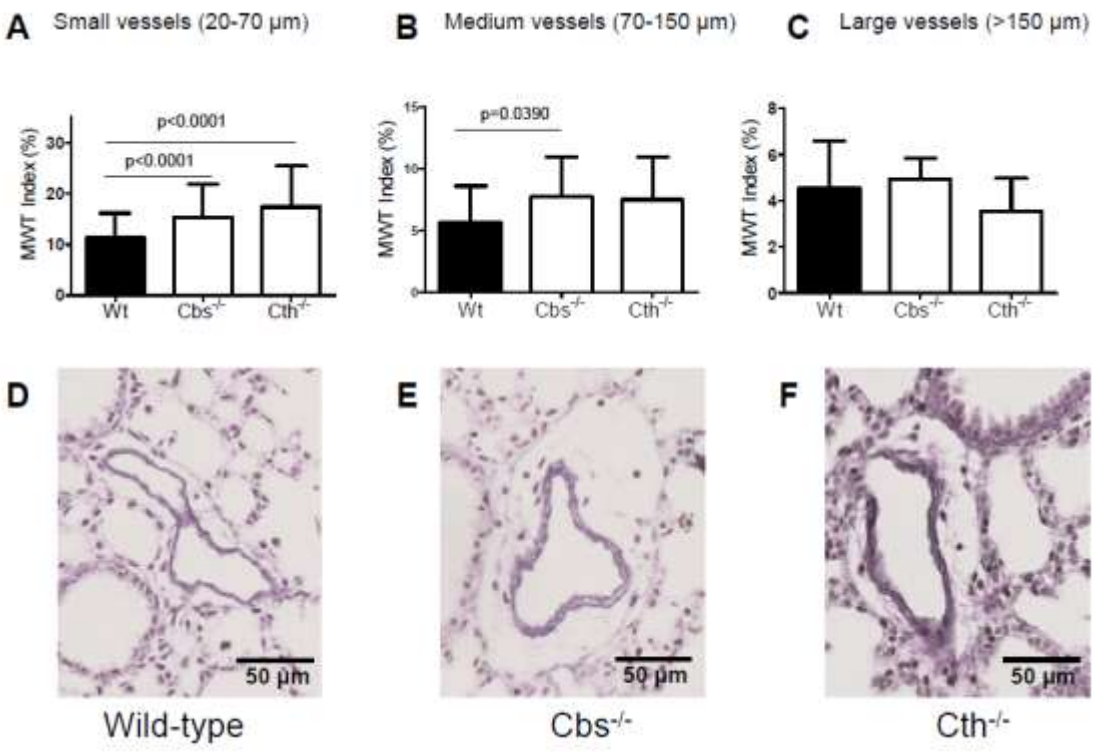

Figure 27 Loss of Cbs or Cth leads to an increase in an index of medial wall thickness in small pulmonary vessels.The index of medial wall thickness (MWT) was determined in van Gieson-stained paraffin embedded lung sections from wild-type mice, *Cbs*$^{-/-}$ mice and *Cth*$^{-/-}$ mice, and differentiated in three different groups: Small vessels (diameter 20-70 µm) (A), medium vessels (diameter 70-150 µm) (B) and large vessels (diameter >150 µm). Illustrative stained sections are represented for wild type mice (D), *Cbs*$^{-/-}$ mice (E) and *Cth*$^{-/-}$ mice (F), 40× magnification, and scale bar of 50 µm. Data represent the mean muscularization (%) ± S.E. (n=3-4, per group). Differences between groups were determined by one-way ANOVA with Tukey's *post hoc* test.

11.2.9 Both Cbs and Cth participate in the angiogenesis of human pulmonary microvascular endothelial cells

To further comprehend the role of CBS in the angiogenesis of HPAEC, a Matrigel assay was performed after transfecting HPAEC cells either with scrambled (200 nM) or siRNA CBS (200 nM) for 48 h, and loaded into the Matrigel for 24 h, represented in Figure 28. Inhibition of CBS expression did not affect the number of tubes formed (Fig. 28D), yet strongly disturbed tube length (Fig. 28C). An immunoblot is represented (Fig. 28E) assessing the efficiency of the CBS knockdown, and quantified in Fig. 28F. The HPAEC were also tested to study the role of CTH in angiogenesis (Fig. 29). Several attempts to use siRNA to inhibit CTH were unsuccessful (results not shown). Still, propargylglycine (PAG) is a small-molecule known to ablate the expression of CTH (Papapetropoulos et al., 2009; Szabó, 2011), and at both 1 mM and 3 mM concentration, PAG effectively reduced the formation of vessels and the length of vessels (Fig. 29C and D). Furthermore, GYY4137, a H_2S donor, increased meaningfully the formation of new tubes when compared to vehicle, and also increased the length of vessels (Fig. 29B). In no case did siRNA, GYY4137 or PAG treatments any consequence on HPAEC viability (results not shown). These data support the idea that both Cbs and Cth play a role in the formation of endothelial tubes formed, since their inhibition interrupts a proper vessel network formation, and that hydrogen sulfide, a byproduct of their reaction, promotes it.

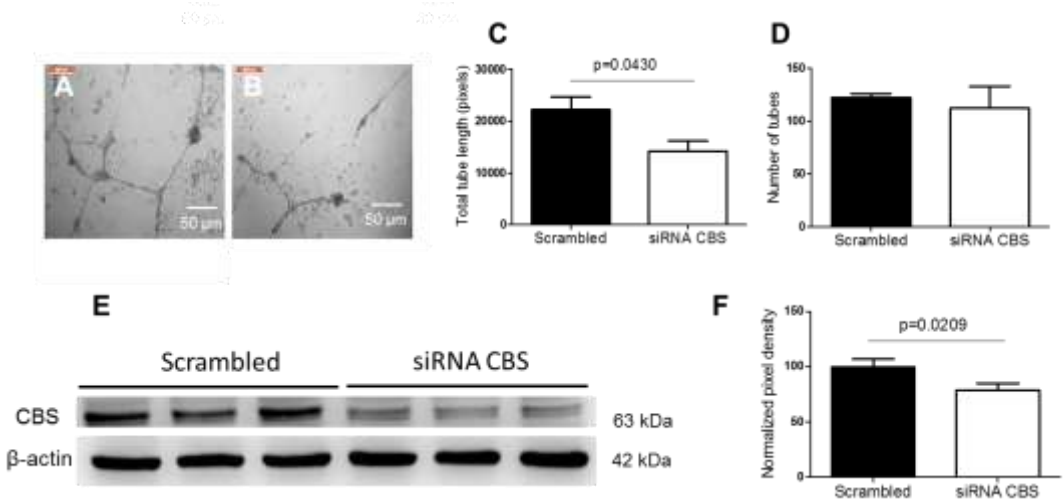

Figure 28 Inhibition of CBS expression alters tube formation *in vitro*.

Tube formation assay of human pulmonary endothelial cells in a Matrigel plate using either scrambled or siRNA CBS. Representative pictures were taken from scrambled 200 nM (A) and siRNA CBS 200 nM (B) after 48 h of transfection and 24 h incubation in a Matrigel plate. Magnification 5×, scale bar 50 µm. Quantification of number of tubes (C) and quantification of tube length (D), protein expression levels of CBS (25 µg) showing the efficiency of CBS knockdown by siRNA treatment was assessed by immunoblot of cell homogenates and probed with anti-CBS antibody (E). The bands from (E) were quantified by densitometry analysis (F). Data represent the mean ± S.E. (n=3, per group). Differences between groups were determined by unpaired Student *t* test.

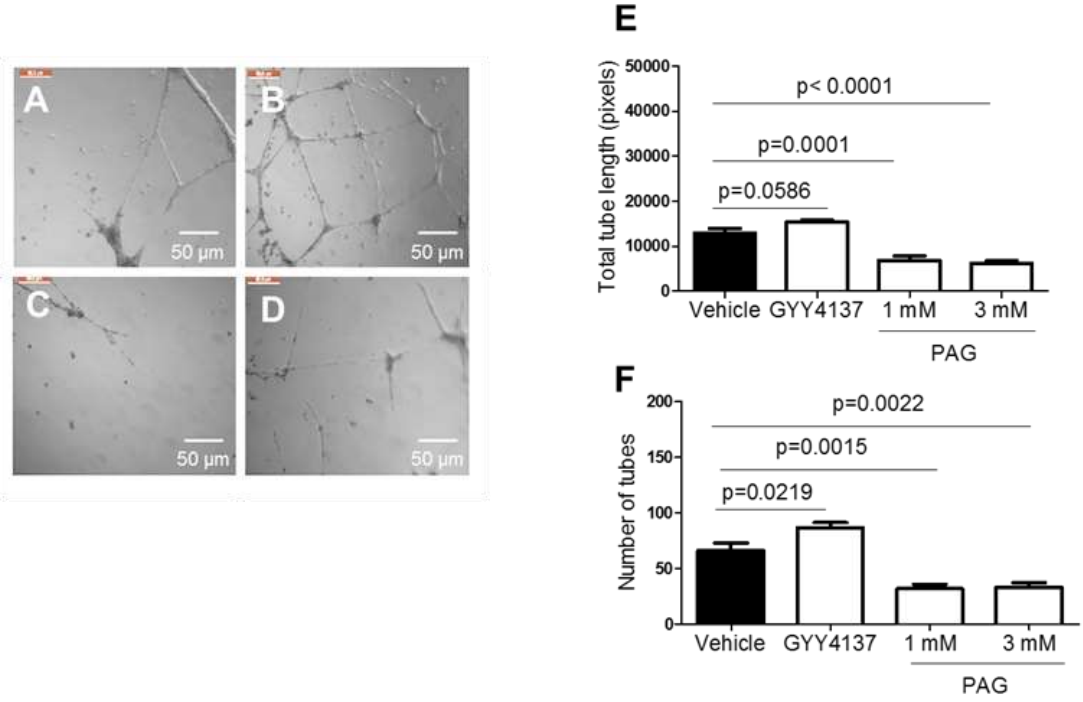

Figure 29 CTH and H_2S modulate endothelial tube formation *in vitro*.

Tube formation assay of human pulmonary endothelial cells in a Matrigel plate after pre-treatment using either vehicle alone, propargylglycine (PAG) or GYY4137. Representative pictures were taken from vehicle alone (A), GYY4137 100 µM (B), PAG 1 mM (C) and PAG 3 mM (D). Magnification 5×, scale bar 50 µm. Quantification of tube length (E) and number of tubes (F), Data represent the mean ± S.E. (n=3, per group). Differences between groups were evaluated by one-way ANOVA with Tukey's *post hoc* test.

12 Discussion

The first central question of this study was: Does systemic administration of H_2S (via the slow-release H_2S donor GYY4137) improve alveolarization of immature lungs that are exposed to 85% O_2 environment over the perinatal period? The starting approach of the study was to perform a stereological analysis to assess changes in the lung structure of developing lungs that were damaged by hyperoxia exposure. The experiment involves the prior maintenance of the lung structure, continued with SUR sampling and followed by the stereological analysis for the determination of the total number of alveoli, MLI and septal thickness (Schneider & Ochs, 2013). Nowadays this approach represents the highest standard in lung structural analysis available, recommended by both the European Respiratory Society and the American Thoracic Society (Hsia et al., 2010). The Green Journal has evaluated the pros and cons of this approach in a recent review (Muhlfeld & Ochs, 2013; Ochs & Muhlfeld, 2013). Up until now, other groups have assessed the stereological analysis of adult lungs (Fehrenbach et al., 2008; Knudsen et al., 2013; Knust et al., 2009; Muhlfeld & Ochs, 2013; Ochs & Muhlfeld, 2013; Schneider & Ochs, 2013, 2014). Still, this study presents for the first time the changes in the lung structure of immature mouse pup lungs during perinatal development (Madurga et al., 2014). From the stereological analysis, it was observed a dramatic reduction in the total number of alveoli in the lung, from $2.10 \pm 0.23 \times 10^6$ alveoli/both lungs in mice exposed to 21% O_2 for the first ten days of life to $0.92 \pm 0.08 \times 10^6$ alveoli/both lungs in mice exposed to 85% O_2 for the first ten days of life. Moreover, the septal thickness was also affected, by a 29% increase. Administering GYY4137, a slow-release H_2S donor, partially restored the lung abnormalities caused by the effects of hyperoxia on mouse late lung development. Administration of GYY4137 doubled the total number of alveoli in GYY4137-treated mouse pups, from $0.92 \pm 0.08 \times 10^6$ alveoli/both lungs in vehicle-treated pups exposed to 85% O_2, to $1.70 \pm 0.15 \times 10^6$ alveoli/both lungs in GYY4137-treated pups exposed to 85% O_2, and normalized septal thickness. Nonetheless, the significant improvement in the number of alveoli caused by the GYY4137 administration, still fell short in comparison to the $2.10 \pm 0.23 \times 10^6$ alveoli/both lungs present in the healthy control group of mouse pups at P10 that breathed 21% O_2. The above mentioned data confirms that H_2S administration can partially reduce the impaired alveolarization of immature mouse lungs caused by exposure to 85% O_2 over the perinatal period (Madurga et al., 2014).

The protective effects of H_2S on disrupted late lung development provoked by hyperoxia, may have been caused by the accredited physiological characteristics of H_2S. These properties include antioxidant, anti-inflammatory, vasoactive and cytoprotective activities ascribed to H_2S (Stein & Bailey, 2013). On the other hand, impaired alveolarization in response to hyperoxia is related to inflammation (Blackwell et al., 2011), oxidative stress (Saugstad, 2010), cell death and apoptosis (Dieperink et al., 2006), and perturbed pulmonary vascular development and hemodynamics (Thebaud & Abman, 2007; Thebaud et al., 2005). In that context, it was demonstrated in this study the anti-inflammatory properties of H_2S in repairing lung development to mouse pups. Hyperoxia induced inflammatory cell infiltration into the alveolar spaces of mouse pups developing lungs, which was reduced when GYY4137 was concomitantly administered. The H_2S donor limited the macrophage, neutrophil, eosinophil and monocyte infiltration into the alveolar air spaces. Thus, the capability of GYY4137 to partially restore normal lung alveolarization may be partially explained through the ability of GYY4137 to blunt the inflammation caused by 85% O_2 in immature developing lungs.

Inflammatory cell dynamics was considered to be one mechanism of action through which GYY4137 could modulate pro- and anti-inflammatory chemokines and cytokines levels in the alveolar airspaces. From the data obtained in this study, hyperoxia exposure increased IL-6 levels and decreased IL-10 levels favoring a pro-inflammatory environment in the immature mouse lungs. These data is consistent with previous work of other groups, where is described that hyperoxia can drive IL-6 production from fetal rat ATII cells (Gavino et al., 2002), and that IL-6 levels are elevated in a baboon model of BPD (Coalson, 2006). Further studies also demonstrated that premature infants express higher IL-6 levels in the BAL which is associated with the development of BPD (Bagchi et al., 1994). Concordant with this data, there are reports describing that IL-10 levels are dramatically reduced in infants with BPD (Jones et al., 1996).

Although GYY4137 did not restore the increased IL-6 levels, GYY4137 did normalize the IL-10 levels to the developing lung exposed to hyperoxia. Hence, the limited inflammation observed in the GYY4137 treated mouse pups exposed to hyperoxia may have been underlie by the anti-inflammatory IL-10 activity. Remarkably, the production of IL-10 by fetal rat ATII cells can be modulated by anti-oxidant treatment with superoxide dismutase (Johnson-Varghese et al., 2004), and it has been suggested that IL-10 may protect fetal rat ATII cells from apoptosis induced by 85% O_2 (Johnson-Varghese et al., 2004; Lee & Kim, 2011). Interestingly, infants that are homozygous for the IL-10 “high producer” 1082G allele – a SNP

that leads to abnormal higher production of IL10 – are thought to have a lower risk for prematurity associated disorders, including BPD (Dordelmann et al., 2006).

One explanation of how IL-10 may play a protective role in BPD includes the idea that IL-10 protects fetal ATII cells from the harmful effects of stretch (Lee et al., 2008), and that IL-10 restricts stretch-induced cytokine secretion by fetal mouse lung fibroblasts (Hawwa et al., 2011). A side observation from the study was that in 21% O_2 GYY4137 treated mouse, GYY4137 decreased IL-10 levels, maybe hinting that H_2S administration to healthy lungs could disturb inflammatory cell lung dynamics. Altogether these data funds the idea that GYY4137 protects the lung from the injuring impact of hyperoxia, and that H_2S delivered by GYY4137 may limit lung inflammation by driving increased IL-10 levels (Madurga et al., 2014).

Apart from the regulation of inflammatory cell dynamics, attention was driven to the modulation of gene expression in the lung. Plus, the impact of H_2S on epithelial cell migration was also considered, since H_2S is known to induce endothelial cell migration (Papapetropoulos et al., 2009). In the *in vitro* studies, the fast-release H_2S donor NaHS replaced the slow-release H_2S donor GYY4137, due to the shorter time-course of the *in vitro* experiments. Prior to following studies it was tested that NaHS provoked no cell toxicity at the dose employed. Using primary ATII cell pools, a microarray analysis was performed, which demonstrated that ATII cells exposed to 85% O_2 *in vitro* for 24 h had a strong impact on gene regulation. Using a very stringent criteria, the expression of 251 genes was up-regulated and the expression of 367 genes was down-regulated in primary ATII cells in response to normobaric hyperoxia conditions. Implementing a PANTHER analysis and taking into account that hyperoxia exposure induces apoptosis of lung cells, the microarray analysis resulted in an increase of the p53 pro-apoptosis pathway activity, and a decreased in activity of the DNA replication pathway. Though, primary ATII cells treated either with H_2S donors had no impact on gene modulation, comparing 21% O_2-treated cells with and without H_2S administration, or comparing 85% O_2-treated cells with and without H_2S administration. These data provides conclusive information that H_2S delivered by NaHS or GYY4137, does not have any direct effect on primary ATII cell gene expression per se, and provides information about what H_2S is not doing in this system.

Though with no modulation on gene expression, exposure of primary ATII cells to NaHS did induce ATII cell migration. Certainly, NaHS administration promoted the migration capacity of primary ATII cells and fastened wound closure in an *in vivo* cell monolayer wounding assay. These data provides supplementary information for a role of H_2S promoting

lung repair and restoring normal alveolarization to oxygen-injured lungs (Madurga et al., 2014).

Considering that H_2S does not influence gene expression in ATII cells, alternative candidate pathways that might drive this effect were studied.

Migration and wound repair of human airway epithelial cells (Trinh et al., 2007) is known to be reliant on upon ATP sensitive potassium (K_{ATP}) channels. Taking into account that the activity of K_{ATP} channels may be modulated by H_2S (Wang, 2011), glibenclamide, a K_{ATP} channels inhibitor, was employed in the ATII cell wound repair assay. Glibenclamide blunted the ability of NaHS to promote wound closure in ATII cell monolayers. These findings support the idea that H_2S, delivered by NaHS, promotes ATII cell wound repair through modulation of K_{ATP} channel activity (Madurga et al., 2014). These data is consistent with previous studies where it has been observed that H_2S activates K_{ATP} channels (Jiang et al., 2010; Siebert et al., 2008). Still, it is important to consider that glibenclamide is a sulfonylurea able to inhibit the cystic fibrosis transmembrane conductance regulator (CFTR) chloride channel (Sheppard & Welsh, 1992), and the plausible interactions between H_2S with CFTR as ATII cell wound repair mediator has not been attempted in this study.

Protein kinase B (Akt), is another anti-oxidant protective protein in the lung (Lu et al., 2001), and H_2S is known to promote angiogenesis through the Akt pathway (Cai et al., 2007). Considering the above mention, primary mouse ATII cells or MLE-12 mouse lung epithelial cells exposed to NaHS, resulted in a fast (less than 30 min) activation of Akt, evaluated through Akt phosphorylation. These experiments might hint a second mechanism, pointing how H_2S may protect the lung against hyperoxia-induced injury, promoting wound repair and epithelial cell migration. This idea is reinforced by the finding of augmented abundance of activated fraction of Akt (phosphorylated) in lung extracts from mouse pup lungs exposed to hyperoxia and treated with GYY4137, versus lung extract from mouse pups exposed to hyperoxia and treated with vehicle (water) alone. Therefore, GYY4137 administration might have activated Akt *in vivo* in mouse pup lungs exposed to hyperoxia, which could have collaborated to the improved lung alveolarization observed in GYY4137-treated mouse pups (Madurga et al., 2014).

In this study, it has been demonstrated that H_2S administration can partially correct defective alveolarization. However, the H_2S administration was systemic and not local, which is a clear caveat of the study. Still, the systemic administration has a series of advantages; (i) enables to properly dose the H_2S donor in a pilot study; (ii) avoids possible irritated effects of H_2S on nursing mothers and the eyes of the newborn pups; and (iii) avoids the quenching of

H_2S by the very high (85% O_2) oxygen levels in the exposure chamber, considering that H_2S and O_2 are highly reactive with one another.

The data presented in this study deal only with the pulmonary system, although systemic administration of H_2S delivered by GYY4137 would also affect other organs apart from the lung. For example, systemic administration of GYY4137 improved liver and kidney failure in an experimental endotoxic shock in rats (determined by attenuated alanine aminotransferase and creatinine levels, respectively) (Li et al., 2009), while systemic NaHS administration improved renal fibrosis in a rat obstructive nephropathy model (Song et al., 2014).

Finally, considering the possible effects of H_2S systemic administration on perinatal development, rat pups treated systemically with H_2S did not suffer growth retardation or behavior abnormalities, without any findings of gross developmental abnormalities of the brain, heart, liver or kidney (Dorman et al., 2000).

The second central question of this study was: Do cystathionine β-synthase (Cbs) and cystathionine γ-lyase (Cth) -both hydrogen sulfide generating and regulatory enzymes- play a role during normal late lung development? A starting point for this study was to measure the expression levels of both enzymes during different time points during late lung development, where the data revealed that both enzymes have a modulated expression in different time points during late lung development almost in an opposite manner.

Secondly, it was measured via laser-capture micro dissection and immunofluorescence stainings, where both enzymes are localized in postnatal lungs during two different time points, on day P7.5 and on day P14.5. These two time points were chosen because P7.5 is an early time point during lung development close to the peak of septation, whereas P14.5 is a later stage closer to the micro vessel maturation of the lung (Choi, 2010; Massaro & Massaro, 2007; Warburton et al., 2010; Warburton et al., 2000). The data indicated that the both enzymes in the mouse, Cbs and Cth, are majoritarely expressed in the vessel and airway compartment with a lower expression in the lung parenchyma. This data is consistent to what it has been previously described in the literature in adult lungs (Olson et al., 2010; Wang et al., 2011).

Next, two transgenic mice, where the genes encoding Cbs and Cth have been deleted respectively, were tested to study the course of normal late lung development during two time points on P7.5 and P14.5. The data from this study describes a dramatic impairment in lung development for both *Cbs*$^{-/-}$ and *Cth*$^{-/-}$ mice that was fully evident on P14.5. The lung volumes of both *Cbs*$^{-/-}$ and *Cth*$^{-/-}$ mice were significantly smaller than wild type mice, the values

decreased from 0.31 ± 0.01 cm^3 in the wild type mice, to 0.23 ± 0.009 cm^3 in the *Cbs*$^{-/-}$ mice and to 0.24 ± 0.02 cm^3 in the *Cth*$^{-/-}$ mice. The number of alveoli were significantly smaller in both *Cbs*$^{-/-}$ and *Cth*$^{-/-}$ mice, it lowered almost 50% when compared to the wild type mice. The number of alveoli decreased from 4.74 ± 0.42 × 10^6 alveoli/both lungs in the wild type mice, to 2.30 ± 0.20× 10^6 alveoli/both lungs in the *Cbs*$^{-/-}$ mice, and to 2.81 ± 0.78 × 10^6 alveoli/both lungs in the *Cth*$^{-/-}$ mice. Regarding the mean linear intercept, it changed increasing from 30.85 ± 1.0 μm in wild type mice to 38.15 ± 3.4 μm in the *Cbs*$^{-/-}$ mice, and it also increased to 43.2 ± 6.8 μm in the *Cth*$^{-/-}$ mice. Moreover, the surface area for gas exchange was smaller in both *Cbs*$^{-/-}$ and *Cth*$^{-/-}$ mice when compared to the wild type mice. The values decreased almost 50 %, ranging from 220.8 ± 13.1 cm^2 in the wild type mice, to 134.2 ± 5.9 cm^2 in the *Cbs*$^{-/-}$ mice and to 154 ± 22.6 cm^2 in the *Cth*$^{-/-}$ mice. These data confirm that the ablation of both genes Cbs and Cth, two generating H_2S enzymes, have an impact in the correct developing of the lung structure during late lung development.

Blood vessels in the lung play an important role promoting normal lung development and preserving correct alveolar structures throughout alveologenesis. An incorrect or poor blood flow distribution may outcome in lung abnormality (Iosef et al., 2012; Pereda et al., 2013; Thebaud, 2007). Hydrogen sulfide is known to play a role in angiogenesis promoting cell growth, motility and capillary morphogenesis, promoting the formation of new vessels both *in vitro* and *in vivo* (Cai et al., 2007; Papapetropoulos et al., 2009; Perry et al., 2011; Szabó, 2011; Vadivel et al., 2014). Prior studies suggest the presence of a vascular network former to the morphological construction of the lung (Peng & Morrisey, 2013), and taking into an account that both enzymes are present in the vessels, the absence of Cbs and Cth and its byproduct H_2S, might lead into an error in the pulmonary vasculature, impacting the correct growth and maturation of the lung. Indeed, the vascular supply was lower for both *Cbs*$^{-/-}$ and *Cth*$^{-/-}$ mice postnatal, especially for the *Cbs*$^{-/-}$ mice, when compared to wild type mice. Furthermore, lung homogenates from postnatal *Cbs*$^{-/-}$ mice and *Cth*$^{-/-}$ had a lower expression of CD31 when compared to wild type mice, which is known to be an effective signaling molecule that have different roles in vascular biology which include: Angiogenesis, platelet function, thrombosis, mechano-sensing of endothelial cell response to fluid shear stress and regulation of multiple stages of leukocyte migration through venular walls (Woodfin et al., 2007).

The *in vitro* experiments corroborated the same findings as the *in vivo* experiments, since the inhibition of both CBS and CTH in HPAECs diminished network formation, but the addition of H_2S, delivered by GYY4137, promoted it. These data is consistent with the

publication of the group of Dr. Thebaud (Vadivel et al., 2014), where they studied the protective effects of H_2S in preventing pulmonary hypertension in the BPD model. They demonstrated *in vitro* that H_2S treatment protects HPAECs from oxygen toxicity and also promotes network formation in hyperoxia conditions. They also indicated that H_2S lessens echographic and structural changes of pulmonary hypertension *in vivo*. They described that in hyperoxia conditions, there is less expression of CD31 in lung homogenates and that the expression levels are comparable to room air exposure when treated with H_2S. They exposed that hyperoxia leads to an arrest of vascular growth by decreasing the number of positive vWF lung vessels, and H_2S treatment attenuated the loss of vWF positive cells. The study presented here also demonstrated that not only the vessel supply is affected in the absence of these two enzymes, but also vessel remodeling occurred during lung development in both *Cbs*$^{-/-}$ mice and *Cth*$^{-/-}$ mice. A thickening of small and medium vessels was present in the *Cbs*$^{-/-}$ mice, and less severe but also present was the remodeling of the small vessels in the *Cth*$^{-/-}$ mice, which correlates with a worse lung development in the case of the *Cbs*$^{-/-}$ mice compared to the *Cth*$^{-/-}$ mice.

The absence of both Cbs and Cth not only inhibit the formation of H_2S, but also promotes the accumulation of homocysteine. Evidence from independent laboratories established that hyperhomocysteinemia is associated with vascular dysfunction and remodeling. One plausible documented mechanism is oxidative stress: NADPH oxidase causes endothelial dysfunction, SMC proliferation and accumulation of extracellular matrix that lead to vessel remodeling (Basu et al., 2011). It has been reported that patients with *Cbs*$^{-/-}$ develop severe hyperhomocysteinemia and experience major clinical manifestations of premature vascular death if not treated, whereas *Cbs*$^{+/-}$ individuals live normally but with cardiovascular defects (Basu et al., 2011). The accumulation of hyperhomocysteine is considered an independent atherogenic risk factor but it has also been shown that administration of NaHS protects rat aortic SMCs from the cytotoxicity caused by this molecule (Mani et al., 2013). Some groups have described similar findings when studying the role of Cth and H_2S in the cardiovascular system, *in vitro* studies indicate that H_2S inhibits SMC proliferation and Cth deficiency increases it (Mani et al., 2013). Decreased endogenous H_2S production predisposes animals to vascular remodeling and early development of atherosclerosis. Some molecular candidates have been proposed as targets from H_2S as inhibitors of vascular SMC proliferation. One known pathway is through the mitogen-activated protein kinase (MAPK) (Li et al., 2013); other results indicate that H_2S via an epigenetic mechanism can involve the inhibition of Brahma-related gene 1 (Brg1) transcription and expression, by reducing the recruitment of

Brg1 to the proliferating cell nuclear antigen, neurotrophin 3 and platelet-derived growth factor subunit A promoting regions (Li et al., 2013). Moreover, other groups have found that the treatment with H_2S can mitigate the vascular remodeling by normalizing the levels of redox stress, matrix metalloproteinase and tissue inhibitor of metalloproteinase (Vacek et al., 2010). Although several explanations have been exposed, it is beyond the scope of this study to elucidate if the vascular remodeling observed in these *Cbs*$^{-/-}$ mice and *Cth*$^{-/-}$ mice is solely due to the accumulation of homocysteine or the absence of H_2S. Further studies are granted to reveal the complex mechanisms that are responsible for the vessel alteration observed in the *Cbs*$^{-/-}$ and *Cth*$^{-/-}$ mice.

The data presented in this study indicate that H_2S administration can diminish the harmful effects of hyperoxia on lung alveolarization, and some candidate mechanisms have been exposed to explain this phenomenon, including the capacity of H_2S to drive production of protective anti-inflammatory cytokines, limit the inflammatory cell recruitment to the alveolar airspaces (mostly macrophages and neutrophils) that was provoked by hyperoxia, and to promote ATII wound healing and cell migration through glibenclamide-sensitive ion channels, and possibly through the activation of the lung-protective Akt pathway.

The data also indicates the possible role of the two generating H_2S enzymes Cbs and Cth, during the course of normal late lung development, the expression and localization of these enzymes in postnatal lung mice have been presented, together with the lung structural analysis of the *Cbs*$^{-/-}$ mice and *Cth*$^{-/-}$ mice showing an aberrant alveolarization and vessel maturation *in vitro* and *in vivo*.

The data presented in this study, provides solid support to continue evaluating H_2S as a novel agent that might prove useful in the management of hyperoxia-induced injury to the developing lung. This possibility is far more attractive, considering the potential delivery of H_2S locally via the trachea to the developing lungs, which would be a feasible process in intubated, ventilated patients.

13 Acknowledgements

I would like to acknowledge the substantive input from Dr. Rory E. Morty and Prof. Dr. Werner Seeger for guiding me during all my PhD. I would like to thank all members of the Morty laboratory, mostly: Dr. Lukasz Wujak, Dr. Gero Niess, Akis Sakkas, Tatyana Likhoshvay, Ivana Mizikova and Jordi Ruiz Camp. I also would like to thank the technicians from our laboratory: Simone Becker, Regina Wagner, Diana Fuchs and Uta Eule, the secretary from our department Monika Haselbauer, the IT department especially Peter Hofmann, the animal facility of the Max Planck Institute, and several students from the Max Planck Institute, among them: Dijana Iloska, Peter Rauschkolb, Dr. Sven Becker and Mario Schmoranzer.

I also would like to thank the assistance of Prof. Dr. Heinz Fehrenbach and Franziska Beyersdorf (Division of Experimental Pneumology, Research Center Borstel, Borstel, Germany), Lisa Fröhlich and Prof. Dr. Norbert Weissmann (ECCPS, University of Giessen School of Medicine, Giessen, Germany), Tamara Papadakis and Prof. Dr. Wolfgang Kummer (Institute for Anatomy and Cell Biology, University of Giessen School of Medicine, Giessen, Germany), Dr. Lars Knudsen and Prof. Dr. Matthias Ochs (Institute of Functional and Applied Anatomy, Hannover Medical School, Hannover, Germany), Dr. Stefan Tschanz (Institute for Anatomy, University of Bern, Bern, Switzerland), and Maike Riese (Molecular Devices, Biberach an der Riss, Germany).

Finally, I would like to thank my family for all their support during this time.

14 References

Abman, S. H. (2007). Recent advances in the pathogenesis and treatment of persistent pulmonary hypertension of the newborn. *Neonatology, 91*(4), 283-290.

Akahoshi, N., Kobayashi, C., Ishizaki, Y., Izumi, T., Himi, T., Suematsu, M., et al. (2008). Genetic background conversion ameliorates semi-lethality and permits behavioral analyses in cystathionine beta-synthase-deficient mice, an animal model for hyperhomocysteinemia. *Hum Mol Genet, 17*(13), 1994-2005.

Alejandre-Alcazar, M. A., Kwapiszewska, G., Reiss, I., Amarie, O. V., Marsh, L. M., Sevilla-Perez, J., et al. (2007). Hyperoxia modulates TGF-beta/BMP signaling in a mouse model of bronchopulmonary dysplasia. *Am J Physiol Lung Cell Mol Physiol, 292*(2), L537-549.

Alejandre-Alcazar, M. A., Michiels-Corsten, M., Vicencio, A. G., Reiss, I., Ryu, J., de Krijger, R. R., et al. (2008). TGF-beta signaling is dynamically regulated during the alveolarization of rodent and human lungs. *Dev Dyn, 237*(1), 259-269.

Alphonse, R. S., Vadivel, A., Coltan, L., Eaton, F., Barr, A. J., Dyck, J. R., et al. (2011). Activation of Akt protects alveoli from neonatal oxygen-induced lung injury. *Am J Respir Cell Mol Biol, 44*(2), 146-154.

Ambalavanan, N., Bulger, A., Murphy-Ullrich, J., Oparil, S., & Chen, Y. F. (2005). Endothelin-A receptor blockade prevents and partially reverses neonatal hypoxic pulmonary vascular remodeling. *Pediatr Res, 57*(5 Pt 1), 631-636.

Ambalavanan, N., & Carlo, W. A. (2004). Bronchopulmonary dysplasia: new insights. *Clin Perinatol, 31*(3), 613-628.

Ambalavanan, N., Carlo, W. A., D'Angio, C. T., McDonald, S. A., Das, A., Schendel, D., et al. (2009). Cytokines associated with bronchopulmonary dysplasia or death in extremely low birth weight infants. *Pediatrics, 123*(4), 1132-1141.

Ambalavanan, N., Van Meurs, K. P., Perritt, R., Carlo, W. A., Ehrenkranz, R. A., Stevenson, D. K., et al. (2008). Predictors of death or bronchopulmonary dysplasia in preterm infants with respiratory failure. *J Perinatol, 28*(6), 420-426.

Ambalavanan, N., Walsh, M., Bobashev, G., Das, A., Levine, B., Carlo, W. A., et al. (2011). Intercenter differences in bronchopulmonary dysplasia or death among very low birth weight infants. *Pediatrics, 127*(1), e106-116.

Aslami, H., Heinen, A., Roelofs, J. J., Zuurbier, C. J., Schultz, M. J., & Juffermans, N. P. (2010). Suspended animation inducer hydrogen sulfide is protective in an in vivo model of ventilator-induced lung injury. *Intensive Care Med, 36*(11), 1946-1952.

Bader, D., Ramos, A. D., Lew, C. D., Platzker, A. C., Stabile, M. W., & Keens, T. G. (1987). Childhood sequelae of infant lung disease: exercise and pulmonary function abnormalities after bronchopulmonary dysplasia. *J Pediatr, 110*(5), 693-699.

Bagchi, A., Viscardi, R. M., Taciak, V., Ensor, J. E., McCrea, K. A., & Hasday, J. D. (1994). Increased activity of interleukin-6 but not tumor necrosis factor-alpha in lung lavage of premature infants is associated with the development of bronchopulmonary dysplasia. *Pediatr Res, 36*(2), 244-252.

Bancalari, E., Abdenour, G. E., Feller, R., & Gannon, J. (1979). Bronchopulmonary dysplasia: clinical presentation. *J Pediatr, 95*(5 Pt 2), 819-823.

Basu, P., Qipshidze, N., Tyagi, S. C., & Sen, U. (2011). Remodeling in vein expresses arterial phenotype in hyperhomocysteinemia. *Int J Physiol Pathophysiol Pharmacol, 3*(4), 266-279.

Benetti, L. R., Campos, D., Gurgueira, S. A., Vercesi, A. E., Guedes, C. E., Santos, K. L., et al. (2013). Hydrogen sulfide inhibits oxidative stress in lungs from allergic mice in vivo. *Eur J Pharmacol, 698*(1-3), 463-469.

Blackwell, T. S., Hipps, A. N., Yamamoto, Y., Han, W., Barham, W. J., Ostrowski, M. C., et al. (2011). NF-kappaB signaling in fetal lung macrophages disrupts airway morphogenesis. *J Immunol, 187*(5), 2740-2747.

Blayney, M., Kerem, E., Whyte, H., & O'Brodovich, H. (1991). Bronchopulmonary dysplasia: improvement in lung function between 7 and 10 years of age. *J Pediatr, 118*(2), 201-206.

Bose, C., Laughon, M., Allred, E. N., Van Marter, L. J., O'Shea, T. M., Ehrenkranz, R. A., et al. (2011). Blood protein concentrations in the first two postnatal weeks that predict bronchopulmonary dysplasia among infants born before the 28th week of gestation. *Pediatr Res, 69*(4), 347-353.

Brion, L. P., & Soll, R. F. (2001). Diuretics for respiratory distress syndrome in preterm infants. *Cochrane Database Syst Rev*(2), CD001454.

Brundage, K. L., Mohsini, K. G., Froese, A. B., & Fisher, J. T. (1990). Bronchodilator response to ipratropium bromide in infants with bronchopulmonary dysplasia. *Am Rev Respir Dis, 142*(5), 1137-1142.

Buczynski, B. W., Maduekwe, E. T., & O'Reilly, M. A. (2013). The role of hyperoxia in the pathogenesis of experimental BPD. *Semin Perinatol, 37*(2), 69-78.

Cai, W. J., Wang, M. J., Moore, P. K., Jin, H. M., Yao, T., & Zhu, Y. C. (2007). The novel proangiogenic effect of hydrogen sulfide is dependent on Akt phosphorylation. *Cardiovasc Res, 76*(1), 29-40.

Chen, Y., & Wang, R. (2012). The message in the air: hydrogen sulfide metabolism in chronic respiratory diseases. *Respir Physiol Neurobiol, 184*(2), 130-138.

Chen, Y. H., Wu, R., Geng, B., Qi, Y. F., Wang, P. P., Yao, W. Z., et al. (2009). Endogenous hydrogen sulfide reduces airway inflammation and remodeling in a rat model of asthma. *Cytokine, 45*(2), 117-123.

Chen, Y. H., Yao, W. Z., Geng, B., Ding, Y. L., Lu, M., Zhao, M. W., et al. (2005). Endogenous hydrogen sulfide in patients with COPD. *Chest, 128*(5), 3205-3211.

Choi, C. W. (2010). Lung interstitial cells during alveolarization. *Korean J Pediatr, 53*(12), 979-984.

Coalson, J. J. (2006). Pathology of bronchopulmonary dysplasia. *Semin Perinatol, 30*(4), 179-184.

Dahal, B. K., Cornitescu, T., Tretyn, A., Pullamsetti, S. S., Kosanovic, D., Dumitrascu, R., et al. (2010). Role of epidermal growth factor inhibition in experimental pulmonary hypertension. *Am J Respir Crit Care Med, 181*(2), 158-167.

Darlow, B. A., & Graham, P. J. (2007). Vitamin A supplementation to prevent mortality and short and long-term morbidity in very low birthweight infants. *Cochrane Database Syst Rev*(4), CD000501.

Deng, H., Mason, S. N., & Auten, R. L., Jr. (2000). Lung inflammation in hyperoxia can be prevented by antichemokine treatment in newborn rats. *Am J Respir Crit Care Med, 162*(6), 2316-2323.

Dieperink, H. I., Blackwell, T. S., & Prince, L. S. (2006). Hyperoxia and apoptosis in developing mouse lung mesenchyme. *Pediatr Res, 59*(2), 185-190.

Dordelmann, M., Kerk, J., Dressler, F., Brinkhaus, M. J., Bartels, D. B., Dammann, C. E., et al. (2006). Interleukin-10 high producer allele and ultrasound-defined periventricular white matter abnormalities in preterm infants: a preliminary study. *Neuropediatrics, 37*(3), 130-136.

Dorman, D. C., Brenneman, K. A., Struve, M. F., Miller, K. L., James, R. A., Marshall, M. W., et al. (2000). Fertility and developmental neurotoxicity effects of inhaled hydrogen sulfide in Sprague-Dawley rats. *Neurotoxicol Teratol, 22*(1), 71-84.

Ehrenkranz, R. A., Walsh, M. C., Vohr, B. R., Jobe, A. H., Wright, L. L., Fanaroff, A. A., et al. (2005). Validation of the National Institutes of Health consensus definition of bronchopulmonary dysplasia. *Pediatrics, 116*(6), 1353-1360.

Enokido, Y., Suzuki, E., Iwasawa, K., Namekata, K., Okazawa, H., & Kimura, H. (2005). Cystathionine beta-synthase, a key enzyme for homocysteine metabolism, is preferentially expressed in the radial glia/astrocyte lineage of developing mouse CNS. *FASEB J, 19*(13), 1854-1856.

Faller, S., Zimmermann, K. K., Strosing, K. M., Engelstaedter, H., Buerkle, H., Schmidt, R., et al. (2012). Inhaled hydrogen sulfide protects against lipopolysaccharide-induced acute lung injury in mice. *Med Gas Res, 2*(1), 26.

Fang, L., Li, H., Tang, C., Geng, B., Qi, Y., & Liu, X. (2009). Hydrogen sulfide attenuates the pathogenesis of pulmonary fibrosis induced by bleomycin in rats. *Can J Physiol Pharmacol, 87*(7), 531-538.

Fehrenbach, H., Voswinckel, R., Michl, V., Mehling, T., Fehrenbach, A., Seeger, W., et al. (2008). Neoalveolarisation contributes to compensatory lung growth following pneumonectomy in mice. *Eur Respir J, 31*(3), 515-522.

Fernandez-Gonzalez, A., Alex Mitsialis, S., Liu, X., & Kourembanas, S. (2012). Vasculoprotective effects of heme oxygenase-1 in a murine model of hyperoxia-induced bronchopulmonary dysplasia. *Am J Physiol Lung Cell Mol Physiol, 302*(8), L775-784.

Gadalla, M. M., & Snyder, S. H. (2010). Hydrogen sulfide as a gasotransmitter. *J Neurochem, 113*(1), 14-26.

Gavino, R., Johnson, L., & Bhandari, V. (2002). Release of cytokines and apoptosis in fetal rat Type II pneumocytes exposed to hyperoxia and nitric oxide: modulatory effects of dexamethasone and pentoxifylline. *Cytokine, 20*(6), 247-255.

Gillman, M. A., & Lichtigfeld, F. J. (1981). A comparison of the effects of morphine sulphate and nitrous oxide analgesia on chronic pain states in man. *J Neurol Sci, 49*(1), 41-45.

Gillman, M. A., & Lichtigfeld, F. J. (1983). Nitrous oxide interacts with opioid receptors: more evidence. *Anesthesiology, 58*(5), 483-484.

Gu, X., & Zhu, Y. Z. (2011). Therapeutic applications of organosulfur compounds as novel hydrogen sulfide donors and/or mediators. *Expert Rev Clin Pharmacol, 4*(1), 123-133.

Halliday, H. L., & Ehrenkranz, R. A. (2001a). Delayed (>3 weeks) postnatal corticosteroids for chronic lung disease in preterm infants. *Cochrane Database Syst Rev*(2), CD001145.

Halliday, H. L., & Ehrenkranz, R. A. (2001b). Early postnatal (<96 hours) corticosteroids for preventing chronic lung disease in preterm infants. *Cochrane Database Syst Rev*(1), CD001146.

Halliday, H. L., & Ehrenkranz, R. A. (2001c). Moderately early (7-14 days) postnatal corticosteroids for preventing chronic lung disease in preterm infants. *Cochrane Database Syst Rev*(1), CD001144.

Hamelet, J., Maurin, N., Fulchiron, R., Delabar, J. M., & Janel, N. (2007). Mice lacking cystathionine beta synthase have lung fibrosis and air space enlargement. *Exp Mol Pathol, 83*(2), 249-253.

Hartling, L., Liang, Y., & Lacaze-Masmonteil, T. (2012). Chorioamnionitis as a risk factor for bronchopulmonary dysplasia: a systematic review and meta-analysis. *Arch Dis Child Fetal Neonatal Ed, 97*(1), F8-F17.

Hawwa, R. L., Hokenson, M. A., Wang, Y., Huang, Z., Sharma, S., & Sanchez-Esteban, J. (2011). IL-10 inhibits inflammatory cytokines released by fetal mouse lung fibroblasts exposed to mechanical stretch. *Pediatr Pulmonol, 46*(7), 640-649.

Hsia, C. C., Hyde, D. M., Ochs, M. & Weibel, E. R.. (2010). An official research policy statement of the American Thoracic Society/European Respiratory Society: standards for quantitative assessment of lung structure. *Am J Respir Crit Care Med, 181*(4), 394-418.

Iosef, C., Alastalo, T. P., Hou, Y., Chen, C., Adams, E. S., Lyu, S. C., et al. (2012). Inhibiting NF-kappaB in the developing lung disrupts angiogenesis and alveolarization. *Am J Physiol Lung Cell Mol Physiol, 302*(10), L1023-1036.

Ishii, I., Akahoshi, N., Yamada, H., Nakano, S., Izumi, T., & Suematsu, M. (2010). Cystathionine gamma-Lyase-deficient mice require dietary cysteine to protect against acute lethal myopathy and oxidative injury. *J Biol Chem, 285*(34), 26358-26368.

Ishii, I., Akahoshi, N., Yu, X. N., Kobayashi, Y., Namekata, K., Komaki, G., et al. (2004). Murine cystathionine gamma-lyase: complete cDNA and genomic sequences, promoter activity, tissue distribution and developmental expression. *Biochem J, 381*(Pt 1), 113-123.

Jiang, B., Tang, G., Cao, K., Wu, L., & Wang, R. (2010). Molecular mechanism for H(2)S-induced activation of K(ATP) channels. *Antioxid Redox Signal, 12*(10), 1167-1178.

Jobe, A. H. (2005). Antenatal associations with lung maturation and infection. *J Perinatol, 25 Suppl 2*, S31-35.

Jobe, A. H. (2011). The new bronchopulmonary dysplasia. *Curr Opin Pediatr, 23*(2), 167-172.

Jobe, A. H., & Bancalari, E. (2001). Bronchopulmonary dysplasia. *Am J Respir Crit Care Med, 163*(7), 1723-1729.

Jobe, A. H., & Ikegami, M. (2001). Prevention of bronchopulmonary dysplasia. *Curr Opin Pediatr, 13*(2), 124-129.

Jobe, A. J. (1999). The new BPD: an arrest of lung development. *Pediatr Res, 46*(6), 641-643.

Johnson-Varghese, L., Brodsky, N., & Bhandari, V. (2004). Effect of antioxidants on apoptosis and cytokine release in fetal rat Type II pneumocytes exposed to hyperoxia and nitric oxide. *Cytokine, 28*(1), 10-16.

Jones, C. A., Cayabyab, R. G., Kwong, K. Y., Stotts, C., Wong, B., Hamdan, H., et al. (1996). Undetectable interleukin (IL)-10 and persistent IL-8 expression early in hyaline membrane disease: a possible developmental basis for the predisposition to chronic lung inflammation in preterm newborns. *Pediatr Res, 39*(6), 966-975.

Kabil, O., Vitvitsky, V., Xie, P., & Banerjee, R. (2011). The quantitative significance of the transsulfuration enzymes for H2S production in murine tissues. *Antioxid Redox Signal, 15*(2), 363-372.

Kajimura, M., Fukuda, R., Bateman, R. M., Yamamoto, T., & Suematsu, M. (2010). Interactions of multiple gas-transducing systems: hallmarks and uncertainties of CO, NO, and H2S gas biology. *Antioxid Redox Signal, 13*(2), 157-192.

Kakkera, D. K., Siddiq, M. M., & Parton, L. A. (2005). Interleukin-1 balance in the lungs of preterm infants who develop bronchopulmonary dysplasia. *Biol Neonate, 87*(2), 82-90.

Kallapur, S. G., & Jobe, A. H. (2006). Contribution of inflammation to lung injury and development. *Arch Dis Child Fetal Neonatal Ed, 91*(2), F132-135.

Kersbergen, K. J., de Vries, L. S., van Kooij, B. J., Isgum, I., Rademaker, K. J., van Bel, F., et al. (2013). Hydrocortisone treatment for bronchopulmonary dysplasia and brain volumes in preterm infants. *J Pediatr, 163*(3), 666-671 e661.

Kimura, H., Shibuya, N., & Kimura, Y. (2012). Hydrogen sulfide is a signaling molecule and a cytoprotectant. *Antioxid Redox Signal, 17*(1), 45-57.

Kirpalani, H., Whyte, R. K., Andersen, C., Asztalos, E. V., Heddle, N., Blajchman, M. A., et al. (2006). The Premature Infants in Need of Transfusion (PINT) study: a randomized, controlled trial of a restrictive (low) versus liberal (high) transfusion threshold for extremely low birth weight infants. *J Pediatr, 149*(3), 301-307.

Knudsen, L., Ochs, K., Boxler, L., Tornoe, I., Lykke-Sorensen, G., Mackay, R. M., et al. (2013). Surfactant protein D (SP-D) deficiency is attenuated in humanised mice expressing the Met(11)Thr short nucleotide polymorphism of SP-D: implications for surfactant metabolism in the lung. *J Anat, 223*(6), 581-592.

Knudsen, L., Ochs, M., Mackay, R., Townsend, P., Deb, R., Muhlfeld, C., et al. (2007). Truncated recombinant human SP-D attenuates emphysema and type II cell changes in SP-D deficient mice. *Respir Res, 8*, 70.

Knust, J., Ochs, M., Gundersen, H. J., & Nyengaard, J. R. (2009). Stereological estimates of alveolar number and size and capillary length and surface area in mice lungs. *Anat Rec (Hoboken), 292*(1), 113-122.

Kresch, M. J., & Clive, J. M. (1998). Meta-analyses of surfactant replacement therapy of infants with birth weights less than 2000 grams. *J Perinatol, 18*(4), 276-283.

Kunzmann, S., Collins, J. J., Kuypers, E., & Kramer, B. W. (2013). Thrown off balance: the effect of antenatal inflammation on the developing lung and immune system. *Am J Obstet Gynecol, 208*(6), 429-437.

Laughon, M. M., Langer, J. C., Bose, C. L., Smith, P. B., Ambalavanan, N., Kennedy, K. A., et al. (2011). Prediction of bronchopulmonary dysplasia by postnatal age in extremely premature infants. *Am J Respir Crit Care Med, 183*(12), 1715-1722.

Lee, H. S., & Kim, C. K. (2011). Effect of recombinant IL-10 on cultured fetal rat alveolar type II cells exposed to 65%-hyperoxia. *Respir Res, 12*, 68.

Lee, H. S., Wang, Y., Maciejewski, B. S., Esho, K., Fulton, C., Sharma, S., et al. (2008). Interleukin-10 protects cultured fetal rat type II epithelial cells from injury induced by mechanical stretch. *Am J Physiol Lung Cell Mol Physiol, 294*(2), L225-232.

Lee, Z. W., Zhou, J., Chen, C. S., Zhao, Y., Tan, C. H., Li, L., et al. (2011). The slow-releasing hydrogen sulfide donor, GYY4137, exhibits novel anti-cancer effects in vitro and in vivo. *PLoS One, 6*(6), e21077.

Li, L., Hsu, A., & Moore, P. K. (2009). Actions and interactions of nitric oxide, carbon monoxide and hydrogen sulphide in the cardiovascular system and in inflammation--a tale of three gases! *Pharmacol Ther, 123*(3), 386-400.

Li, L., Liu, D., Bu, D., Chen, S., Wu, J., Tang, C., et al. (2013). Brg1-dependent epigenetic control of vascular smooth muscle cell proliferation by hydrogen sulfide. *Biochim Biophys Acta, 1833*(6), 1347-1355.

Li, L., Rose, P., & Moore, P. K. (2011). Hydrogen sulfide and cell signaling. *Annu Rev Pharmacol Toxicol, 51*, 169-187.

Li, L., Salto-Tellez, M., Tan, C. H., Whiteman, M., & Moore, P. K. (2009). GYY4137, a novel hydrogen sulfide-releasing molecule, protects against endotoxic shock in the rat. *Free Radic Biol Med, 47*(1), 103-113.

Li, L., Whiteman, M., Guan, Y. Y., Neo, K. L., Cheng, Y., Lee, S. W., et al. (2008). Characterization of a novel, water-soluble hydrogen sulfide-releasing molecule (GYY4137): new insights into the biology of hydrogen sulfide. *Circulation, 117*(18), 2351-2360.

Lu, Y., Parkyn, L., Otterbein, L. E., Kureishi, Y., Walsh, K., Ray, A., et al. (2001). Activated Akt protects the lung from oxidant-induced injury and delays death of mice. *J Exp Med, 193*(4), 545-549.

Madurga, A., Mizikova, I., Ruiz-Camp, J., & Morty, R. E. (2013). Recent advances in late lung development and the pathogenesis of bronchopulmonary dysplasia. *Am J Physiol Lung Cell Mol Physiol, 305*(12), L893-905.

Madurga, A., Mizikova, I., Ruiz-Camp, J., Vadasz, I., Herold, S., Mayer, K., et al. (2014). Systemic hydrogen sulfide administration partially restores normal alveolarization in an experimental animal model of bronchopulmonary dysplasia. *Am J Physiol Lung Cell Mol Physiol, 306*(7), L684-697.

Malczyk, M., Veith, C., Fuchs, B., Hofmann, K., Storch, U., Schermuly, R. T., et al. (2013). Classical transient receptor potential channel 1 in hypoxia-induced pulmonary hypertension. *Am J Respir Crit Care Med, 188*(12), 1451-1459.

Mani, S., Li, H., Untereiner, A., Wu, L., Yang, G., Austin, R. C., et al. (2013). Decreased endogenous production of hydrogen sulfide accelerates atherosclerosis. *Circulation, 127*(25), 2523-2534.

Massaro, D., & Massaro, G. D. (2007). Developmental alveologenesis: longer, differential regulation and perhaps more danger. *Am J Physiol Lung Cell Mol Physiol, 293*(3), L568-569.

Massie, S. E., Tolleson-Rinehart, S., DeWalt, D. A., Laughon, M. M., Powell, L. M., & Price, W. A. (2011). Development of a proxy-reported pulmonary outcome scale for preterm infants with bronchopulmonary dysplasia. *Health Qual Life Outcomes, 9*, 55.

Mathew, N. D., Schlipalius, D. I., & Ebert, P. R. (2011). Sulfurous gases as biological messengers and toxins: comparative genetics of their metabolism in model organisms. *J Toxicol, 2011*, 394970.

Mbuyamba, M., Holman, M., & Kresch, M. J. (1998). Gestational age can predict the need for prophylaxis with surfactant therapy. *Am J Perinatol, 15*(4), 263-267.

Morley, C. J., Davis, P. G., Doyle, L. W., Brion, L. P., Hascoet, J. M., Carlin, J. B., et al. (2008). Nasal CPAP or intubation at birth for very preterm infants. *N Engl J Med, 358*(7), 700-708.

Morrisey, E. E., Cardoso, W. V., Lane, R. H., Rabinovitch, M., Abman, S. H., Ai, X., et al. (2013). Molecular determinants of lung development. *Ann Am Thorac Soc, 10*(2), S12-16.

Morty, R. E., Nejman, B., Kwapiszewska, G., Hecker, M., Zakrzewicz, A., Kouri, F. M., et al. (2007). Dysregulated bone morphogenetic protein signaling in monocrotaline-induced pulmonary arterial hypertension. *Arterioscler Thromb Vasc Biol, 27*(5), 1072-1078.

Muhlfeld, C., & Ochs, M. (2013). Quantitative microscopy of the lung: a problem-based approach. Part 2: stereological parameters and study designs in various diseases of the respiratory tract. *Am J Physiol Lung Cell Mol Physiol, 305*(3), L205-221.

Nagahara, N. (2011). Catalytic site cysteines of thiol enzyme: sulfurtransferases. *J Amino Acids, 2011*, 709404.

Namekata, K., Enokido, Y., Ishii, I., Nagai, Y., Harada, T., & Kimura, H. (2004). Abnormal lipid metabolism in cystathionine beta-synthase-deficient mice, an animal model for hyperhomocysteinemia. *J Biol Chem, 279*(51), 52961-52969.

Nanan, R. K., Liu, A. J., & Poulton, A. (2008). Nasal CPAP for very preterm infants. *N Engl J Med, 358*(23), 2520-2521; author reply 2521.

Network, S. S. G. o. t. E. K. S. N. N. R., Carlo, W. A., Finer, N. N., Walsh, M. C., Rich, W., Gantz, M. G., et al. (2010). Target ranges of oxygen saturation in extremely preterm infants. *N Engl J Med, 362*(21), 1959-1969.

Nicholson, C. K., & Calvert, J. W. (2010). Hydrogen sulfide and ischemia-reperfusion injury. *Pharmacol Res, 62*(4), 289-297.

Northway, W. H., Jr. (1992). Bronchopulmonary dysplasia: twenty-five years later. *Pediatrics, 89*(5 Pt 1), 969-973.

Northway, W. H., Jr., Rosan, R. C., & Porter, D. Y. (1967). Pulmonary disease following respirator therapy of hyaline-membrane disease. Bronchopulmonary dysplasia. *N Engl J Med, 276*(7), 357-368.

O'Reilly, M., Sozo, F., & Harding, R. (2013). Impact of preterm birth and bronchopulmonary dysplasia on the developing lung: long-term consequences for respiratory health. *Clin Exp Pharmacol Physiol, 40*(11), 765-773.

Ochs, M. (2006). A brief update on lung stereology. *J Microsc, 222*(Pt 3), 188-200.

Ochs, M., & Muhlfeld, C. (2013). Quantitative microscopy of the lung: a problem-based approach. Part 1: basic principles of lung stereology. *Am J Physiol Lung Cell Mol Physiol, 305*(1), L15-22.

Olson, K. R. (2011). The therapeutic potential of hydrogen sulfide: separating hype from hope. *Am J Physiol Regul Integr Comp Physiol, 301*(2), R297-312.

Olson, K. R., Whitfield, N. L., Bearden, S. E., St Leger, J., Nilson, E., Gao, Y., et al. (2010). Hypoxic pulmonary vasodilation: a paradigm shift with a hydrogen sulfide mechanism. *Am J Physiol Regul Integr Comp Physiol, 298*(1), R51-60.

Papapetropoulos, A., Pyriochou, A., Altaany, Z., Yang, G., Marazioti, A., Zhou, Z., et al. (2009). Hydrogen sulfide is an endogenous stimulator of angiogenesis. *Proc Natl Acad Sci U S A, 106*(51), 21972-21977.

Papile, L. A., Tyson, J. E., Stoll, B. J., Wright, L. L., Donovan, E. F., Bauer, C. R., et al. (1998). A multicenter trial of two dexamethasone regimens in ventilator-dependent premature infants. *N Engl J Med, 338*(16), 1112-1118.

Peng, T., & Morrisey, E. E. (2013). Development of the pulmonary vasculature: Current understanding and concepts for the future. *Pulm Circ, 3*(1), 176-178.

Pereda, J., Sulz, L., San Martin, S., & Godoy-Guzman, C. (2013). The human lung during the embryonic period: vasculogenesis and primitive erythroblasts circulation. *J Anat, 222*(5), 487-494.

Perry, M. M., Hui, C. K., Whiteman, M., Wood, M. E., Adcock, I., Kirkham, P., et al. (2011). Hydrogen sulfide inhibits proliferation and release of IL-8 from human airway smooth muscle cells. *Am J Respir Cell Mol Biol, 45*(4), 746-752.

Predmore, B. L., Lefer, D. J., & Gojon, G. (2012). Hydrogen sulfide in biochemistry and medicine. *Antioxid Redox Signal, 17*(1), 119-140.

Prevention of respiratory syncytial virus infections: indications for the use of palivizumab and update on the use of RSV-IGIV. American Academy of Pediatrics Committee on Infectious Diseases and Committee of Fetus and Newborn. (1998). *Pediatrics, 102*(5), 1211-1216.

Rabinovitch, M., Gamble, W., Nadas, A. S., Miettinen, O. S., & Reid, L. (1979). Rat pulmonary circulation after chronic hypoxia: hemodynamic and structural features. *Am J Physiol, 236*(6), H818-827.

Regal, J. F. (2004). Murine asthma models. *Curr Protoc Toxicol, Chapter 18*, Unit18 13.

Rieger, A. M., Nelson, K. L., Konowalchuk, J. D., & Barreda, D. R. (2011). Modified annexin V/propidium iodide apoptosis assay for accurate assessment of cell death. *J Vis Exp*(50).

Robert, K., Vialard, F., Thiery, E., Toyama, K., Sinet, P. M., Janel, N., et al. (2003). Expression of the cystathionine Synthase (CBS) gene during mouse development and immunolocalization in adult brain. *Journal of Histochemistry & Cytochemistry, 51*(3), 363-371.

Rocha, G., Ribeiro, O., & Guimaraes, H. (2010). Fluid and electrolyte balance during the first week of life and risk of bronchopulmonary dysplasia in the preterm neonate. *Clinics (Sao Paulo), 65*(7), 663-674.

Saugstad, O. D. (2010). Oxygen and oxidative stress in bronchopulmonary dysplasia. *J Perinat Med, 38*(6), 571-577.

Schelonka, R. L., Katz, B., Waites, K. B., & Benjamin, D. K., Jr. (2005). Critical appraisal of the role of Ureaplasma in the development of bronchopulmonary dysplasia with metaanalytic techniques. *Pediatr Infect Dis J, 24*(12), 1033-1039.

Schmidt, B., Roberts, R. S., Davis, P., Doyle, L. W., Barrington, K. J., Ohlsson, A., et al. (2006). Caffeine therapy for apnea of prematurity. *N Engl J Med, 354*(20), 2112-2121.

Schneider, J. P., & Ochs, M. (2013). Stereology of the lung. *Methods Cell Biol, 113*, 257-294.

Schneider, J. P., & Ochs, M. (2014). Alterations of mouse lung tissue dimensions during processing for morphometry: a comparison of methods. *Am J Physiol Lung Cell Mol Physiol, 306*(4), L341-350.

Shennan, A. T., Dunn, M. S., Ohlsson, A., Lennox, K., & Hoskins, E. M. (1988). Abnormal pulmonary outcomes in premature infants: prediction from oxygen requirement in the neonatal period. *Pediatrics, 82*(4), 527-532.

Sheppard, D. N., & Welsh, M. J. (1992). Effect of ATP-sensitive K+ channel regulators on cystic fibrosis transmembrane conductance regulator chloride currents. *J Gen Physiol, 100*(4), 573-591.

Siebert, N., Cantre, D., Eipel, C., & Vollmar, B. (2008). H2S contributes to the hepatic arterial buffer response and mediates vasorelaxation of the hepatic artery via activation of K(ATP) channels. *Am J Physiol Gastrointest Liver Physiol, 295*(6), G1266-1273.

Smith, L. J., McKay, K. O., Asperen, v., Selvadurai, & Fitzgerald. (2010). Normal development of the lung and premature birth. *Paediatr Respir Rev, 11*(3), 135-142.

Smith, V. C., Zupancic, J. A., McCormick, M. C., Croen, L. A., Greene, J., Escobar, G. J., et al. (2005). Trends in severe bronchopulmonary dysplasia rates between 1994 and 2002. *J Pediatr, 146*(4), 469-473.

Song, K., Wang, F., Li, Q., Shi, Y. B., Zheng, H. F., Peng, H., et al. (2014). Hydrogen sulfide inhibits the renal fibrosis of obstructive nephropathy. *Kidney Int, 85*(6), 1318-1329.

Stein, A., & Bailey, S. M. (2013). Redox Biology of Hydrogen Sulfide: Implications for Physiology, Pathophysiology, and Pharmacology. *Redox Biol, 1*(1), 32-39.

Stoelhorst, G. M., Rijken, M., Martens, S. E., Brand, R., den Ouden, A. L., Wit, J. M., et al. (2005). Changes in neonatology: comparison of two cohorts of very preterm infants (gestational age <32 weeks): the Project On Preterm and Small for Gestational Age Infants 1983 and the Leiden Follow-Up Project on Prematurity 1996-1997. *Pediatrics, 115*(2), 396-405.

Szabó, C. a. P., A. (2011). Hydrogen sulphide and angiogenesis: mechanisms and applications. *British Journal of Pharmacology, 164*(3), 13.

Thebaud, B. (2007). Angiogenesis in lung development, injury and repair: implications for chronic lung disease of prematurity. *Neonatology, 91*(4), 291-297.

Thebaud, B., & Abman, S. H. (2007). Bronchopulmonary dysplasia: where have all the vessels gone? Roles of angiogenic growth factors in chronic lung disease. *Am J Respir Crit Care Med, 175*(10), 978-985.

Thebaud, B., Ladha, F., Michelakis, E. D., Sawicka, M., Thurston, G., Eaton, F., et al. (2005). Vascular endothelial growth factor gene therapy increases survival, promotes lung angiogenesis, and prevents alveolar damage in hyperoxia-induced lung injury: evidence that angiogenesis participates in alveolarization. *Circulation, 112*(16), 2477-2486.

Trinh, N. T., Prive, A., Kheir, L., Bourret, J. C., Hijazi, T., Amraei, M. G., et al. (2007). Involvement of KATP and KvLQT1 K+ channels in EGF-stimulated alveolar epithelial cell repair processes. *Am J Physiol Lung Cell Mol Physiol, 293*(4), L870-882.

Tschanz, S. A., Burri, P. H., & Weibel, E. R. (2011). A simple tool for stereological assessment of digital images: the STEPanizer. *J Microsc, 243*(1), 47-59.

Vacek, T. P., Gillespie, W., Tyagi, N., Vacek, J. C., & Tyagi, S. C. (2010). Hydrogen sulfide protects against vascular remodeling from endothelial damage. *Amino Acids, 39*(5), 1161-1169.

Vadivel, A., Alphonse, R. S., Ionescu, L., Machado, D. S., O'Reilly, M., Eaton, F., et al. (2014). Exogenous hydrogen sulfide (H2S) protects alveolar growth in experimental O2-induced neonatal lung injury. *PLoS One, 9*(3), e90965.

Van Marter, L. J. (2009). Epidemiology of bronchopulmonary dysplasia. *Semin Fetal Neonatal Med, 14*(6), 358-366.

Van Marter, L. J., Allred, E. N., Pagano, M., Sanocka, U., Parad, R., Moore, M., et al. (2000). Do clinical markers of barotrauma and oxygen toxicity explain interhospital variation in rates of chronic lung disease? The Neonatology Committee for the Developmental Network. *Pediatrics, 105*(6), 1194-1201.

Voswinckel, R., Motejl, V., Fehrenbach, A., Wegmann, M., Mehling, T., Fehrenbach, H., et al. (2004). Characterisation of post-pneumonectomy lung growth in adult mice. *Eur Respir J, 24*(4), 524-532.

Wallace, J. L., Ferraz, J. G., & Muscara, M. N. (2012). Hydrogen sulfide: an endogenous mediator of resolution of inflammation and injury. *Antioxid Redox Signal, 17*(1), 58-67.

Walsh, M. C., Szefler, S., Davis, J., Allen, M., Van Marter, L., Abman, S., et al. (2006). Summary proceedings from the bronchopulmonary dysplasia group. *Pediatrics, 117*(3 Pt 2), S52-56.

Walsh, M. C., Yao, Q., Gettner, P., Hale, E., Collins, M., Hensman, A., et al. (2004). Impact of a physiologic definition on bronchopulmonary dysplasia rates. *Pediatrics, 114*(5), 1305-1311.

Wang, K., Ahmad, S., Cai, M., Rennie, J., Fujisawa, T., Crispi, F., et al. (2013). Dysregulation of hydrogen sulfide producing enzyme cystathionine gamma-lyase contributes to maternal hypertension and placental abnormalities in preeclampsia. *Circulation, 127*(25), 2514-2522.

Wang, P., Zhang, G., Wondimu, T., Ross, B., & Wang, R. (2011). Hydrogen sulfide and asthma. *Exp Physiol, 96*(9), 847-852.

Wang, R. (2003). The gasotransmitter role of hydrogen sulfide. *Antioxid Redox Signal, 5*(4), 493-501.

Wang, R. (2010). Hydrogen sulfide: the third gasotransmitter in biology and medicine. *Antioxid Redox Signal, 12*(9), 1061-1064.

Wang, R. (2011). Signaling pathways for the vascular effects of hydrogen sulfide. *Curr Opin Nephrol Hypertens, 20*(2), 107-112.

Warburton, D. (2012). Developmental responses to lung injury: repair or fibrosis. *Fibrogenesis Tissue Repair, 5*, S2.

Warburton, D., El-Hashash, A., Carraro, G., Tiozzo, C., Sala, F., Rogers, O., et al. (2010). Lung organogenesis. *Curr Top Dev Biol, 90*, 73-158.

Warburton, D., Schwarz, M., Tefft, D., Flores-Delgado, G., Anderson, K. D., & Cardoso, W. V. (2000). The molecular basis of lung morphogenesis. *Mech Dev, 92*(1), 55-81.

Watanabe, M., Osada, J., Aratani, Y., Kluckman, K., Reddick, R., Malinow, M. R., et al. (1995). Mice deficient in cystathionine beta-synthase: animal models for mild and severe homocyst(e)inemia. *Proc Natl Acad Sci U S A, 92*(5), 1585-1589.

Weibel, E. R., Hsia, C. C., & Ochs, M. (2007). How much is there really? Why stereology is essential in lung morphometry. *J Appl Physiol (1985), 102*(1), 459-467.

Woodfin, A., Voisin, M. B., & Nourshargh, S. (2007). PECAM-1: a multi-functional molecule in inflammation and vascular biology. *Arterioscler Thromb Vasc Biol, 27*(12), 2514-2523.

Zhang, G., Wang, P., Yang, G., Cao, Q., & Wang, R. (2013). The inhibitory role of hydrogen sulfide in airway hyperresponsiveness and inflammation in a mouse model of asthma. *Am J Pathol, 182*(4), 1188-1195.